10 EUR

HUNGARIAN GROUP OF *fib*

CONCRETE STRUCTURES

ANNUAL TECHNICAL JOURNAL

2016

Vol. 17

Statik mit Dynamik

AxisVM
Finite Element Program

Kombiniert beliebig

Kurhaus Oberwaid, St.Gallen
Grünenfelder + Lorenz AG Bauingenieure, St. Gallen

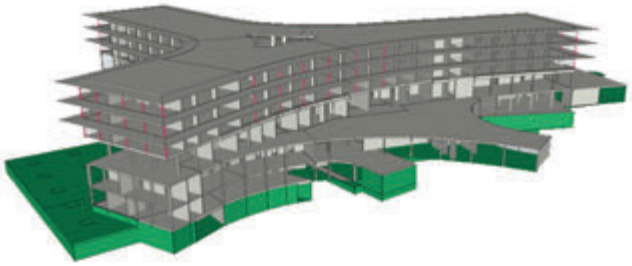

Clinique des Grangettes, Chêne-Bougeries
INGENI SA Genève
Architecte: Brodbeck & Roulet SA

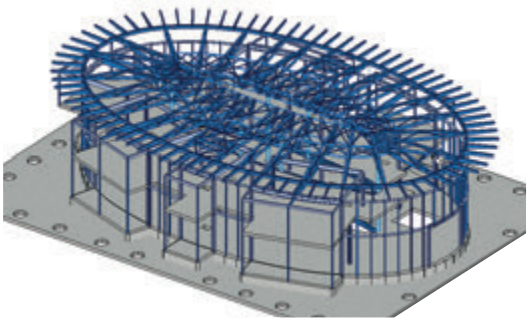

Vielseitig einsetzbar

Solothurn Entlastung West, Aaresteg
Fürst Laffranchi Bauingenieure GmbH, Aarwangen

Centro d'esercizio FFS, Pollegio
Borlini & Zanini SA, Pambio Noranco

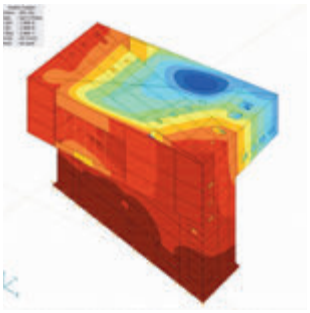

Dynamisch flexibel

Richti-Areal, Wallisellen ZH · JägerPartner AG Bauingenieure sia Zürich · Wiel Arets Architects Zürich

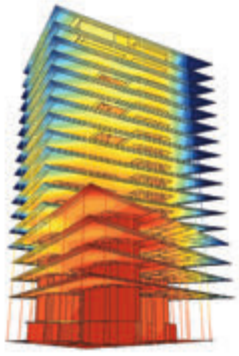

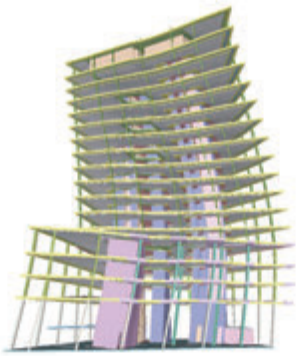

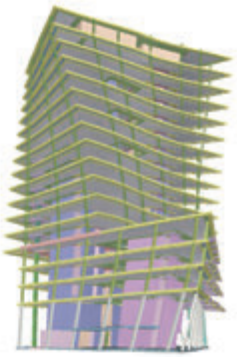

IngWare GmbH · CH-8703 Erlenbach · fon +41 (44) 910 34 34
www.ingware.ch · info@ingware.ch

IngWare

CONCRETE STRUCTURES
Journal of the Hungarian Group of ***fib***

Editor-in-chief:
Prof. György L. Balázs

Editors:
Prof. Géza Tassi
Dr. Herbert Träger

Founded by: Hungarian Group of ***fib***
Publisher: Hungarian Group of ***fib***
(***fib*** = International Federation for Structural Concrete)

Editorial office:
Budapest University of Technology and Economics (BME)
Department of Construction Materials and Engineering Geology
Műegyetem rkp. 3., H-1111 Budapest
Phone: +36-1-463 4068
Fax: +36-1-463 3450
WEB http://www.fib.bme.hu
WEB editor: Olivér Czoboly

Layout and print:
Csaba Halmai
Navigar Ltd.

Price: 10 EUR
Printed in 1000 copies

HU ISSN 2062-7904
online ISSN: 1586-0361

Cover photo:
Bridge beams of M6 motorway viaduct in Hugary produced by FERROBETON Co, CRH Group

FERROBETON

CONTENT

Sponsors:
Railway Bridges Foundation, ÉMI Nonprofit Ltd., HÍDÉPÍTŐ Co., Holcim Hungary Co., MÁV Co., MSC Consulting Co., Lábatlani Vasbetonipari Co., Pont-*TERV* Co., UVATERV Co., MÉLYÉPTERV KOMPLEX Engineering Co., SW Umwelttechnik Hungary Ltd., Betonmix Consulting Ltd., BVM Épelem Ltd., CAEC Ltd., Pannon Freyssinet Ltd., STABIL PLAN Ltd., UNION PLAN Ltd., DCB Consulting Ltd., BME Dept. of Structural Engineering, BME Dept. of Construction Materials and Technologies

UNIFIED DIMENSIONING FOR BENDING AND SHEAR

Dedicated to the 90th birthday of Prof. Géza Tassi

Andor Windisch

The 5th axiom is decisive in the geometry: only one parallel line through a point outside another line: geometry of Euclid; many lines: spherical geometry. Similarly important is in the theory of structural concrete whether at dimensioning bending and shear are considered separately or together. The paper reviews the shear theories which were developed during the last 90 years in order to eliminate the drawbacks of the common praxis, i.e. the separated dimensioning. It summarizes the advantages of unified/combined dimensioning method for bending and shear (torsion can be easily incorporated, too).

Keywords: bending, shear, dimensioning, cracked continuum model, compression zone

1. INTRODUCTION

In the geometry the axiom of parallels is one of the assumptions related to the properties of the line in the plane. Already the first analysts pointed out that Euclid classified this statement as axiom but not as postulate (claim) because he realized that it cannot be proven by experience.

Nevertheless, during 2000 years the whole galaxy was happy with this axiom: Columbus discovered America, Shakespeare wrote his dramas and sonnets and Newton stated the foundations of the science of mechanics.

At the beginning of the 19th century Bólyai and Lobachevski successfully modified the parallelism postulate. The new postulate led to the consistent system of hyperbolic geometry. The «new» geometry was indispensable for Einstein when describing the theory of relativity.

The "old 5th axiom" of structural concrete is: the dimensioning for bending and shear can be performed independently of each other. For bending in a beam the top and bottom flanges are included whereas for shear the web is "responsible". Slabs are displayed as sandwiches: for bending the upper and bottom layers, for shear the core are considered. This presumption was practical and most inconsistencies which occurred and were perceived by the engineers during practice were smoothened out during the last decades with more and more sophisticated models, concepts, e.g.:

- Varying angle truss model
- Aggregate interlock
- Size effect underlined with the theory of fracture energy
- Strut and tie model
- Stress field model
- Modified Compression Field Theory,
- Compressive Force Path-Model.

Moreover, most of these models disregard basic requirements of equilibrium, compatibility and kinematics.

This paper shortly evaluates these models, reveals their shortages and lists the advantages of the unified method of dimensioning.

2. CONSEQUENCES OF THE „OLD 5TH AXIOM" FOR THE DIMENSIONING FOR BENDING MOMENT

In the 1950's the proper stress-strain curve for concrete in the compression zone was looked for. In his PhD thesis Scholz (1960) tried to deduce the best fit form evaluating the results of beam tests, whether the σ-ε curve determined in the axial compression test could be accepted for the compression zone, too. His conclusion was: no correct and unequivocal curve can be found (nevertheless, he got the degree). The source of this flop was that the failure moments of members failing in pure bending and along the shear span, resp. were treated as one coherent dataset. Nevertheless, along the shear span the concrete compression zone is loaded with axial and shear stresses, too, hence – depending on the shear stress-axial stress ratios – the failures occurred at different outer fiber axial strains. If the datasets would have been evaluated separately, a proper curve could have been found.

Note: as the failure moment is quite insensitive to the variations of the concrete compressive strength hence the deficiencies of the curve have slight impacts only.

Note: at dimensioning for bending along the shear span a stress-strain diagram for compressed concrete should be taken into account where the impact of the shear stresses along the compression zone are considered, i.e. depending on the size of shear stresses $f_{cd}^* < f_{cd}'$ must be used.

Note: In this paper the deficiencies of the concrete compressive strength as the fundamental characteristics of the building material concrete will not be discussed. The form-dependence of the compressive strength and the failure patterns of the test specimens reveal that the compressive strength is a derived quantity, nevertheless very comfortable one (Windisch, 1992).

3. FUNDAMENTAL PROBLEMS AT DIMENSIONING FOR SHEAR

3.1 Generalities

Shear stresses are the "result" of the use of global coordinate system only. A significant drawback of the traditional dimensioning practice is that it adheres to the global coordinate system thus creating problems/obstacles for itselves.

In all shear tests on beams without shear reinforcement an explicit shear failure load was found, whereas beams with shear reinforcement failed at a higher load than predicted by the 45° truss model of Mörsch i.e. higher than resisted by the stirrups crossing the 45° inclined shear crack.

Following the old principle of the "5th axiom" i.e. for shear the web is "responsible", a uniformly distributed shear stress in the web with dimensions of $b_{ef} \cdot d$ must develop as "concrete contribution".

The American Concrete Institute set this "shear" strength equal to the tensile strength of concrete.

Fenwick and Paulay (1968) attributed the shear contribution of concrete to the aggregate interlock along the shear crack.

Analyzing the failure mechanism of a R. C. beam without transverse (shear) reinforcement Kani (1964) "noticed" the following correlation: The resultant bending moment (see *Fig. 1a*) is given by

$$M_c = V_c \cdot x = T \cdot jd$$

where

V_c is the shear force due to concrete resisting contribution,
T is tensile force in the longitudinal reinforcement and
x is the distance between the support and the point where crack has been appeared
jd is the inner lever arm.

The shear force is the derivative of the bending moment

$$V_c = dM_c/dx$$

$$V_c = jd\left[\frac{d}{dx}T\right] + T \cdot \frac{d}{dx}jd$$

The first term was identified as the resistance to shear as contribution of the "beam action", whereas the second part was called "arch action" (see *Fig. 1b*).

It is easy to recognize that these internal arches cannot exist at all nevertheless – as structural engineers like to assist their understanding making use of the simplest structures (truss, arch) – these actions are used and misused since by many researchers.

In *Fig. 1a* the angle α is indicated: this angle is used/misused in many of the following models/concepts.

3.2 Varying angle truss model

Kupfer (1962) declared that far enough from the support and the concentrated load "it can be assumed that the inclined compressive stresses change their direction only gradually, as the experimental practice shows the beam web is in the position to form flatter diagonal compressive struts (flatter than the 45°, adopted by Mörsch). The main proof is that even with a reduction of the stirrups under 50% of the amount calculated according to Mörsch, bending failure may occur before shear failure develops. The flatter slope of the compression diagonals is made possible by three main factors:

a) In experiments, the average inclination of cracks is often a little under 45°.
b) The inclined concrete strut formed by two adjacent cracks is able to take up an oblique normal force, which is inclined by a few degrees flatter than the cracks.
c) Finally, between the two flanks of a crack strong teeth are always present, so that small shear stresses can be transferred parallel to the crack direction."

Note the wording in a) little under, b) few degrees and c) "small shear stresses": nevertheless at recalculations of test results the "necessary" inclination of the struts was to be chosen many degrees flatter and the shear stresses transferred was considerable.

Thereafter Kupfer determines the minimum of strain energy of a truss composed of elastic materials. During the derivation he makes a mistake, and arrives at a complicated higher order trigonometrical equation. The tgα values (between 0 and 1.0) can be determined as functions of the rate of the axial, shear and the stirrup stresses. These curves were never used in practice hence their correctness was never proven. Nevertheless since 50 years many researchers refer on this paper (maybe they never read it, otherwise they should have found the mistake in the derivation). In effect, allowing for flatter compression struts Kupfer increases the number of the stirrups thus hiding the concrete contribution as that of surplus stirrups. The falseness of this method could be directly detected as in many experiments the number of the recalculated stirrups is larger than those existing along the shear span.

3.3 Aggregate interlock

In his thesis Walraven (1980) performed detailed theoretical and experimental work on this topic. *Fig. 2* gives an impression on the high level of this work.

Walraven's results were considered by many researchers. Nevertheless, all these theories do not consider the real kinematics of the crack faces. Muttoni et al. (2010) presented the

Fig. 1: Forces acting in a beam element within the shear span (a) and one of the internal arches in a R.C. beam (b) (Kani, 1964)

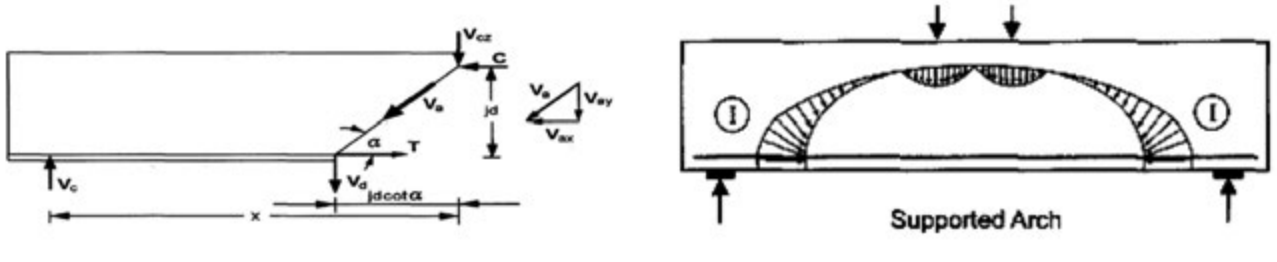

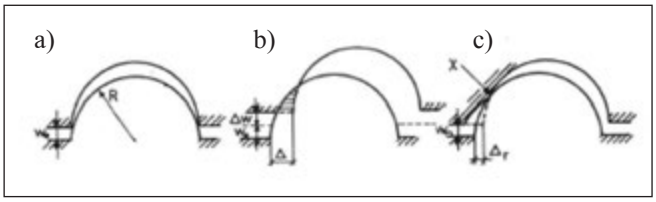

Fig. 2: *Three characteristic stages of crack faces a) before loading, b) peak stress, c) after unloading, Walraven (1980)*

relative displacements between crack faces measured in their tests (*Fig. 3, V* – actual shear force, V_{max} – shear force at failure). When a crack just occurs then the relative displacement between its faces is approximately orthogonal to the crack. The trend of the subsequent relative displacement recorded reveals that the instantaneous relative displacements had dominant rotational components and that the centre of rotation is located close to perpendicular to the radius drawn from the current tip of the crack to the point observed.

The crack kinematics and the crack widths reveal that aggregate interlock in the tensile zone through the web cannot be effective. In a test series Völgyi et al. (2016) showed that beams loaded in bending and shear failed practically at the same load when aggregate interlock could be effective or it was eliminated through plastic inlets along the failure shear crack. This reveals that the source of the "concrete contribution" is the concrete compression zone.

3.4 Size effect underlined with the theory of fracture energy

Already Kani (1967) found that increasing the depth of shear unreinforced beams leads to considerable reduction in the relative shear strength. Experiments showed that the (relative) shear strength of 3000 mm deep beams was merely one third of the (relative) shear strength of 600 mm deep beams without shear reinforcement. Important are the words "relative" and "without shear reinforcement". Relative means that the shear failure load is divided with the (increasing) depth of the web resulting in decreasing "shear strength". When the concrete contribution to shear strength originates from the compression zone then this is a constant value, independent from the depth of the beam, thus dividing this constant value with the increasing depth gives the size effect.

The application of fracture mechanics as explanation involves numerical modeling of the complex tensile stress vs. crack displacement relationship at the tip of the critical crack and also empirical relationships having little explanation of the structural behavior.

3.5 Strut and Tie Model

The Strut and Tie Models have as free parameters the inclination of the struts and the effective concrete crushing strength. In many cases very radical reductions were necessary in order to recalculate the test results. The researchers attribute this reduction to the spreading of the concrete stresses in the bottle shaped strut or to the effect of crossing shear cracks. Pujol et al. (2011) showed in tests that increasing the width of the "bottle" does not let decrease the failure load. All other results would have contradicted the fundamental law of plasticity theory. The crossing shear cracks reveal only that the assumed strut geometry is not correct: the compression in the strut acts like prestressing hence cracks cannot enter/cross it.

3.6 Stress field approaches

Stress field approaches should serve as simple and transparent design tools. In regions where no main reinforcement is required a well distributed minimum reinforcement shall be applied. As a matter of fact stress fields are smeared compression struts in the web concrete loaded in uniaxial compression. Important characteristic of the stress field is its inclination, Θ. The most important impact of the stress field approach is the increase of the number of stirrups taken into account, hence the displacement of a part of the concrete contribution to the shear reinforcement. As the inclination does not correspond to the inclination of the shear cracks thus it remains open how those stirrups which are not crossed by any shear crack are stressed up to their yield strength. In MC2010 (2013) the inclination Θ can be selected between certain limits (which were confirmed by experimental observations, thus this approach is not a theoretical but an empirical best-fit method). The inclination can be calculated in function of the longitudinal strain at the mid-depth of the effective shear depth. The minimum value of Θ can be taken from 25° for members with significant axial compression or prestress and 30° for reinforced concrete members (we refer to the starting comment of Kupfer (see Section 3.2) for the variable angle truss model approach (little under, few degrees): the difference increased up to 20°!)

3.7 Modified Compression Field Theory

This theory presented by Vecchio et al. (1986) is based on a questionable evaluation of a series of questionable tests. *Fig. 4* shows the test rig.

The ~ 800 * 800 mm big, 80 mm thick panels were reinforced with different rate of smooth (!) rebars (parallel to the

Fig. 3: *Propagation of critical crack and relative displacements between crack faces, Muttoni et al. (2010)*

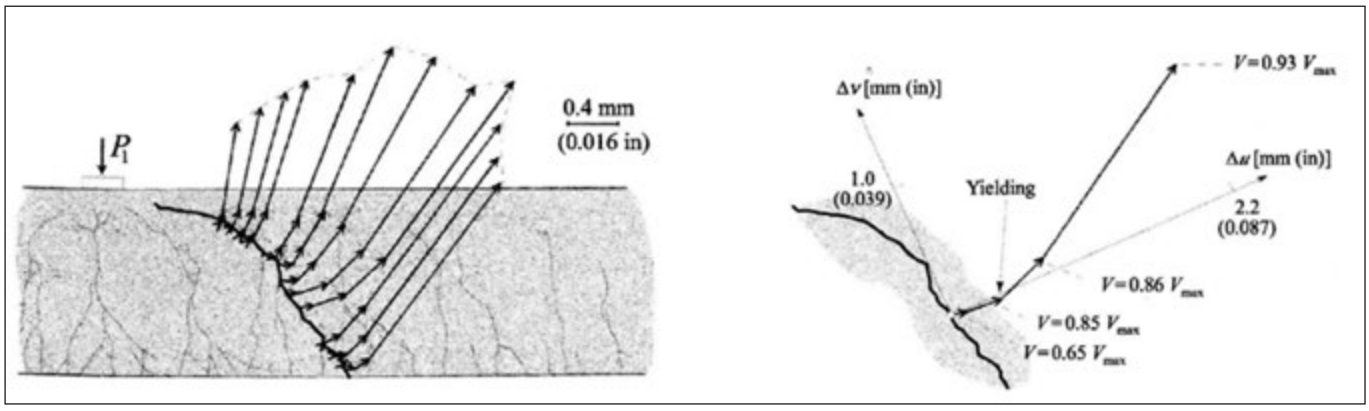

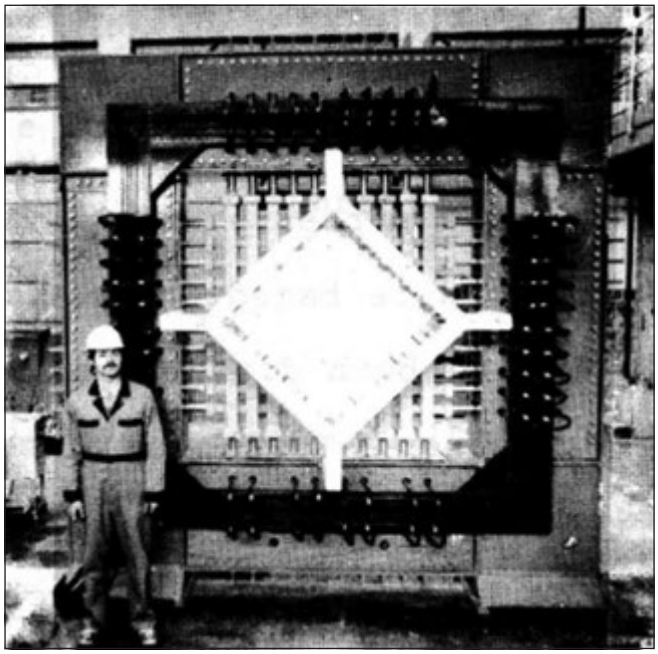

Fig. 4: The Toronto-Panel-Tester

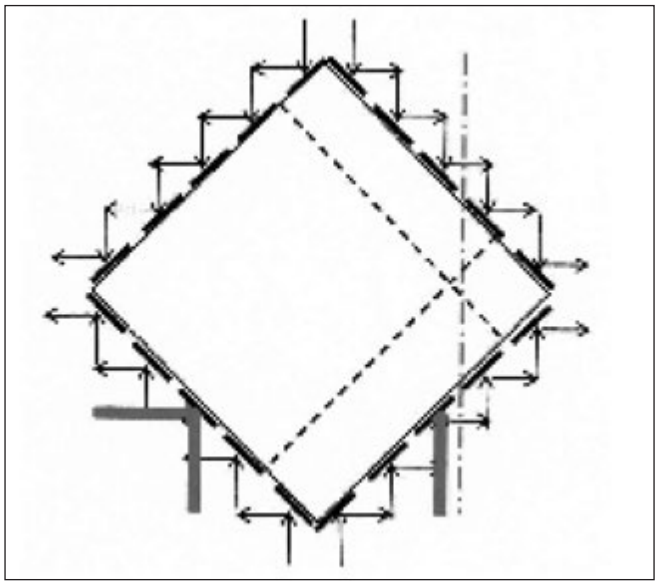

Fig. 5: The principle of the panels and the Tester

borders as shown in *Fig. 5* with the dashed lines). Along each border five stiff "shear keys" were concreted into the panels. To each shear key two double-acting hydraulic jacks were attached. All were simultaneously operated by a single pump. The jacks compose two systems by which different rates of normal and shear stresses can be applied to the panels. As the panel would uncontrolled "swim" in the "Tester" therefore three jacks were substituted by fix links, as shown by the gray arrows in *Fig. 5*.

All panels were declared as failed when the pressure in the hydraulic loading system could not be increased further. (This occurred when the weaker of both reinforcements yielded.) Although – as testified by the photos of the failed panels – not a single panel failed in concrete compression all failures were interpreted as concrete failure showing a softening in compression which was attributed to the mean value of the transverse (smooth) steel elongation. It can be easily recognized that a) the three rigid links with their unknown reaction forces fundamentally influenced the strains and deformations (this could be realized by the testing personal, too, as the lowest corner was teared off as the shear loading was directed in direction of the rigid links and the test must be stopped; the direction of shear load was changed thus all following tests run without problems; nevertheless the reaction forces were not published.), b) the shear keys which stiffened 94% of the border lines of the panels predetermined the possible crack positions and directions.

The principal compressive stresses taken as the basis, the formula

$$\frac{f_p}{f_c'} = \frac{1}{0.85 + 0.27\,\varepsilon_{dt}/\varepsilon_d}$$

with

f_p peak compressive stress in cracked concrete (measured)
f_p peak compressive stress in cracked concrete (theoretical)
f_c' concrete cylinder compressive strength
ε_{dt} principal tensile strain in diagonally cracked concrete
ε_d principal compressive strain in diagonally cracked concrete,

was derived directly from the average principal stresses (*Fig. 6*). The additional compressive forces developing due to the fixed links were not considered. It can be shown that the principal compressive stresses do not govern the failure of the panels they are by-products of the events only.

The panels reinforced in two directions (with $\mu_{longitudinal} = \mu_{transversal}$ or $\mu_{longitudinal} > \mu_{transversal}$) and loaded with different rates of the principal stresses can be considered as skew reinforced panels which fail when the weaker band of reinforcement begins to yield. *Fig. 7* shows the result of the evaluation: all failure loads, V_u, lie along the line $V_{u,\,pred} = V_u$ line or over it (due to dowel effect the yielding weaker reinforcement allows for an increase of the load until the stronger reinforcement also yields).

As at the application of the Modified Compression Field Theory at modelling of a web the boundary conditions to the tensile and compression zones, resp. are not considered/fulfilled, it is questionable whether this theory is capable of predicting the response of reinforced concrete elements subjected to in-plane shear and axial forces. The failure of the specimens was mostly presented as concrete shear, nevertheless, in each and every usable case the failure was initiated through yielding of the weaker band of reinforcement. The concrete has no shear strength, concrete fails in all cases due to principal tensile stresses exceeding the local tensile strength. No strain softening of the concrete could be perceived either, the tension stiffening effects perceived could not be general as smooth reinforcing bars were used. The analytical model developed is tedious but the layer representation, the assumed shear flow and shear strain distributions do not fit the basic characteristics of cracked reinforced- or prestressed concrete members.

3.8 Compressive Force Path-Model

Kotsovos (1986) analyzed the shear behavior of R.C. beams with web reinforcement and having shear span to depth ratio greater than 2.5 under two point loads. He compared the test results with the Finite Element Analysis results of the same beams and made - among others - the following significant conclusions:

I. The predicted behavior of the beams by FEA is incompatible with the actual shear behavior at critical section of R.C. beams with various arrangements of stirrups.
II. Shear behavior is associated with the development of tensile stresses within the compression zone and particu-

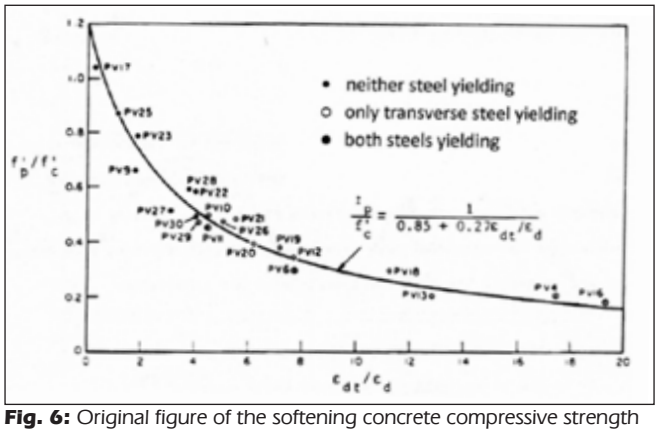

Fig. 6: *Original figure of the softening concrete compressive strength (Vecchio et al., 1982)*

larly in the region of compression zone between sections at load and sections twice the beam depth.

III. The stirrups resist the tensile stresses within the compression zone rather than transforming the beam into truss as widely considered.

Kotsovos's model is an important step into the direction of the "new 5th axiom".

4. THE "NEW 5TH AXIOM"

The "new 5th axiom" for structural concrete is: the dimensioning for bending and shear are strongly interrelated.

In the Shear Failure Theory of Walther (1962) the interdependence of failures in bending and shear through the concrete compression zone is clearly demonstrated. The failure criterion for the compression zone is derived using the failure criterion of Mohr. (Why was this theory during decades almost forgotten??)

As presented by Windisch (1988) the dimensioning for bending and shear shall not be carried out independently. The source of the concrete contribution for shear is the concrete compression zone above the critical shear crack. R.C. and P.C. members do not work like trusses or stress fields but like cracked continuums. The characteristic (critical) bending-shear cracks run along the compression trajectories. The mechanical behavior of concrete is characterized with a modified Mohr-Coulomb failure criterion. Along the bending-shear-cracks separation failure mode occurs which excludes the activation of forces from aggregate interlock there. The compression zone fails developing a sliding surface beginning at the tip of the shear crack. Accordingly the methods of soil mechanics can be applied (Völgyi et al. 2014). Along the sliding surface aggregate interlock is acting. In addition to the equilibrium in the bending-shear crack and the sliding surface – which form the failure cross-section – the requirements of compatibility and kinematics must and can be considered.

All known influencing factors and perceptions gathered in tests during the past can be understood/incorporated/taken into account, e.g.:

- The max. concrete compressive stress reduced through the shear stress acting simultaneously in the compression zone hence more reliable calculation of load bearing capacity for bending and shear
- Size effect in shear
- The effective slab width in T-beams
- The impact of the bond characteristics on the failure load
- The impact of the additional flexural tensile reinforcement on the concrete shear contribution
- The necessity of shifting of the flexural reinforcement

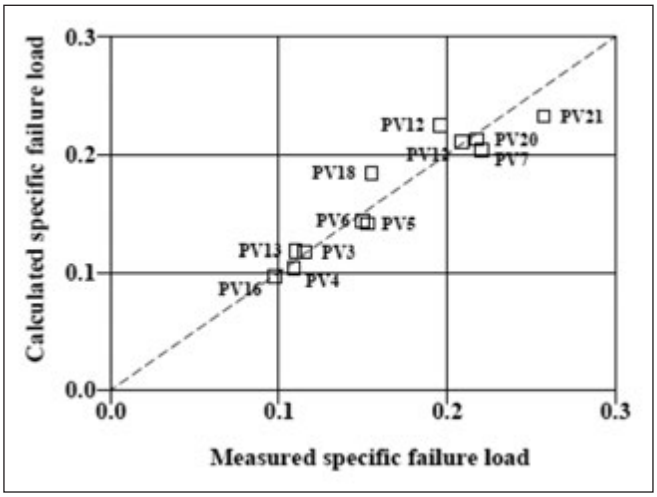

Fig. 7: *Comparison of measured vs. calculated failure loads of then Toronto-test panels (Windisch, 2000)*

- The scatter of the failure loads depending on the relative position of the failure section to the loads
- Direct/simple dimensioning for biaxial bending and shear.

5. CONCLUSIONS

The shortages of shear theories developed during the last century can be overcome if the dimensioning for bending and shear are carried out interrelated. In cross sections loaded in bending and shear the concrete compression zone yields both, the contribution in compression and shear. On this theoretically sound basis the influencing factors on bending and shear can be explained.

6. REFERENCES

Fenwick, R. C. and Paulay, T. (1968), "Mechanisms of Shear Resistance of Concrete Beams". *Journal of the Structural Division,* American Society of Civil Engineers, Vol. 94, No. ST10, pp. 2325−2350.

fib Model Code for Concrete Structures 2010, (2013) Ernst & Sohn, Oct. 2013, 434 p. ISBN: 978-3-433-03061-5

Kani, G. N. J. (1964), "The Riddle of Shear Failure and its Solution", *ACI Journal* Vol. 61, pp. 441-467.

Kotsovos, M. D. (1986), "Behaviour or RC beams with shear span to depth ratios greater han 2.5" *ACI J. Proceedings 83* (115) Nov-Dec 1986, pp. 1026-1034.

Kupfer, H. (1962), "Erweiterung der Mörsch'schen Fachwerkanalogie mit Hilfe des Prinzips vom Minimum der Formänderungsarbeit", nach einem *Vortrag auf dem Schub-Kolloquium*, Oktober 1962 in Stuttgart, 12. p.

Muttoni, R. V., Ruiz, M. F. (2011), „Influence of Capacity of Reinforced Members without Shear Reinforcement", *ACI Structural Journal,* Sept-Oct. 2010, pp. 516-525.

Pujol, S., Rautenberg, J. M., and Sozen, M.A., (2011) „Compressive Strength of Concrete in Nonprismatic Elements". *Concrete International 33* (9) pp. 42-49.

Scholz, G. (1960), „Festigkeit der Biegedruckzone. Theoretische Auswertung von Heft 120". *Heft 139, Deutscher Ausschuss für Stahlbeton.* Verlag Wilhelm Ernst & Sohn, 1960. p. 40.

Vecchio, F. J., and Collins, M. P. (1982), "The Response of Reinforced Concrete to In-Plane Shear and Normal Stresses," *University of Toronto, Department of Civil Engineering,* March 1982, 332 p.

Vecchio, F. J., and Collins, M. P. (1986), "The Modified Compression Field Theory for Reinforced Concrete Elements Subjected to Shear," *ACI JOURNAL,* Proceedings V. 83, No. 2, Mar.-Apr. 1986, pp. 219-231.

Völgyi, I. and Windisch A. (2014), "Resistance of reinforced concrete members with hollow circular cross-section under combined bending and shear – Part II: New calculation model", *Structural Concrete 15* (2014), No. 1, pp. 21-29.

Völgyi, I. and Windisch, A., (2016): "Contribution of aggregate interlock to the shear resistance of RC beams", in press

Walraven, J. C. (1980), "Aggregate interlock: A theoretical and experimental analysis", 1980, *Delft University Press*

Walther, R. (1962), "Über die Berechnung der Schubtragfähigkeit von Stahl- und Spannbetonbalken – Schubbruchtheorie", *Beton- und Stahlbetonbau,* 11/1962, pp. 261-271.

Windisch, A. (1987), Discussion: M. D. Kotsovos „Behavior of Beams with Shear-to-Span Ratios Greater than 2.5“ *ACI Structural Journal, Vol. 84,* No. 5, Sep-Oct 1987, p. 450

Windisch, A. (1988), Discussion 85-S8: M. D. Kotsovos „Compressive Force Path Concept: Basis for Reinforced Concrete Ultimate Limit State Design“, *ACI Structural Journal, Vol. 85,* No. 5, Nov-Dec 1988

Windisch, A. (1988), „Das Modell der charakteristischen Bruchquerschnitte. Ein Beitrag zur Bemessung der Sonderbereiche von Stahlbetontragwerken“, *Beton- und Stahlbetonbau, Vol. 83,* Heft 9, pp. 251-255, Heft. 10, pp. 271-274.

Windisch, A. (1989), Discussion 85-S27: F. J. Vecchio, M. P. Collins “Predicting the Response of Reinforced Concrete Beams Subjected to Shear Using Modified Compression Field Theory“ *ACI Structural Journal, Vol. 86,* No. 2, Mar.-Apr. 1989

Windisch A (1991), „Tensile Strength of Concrete: Prodigal Son or Primary Source?”, *IABSE Colloquium, “Structural Concrete, Stuttgart,* 1991, pp. 773-777.

Windisch A. (1992), Discussion 88-S29: Z. Bažant, M. T.Kazemi: “Size Effect on Diagonal Shear-Failure of Beams without Stirrups“, *ACI Structural Journal, Vol. 89,* No. 2, March-Apr. 1992

Windisch A. (2000), “On the design of two-way reinforcements in R/C”, *Studi e ricerche, Vol. 21,* 2000, Scuola di specializzazione in Costruzioni in C. A. Fratelli Pesenti, Politecnico di Milano, pp. 283-302

Windisch A. (2002), “Towards a Consistent Design Model for Punching Shear Capacity”, I*nternational Workshop on Punching Shear Capacity on RC Slabs.* Stockholm, 2002, pp. 293-301.

Andor Windisch PhD, Prof. h.c. retired as Technical Director of DYWIDAG-Systems International in Munich, Germany. He made his MSc and PhD at Technical University of Budapest, Hungary, where he served 18 years and is now Honorary Professor. Since 1970 he is member of different commissions of FIP, CEB and fib. He is author of more than 120 technical papers.

A COMPARATIVE STUDY ON ULTRASONIC PULSE VELOCITY FOR NORMALLY VIBRATED AND SELF-COMPACTING CONCRETES


Abdulkader El Mir - Salem G. Nehme

There is a growing interest in non-destructive testing of cement based materials in the construction industry, especially when it comes to high performance concretes. In this paper, the compressive strength of 2 concrete types, normally vibrated concrete (NVC) and self-compacting concrete (SCC), is evaluated by ultrasonic pulse velocity (UPV) non-destructive method. Therefore, a total of 30 mixtures arranged between NVC and SCC, were designed and placed. The influence of several-factors such as concrete type, water-binder ratio, total powder content, supplementary cementitious materials and total porosity, on the relation between compressive strength and UPV was examined. According to the results, total powder content highly affected the response of NVC whereas no significant variations in SCC. Nevertheless, total porosity measurement was performed and compared with UPV results.

Keywords: normally vibrated concrete, self-compacting concrete, compressive strength, ultrasonic pulse velocity, supplementary cementitious materials, porosity

1. INTRODUCTION

Self-compacting concrete (SCC) provides better results in terms of homogeneity and performance since it can be placed and compacted under its own weight without segregation (Khayat, 1999). Not only productivity is enhanced but also a more sustainable material is reached (Skarendahl, 2000). The cost of SCC production associated with high amount of Portland cement and chemical admixture remarkably increased, hence the application of mineral admixtures such as fly ash, blast furnace slag, and others reduced the production cost of SCCs (Sahmaran, 2006; Bouzoubaa, 2001). Variation in the mix design or adopted placing method can lead to changes of the porous microstructure of concrete and thereby also permeability properties. SCC is characterized by the powder content which is higher than in normally vibrated concrete (NVC). Previous studies which provide analysis on SCC porous structure, revealed that SCC with a high amount of filler material and exceptional rheological properties, gives the concrete a denser microstructure than NVC with the same water-binder ratio (Trägardh,1999; Zhu, 2005).

Quality control of concrete structures, by means of non-destructive test methods, is highly required in the field of concrete technology. Based on the calculation of transmission speed of ultrasonic pulses in concrete, diagnostic assessment of the properties of concrete structures is possible to be fulfilled (ASTM C597-97). Several earlier studies on various concretes with the application of ultrasonic pulse velocity (UPV) proved the efficiency of such non-destructive test (Abo-Qudais, 2005; Zhu, 2011; Hamid, 2010). However, this instrument highly depends on many parameters affecting its response such as the concrete age, type of cement, water-binder ratio, applied aggregates, curing conditions, measured distance length and temperature of the evaluated element (Ravindrarajah, 1997; Neville, 1981). For instance, Rommel and Malhotra have evaluated the UPVs of concrete for different water-binder ratios and aggregate content. Thereby they were able to introduce the concrete specimen and the range of ultrasonic velocities in terms of variables affecting concrete quality (Rommel, 2008; Malhotra, 1976).

The purpose of this paper is to investigate and compare the effect of using different powder content, water-binder ratios combining binary and ternary cementitious materials on the response of ultrasonic transmission and compressive strength of NVC and SCC mixtures.

2. MATERIALS

"Danube" quartz gravel and sand with maximum aggregate size of 16 mm lies in the grading curve of EN standards (MSZ 4798-1:2004). Sand (0-4 mm), small gravel (4-8 mm) and medium gravel (8-16 mm) are divided in the following percentages of particle size fractions 45%, 20% and 35% respectively. *Fig. 1* shows the particle size distribution of aggregates in terms of standard limits. Slag cement, CEM III/A 32.5 R-MSR, is the binary cementitious material. Metakaolin and silica fume slurry are the ternary cementitious materials. Limestone powder is the filling material for SCC. "Sika Viscocrete 5 Neu" presents the applied high range reducing admixture (HRWRA) for achieving adequate rheological properties (EN 934-2:2009).

3. EXPERIMENTAL METHOD AND MIX PLAN

UPV and compressive strength determining tests of the cube specimen (150× 150 × 150 mm) at the age of 28 and 56 days

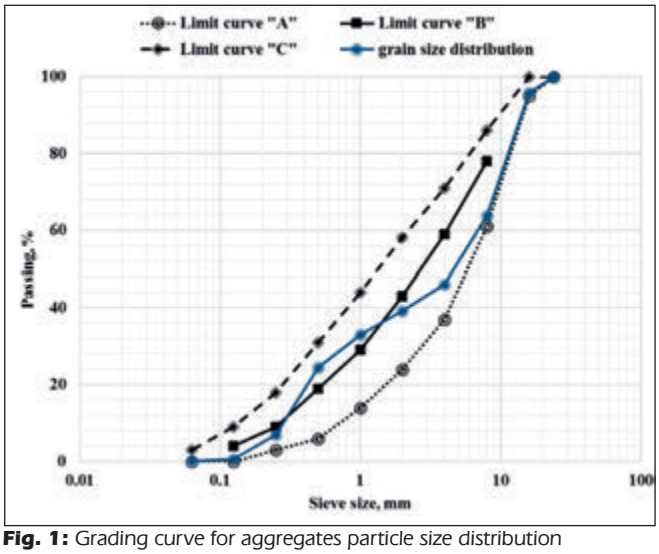

Fig. 1: Grading curve for aggregates particle size distribution

were the hardened test according to EN standards (EN 12390-3:2009, 12504-4:2004).

Several SCC and NVC mixtures were designed and tested with various laboratory methods. The following parameters were kept unchanged in each concrete mixture:

- The particle size distribution, MSA = 16 mm,
- The type of cement, CEM III 32.5/A R-MSR,
- The water content,180 kg/m^3,
- The mass of metakaolin and silica fume slurry materials, 40 kg/m^3

The varied parameters:

- Concrete type, SCC or NVC,
- The water-binder ratio, w/b = 0.562- 0.5- 0.45-0.41,
- The total powder content, 320-360-400-520-580-620 kg/m^3,
- Supplementary cementitious materials, none, metakaolin or silica fume.

A total of 30 concrete mixtures were produced (27 SCC and 3 NVC). SCC mixtures were divided into 3 series: Reference series (R), Metakaolin series (M) and silica fume series (S). Each of these series is categorized by the type of implemented supplementary cementitious material. So that R, M and S refer as the followings: R (reference mixture without supplementary cementitious material), M (metakaolin as the applied supplementary cementitious material) and S (silica fume as the applied supplementary cementitious material). Regarding NVC mixtures which are symbolized by (N), only 3 mixtures were produced with the same cement content of SCC mixtures. For more information, *Table 1* summarizes the mixtures composition.

Fig. 2: Scheme of the ultrasonic pulse velocity measurement in concrete cube specimens

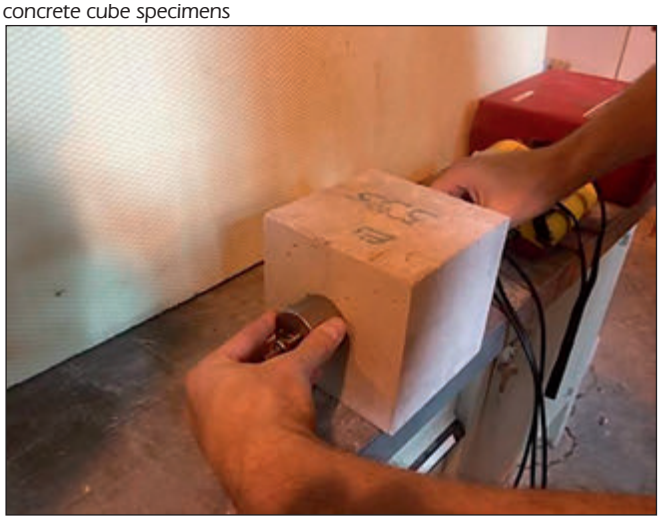

Ultrasonic non-destructive test was the first conducted on the specimens at mentioned ages by means of direct transmission method, using the device illustrated in *Fig.2*. In all the tested cubes, refractory grease was applied on the concrete surface to connect transducers. Demolded concrete surfaces were the tested surfaces. According to Fig. 2, transducers were placed centrically on the tested surface in which 3 ultrasonic pulse velocities reading were recorded, by this means, average velocity values for each specimen can be calculated. Following the non-destructive test on concrete specimens, a compressive test was also performed on them with a rate of 11.22 kN/s.

Total porosity in hardened concrete was calculated. It was determined based on the ratio of bulk (containing open and closed pores) and particle (containing no pores) densities of concrete specimens. Bulk density was measured referring to American standards (ASTM C642, 1992). Shredded specimens were crushed and grounded into fine powder in order to evaluate true densities using pycnometers (EN ISO 17892-3, 2014). Hence total porosity was obtained from the following equation:

$$P_T = 1 - \frac{\rho_b}{\rho_p} \quad (1)$$

Where ρ_b *and* ρ_t are the bulk and particle densities (g/cm^3) respectively.

4. RESULTS AND DISCUSSION

All average UPV, compressive strength and total porosity values are presented in *Table 1*. UPV results showed a range between 4080 to 4655 m/s. SCC mixture M3 with lowest water-binder ratio of 0.41 had the highest UPV value while the lowest UPV value corresponded to NVC mixture R1 at 0.562 water-binder ratio. According to Whitehurst, concrete UPV classification is arranged as very poor, poor, doubtful, good and excellent for UPV values of 2000, 2000-3000,3000-3500, 3500-4500, 4500 m/s and above, respectively (Whitehurst, 1951). All produced concretes were classified either under good or excellent categories. In this section, diagrams are introduced for the test results and are discussed under the following sub-heads.

4.1 Influence of water-binder ratio on UPV

The experimental evolution of UPV in terms of water-binder ratio at 28 days has been shown in *Figs. 3,4* and *5* for 3 different total powder content (620-580-520 kg/m^3), corresponding to SCC mixtures and compared with NVC mixtures N. Different water-binder ratios were obtained by varying the amount of cement or supplementary cementitious materials and keeping a constant amount of water. The trend of variation in all concrete mixtures shows the increase of UPV with the decrease of water-binder ratio. For the same water-binder ratio and different total powder content, UPV values can vary more than 250 m/s. The highest level of UPV was achieved for the SCC (M3) prepared by water-binder ratio of 0.41, enhanced by metakaolin, and combines a total powder content of 620 kg/m^3. In contrast, the lowest UPV was obtained for the NVC (N1) produced with water-binder ratio of 0.562. The

Table. 1: Mixtures composition and hardened properties for SCC (R, M and S) and NVC mixtures (N)

	kg/m³						28 days		56 days		400 days
Mix ID	**Cement**	**Metakaolin**	**Silica fume**	**Filler**	**Aggregates**	**HRWRA**	**V (m/s)**	**f_{cm} (Mpa)**	**V (m/s)**	**f_{cm} (Mpa)**	**P_T (V%)**
R1	320	-	-	300	1520	3.04	4390	58	4410	65	12.78
R2	360	-	-	260	1524	3.06	4420	63	4495	70	11.11
R3	400	-	-	220	1529	3.56	4530	70	4525	76	9.06
R4	320	-	-	260	1560	1.92	4360	47	4380	52	13.03
R5	360	-	-	220	1565	2.02	4440	53	4435	59	12.07
R6	400	-	-	180	1569	2.72	4480	58	4510	65	11.20
R7	320	-	-	200	1618	1.74	4320	41	4390	46	14.84
R8	360	-	-	160	1624	1.55	4380	48	4410	57	13.04
R9	400	-	-	120	1629	1.76	4415	52	4445	60	10.85
M1	320	40	-	260	1518	3.36	4430	61	4485	69	10.98
M2	360	40	-	220	1524	3.96	4485	69	4510	75	11.54
M3	400	40	-	180	1524	4.40	4620	77	4655	79	6.34
M4	320	40	-	220	1557	2.72	4370	56	4390	61	12.50
M5	360	40	-	180	1562	2.92	4400	62	4440	70	11.89
M6	400	40	-	140	1564	4.00	4550	70	4580	74	8.98
M7	320	40	-	160	1616	2.27	4375	51	4445	58	13.12
M8	360	40	-	120	1620	2.34	4455	64	4475	71	10.23
M9	400	40	-	80	1625	2.84	4510	65	4510	71	8.63
S1	320	0	40	260	1506	5.44	4395	59	4453	64	7.59
S2	360	0	40	220	1514	4.86	4447	65	4475	70	5.65
S3	400	0	40	180	1520	5.20	4548	74	4570	77	5.15
S4	320	0	40	220	1551	2.88	4385	50	4410	60	9.26
S5	360	0	40	180	1556	3.17	4415	59	4425	69	8.86
S6	400	0	40	140	1560	3.76	4510	70	4585	75	6.25
S7	320	0	40	160	1611	2.31	4385	49	4405	58	12.48
S8	360	0	40	120	1616	2.34	4400	59	4465	65	10.12
S9	400	0	40	80	1620	2.72	4425	62	4485	69	8.16
N1	320	0	0	-	1851	0.78	4080	43	4160	50	15.89
N2	360	0	0	-	1817	0.70	4260	46	4310	55	13.84
N3	400	0	0	-	1782	0.96	4316	59	4410	62	12.21

enhancement of UPV at a lower water-binder ratio was due to the reduced porosity of concrete, the filling effect of the limestone powder and the enhancement of pozzolanic activity by metakaolin in SCC mixtures. Therefore, the relation between UPV and water-binder ratio depends on the type and amount of materials applied in concrete matrix and how the water-binder ratio is varied in UPV measurement.

Referring to *Table 1*, SCC series which contain metakaolin or silica fume as a supplementary cementitious material (M and S), showed almost the same mean UPV values reference series (R). Therefore, UPV response does not depend on the presence of such active mineral additives.

4.2 Influence of total powder content on UPV

The variation of UPV and compressive strength over the total powder content of concrete at the age of 28 and 56 days is illustrated in *Figs. 6* and *7*. Note that UPV and compressive strength properties provide the mean values of SCC mixtures which fall into the same total powder content category: 620, 580, or 520 kg/m³.

The UPV of concrete was affected by the total powder content. The lowest UPV and compressive strength values are found for NVC N1 made with lowest total powder content of 320 kg/m³ where the highest values correspond to SCC mixtures made with highest total powder content of 620 kg/m³. The importance of the total powder content is highlighted in *Figs. 6* and *7* since this parameter differentiates between NVC and SCC. The latter requires special rheological properties in order to provide the self-compact ability, thereby higher powder content is required.

It can be seen in *Figs. 6* and *7*, NVC mixtures at 400 kg/m³ of total powder content, showed a significant increase 300 m/s of the UPV with respect to 320 kg/m³ total powder content. However, it can be noticed from SCC total powder content, a slight variation of 66 m/s between UPV values corresponding to 520, 580 and 620 kg/m³.This confirms that UPV values are affected by total powder content in case of NVC. Yet SCC mixtures showed insignificant differences between UPV values. Therefore, this behaviour would be explained by the dispersion effect caused by concrete heterogeneity, which is highly related to the total powder content. In comparison with NVC, SCC is characterized by the high paste volume, there-

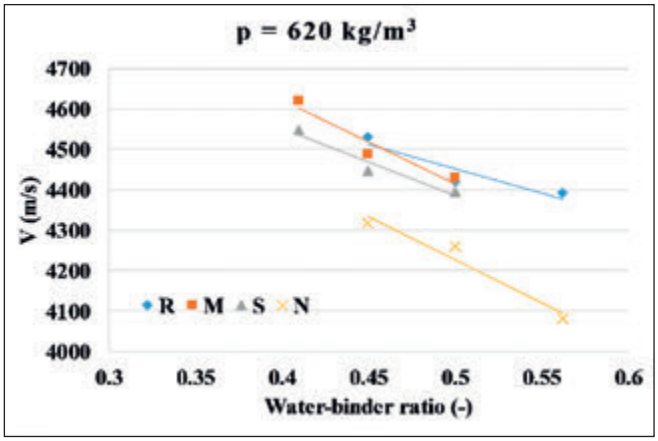

Fig. 3: Water-binder ratio versus the UPV for SCC series (R, M and S) corresponding to total powder content (p) of 620 kg/m3 and NVC mixtures (N) at 28 days

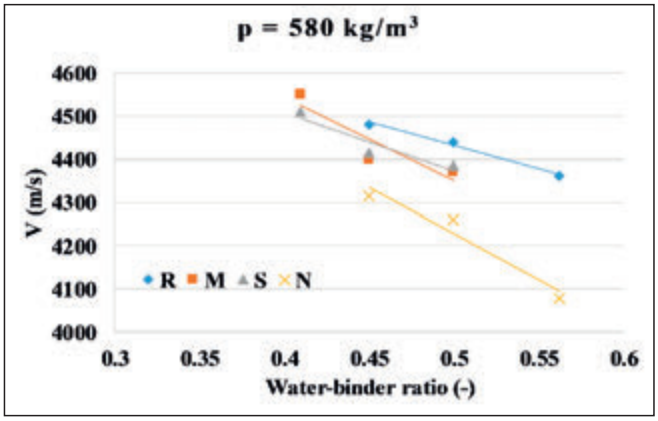

Fig. 4: Water-binder ratio versus the UPV for SCC series (R, M and S) corresponding to total powder content (p) of 580 kg/m3 and NVC mixtures (N) at 28 days

by the transmission wave is able to propagate more easily in SCC mixtures since the microstructure is refined with less aggregates and pores. However, in case of NVC, that has a more porous microstructure and lower total powder content; it may delay the propagation of the UPV, thus reducing the velocity through the concrete.

4.3 Influence of porosity measurements on UPV

Absolute values of total porosity at 400 days are provided in *Table 1*. The total porosity of both NVC and SCC are correlated in terms of their UPV values (*Fig. 7*). The total porosity varied in the range of 5.15-15.89%. In general, total porosity results are considered to classify the quality of concrete as good. According to (Hearn, 2006), high quality concrete has a total porosity of 7% whereas average quality concrete owns 15%. The lowest level of porosity was reached in case of SCC S3 incorporating silica fume and with lowest water-binder ratio of 0.41. Aggregate packing is improved and by the filling effect of the powder content, hence higher range of fines is provided for less porous network. Moreover, one can observe the decreasing trend of total porosity with the increase of UPV. Accordingly, it can be concluded that the porous network highly affects the response of UPV in concrete.

4.4 Relationship between compressive strength and UPV

Earlier studies demonstrated that there is no unique relationship between compressive strength and UPV of concrete

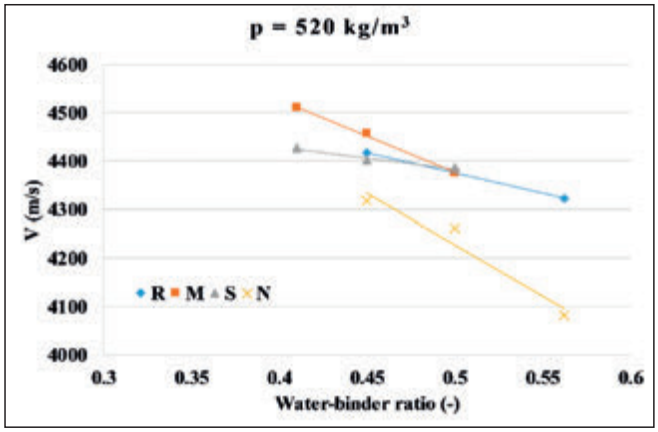

Fig. 5: Water-binder ratio versus the UPV for SCC series (R, M and S) corresponding to total powder content (p) of 520 kg/m3 and NVC mixtures (N) at 28 days.

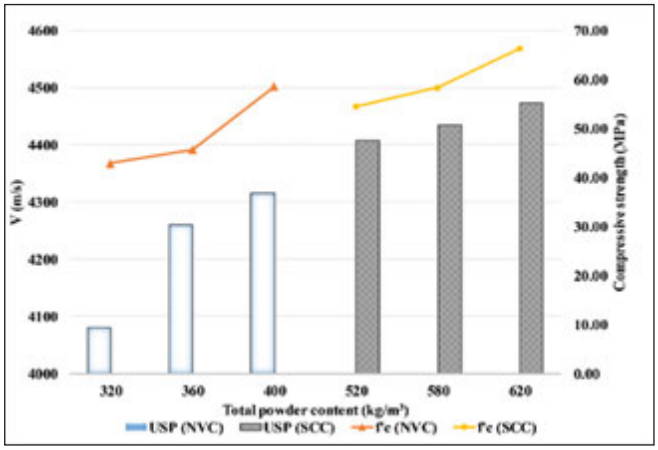

Fig. 6: Total powder content versus the UPV and compressive strength for SCC series (R, M and S) to total powder and NVC mixtures at 28 days

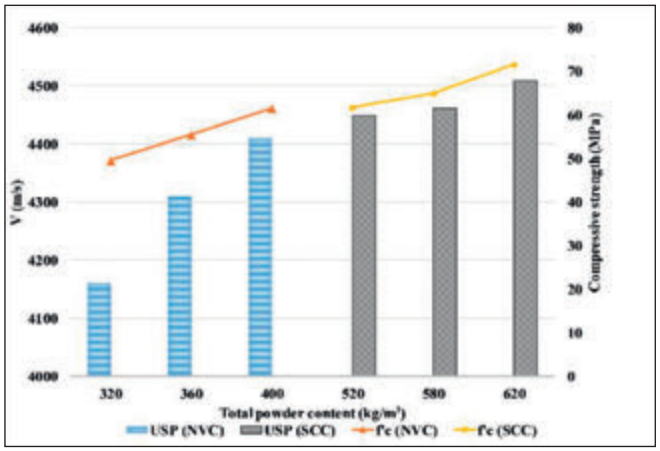

Fig. 7: Total powder content versus the UPV and compressive strength for SCC series (R, M and S) to total powder and NVC mixtures at 56 days

(Neville, 2005). Yet, the UPV of concrete is highly influenced by cement paste state. The latter is directly affected by the water-binder ratio.

$$f'_c = 0.0745e^{0.0015x} \quad (2)$$

Based on regressing an exponential curve among the available data, *Fig.8* shows the relationship between compressive strength and UPV of all tested concretes, the regressed curve and the EN 13791 recommendation (EN 13791:2007). According to the experimental results, exponential relationship between compressive strength and UPV is plotted and com-

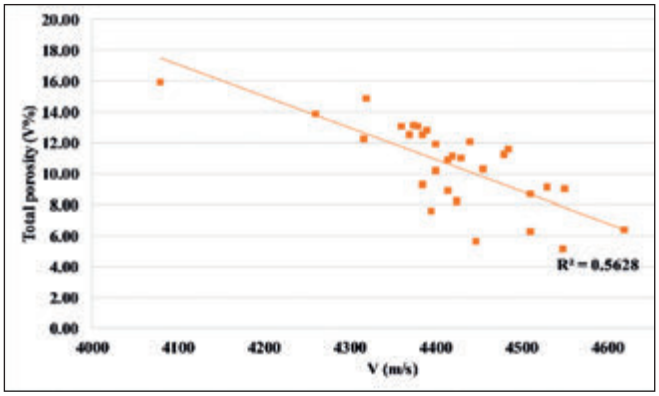

Fig. 8: *Total porosity versus the UPV for different types of all concrete mixtures at 28 days*

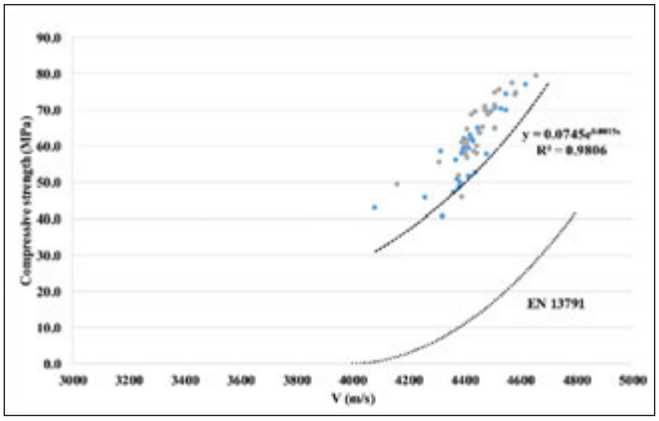

Fig. 9: *Relationship between compressive strength and UPV for all tested concretes in terms of EN 13791 recommendations*

pared with EN 13791 standards. One can observe how highly EN 13791 underestimates the actual compressive strength. Furthermore, in order to assess the compressive strength of produced concrete, authors suggested the following equations which is located at the lowest boundaries of the plotted data. Hence a more reliable estimate would be fulfilled.

5. CONCLUSIONS

Ultrasonic pulse velocity is a valuable non-destructive technique in assessing cement based materials. Many factors could affect the response of such measurement; hence the conclusions derived from the above experimental study are the followings:

- Ultrasonic pulse velocity is inversely proportional by the water-binder ratio.
- The total porosity of concrete decreased with lower water-binder ratio and higher total powder content.
- The increase of compressive strength, ultrasonic pulse velocity is directly affected by the decrease of total porosity.
- The excellent hardened properties were obtained in case of water-binder ratio of 0.41.
- The total powder content highly affects the response of ultrasonic pulse velocity in NVC, whereas insignificant influence is observed in case of SCC mixtures.
- EN 13791 recommendations underestimate the compressive strength.

6. ACKNOWLEDGEMENTS

The authors appreciate the assistance of Szijártó Anna, Péter Molnár, Vági István, Viktor Hlavička, András Jakab, András Eipl and Zsombor Pintye in fulfilling the laboratory tests.

7. REFERENCES

Abo-Qudais, Saad A. (2005), "Effect of concrete mixing parameters on propagation of ultrasonic waves", *Construction and Building Materials*, 19 (4), pp. 257–263.

ASTM C597-97 (1997), "Standard test method for pulse velocity through concrete.", *American Society for Testing and Materials,* 4 p.

ASTM C642-97 (1997), "Standard Test Method for Density, Absorption, and Voids in Hardened Concrete" *American Society for Testing and Materials,* 3 p.

Bouzoubaa N, Lachemi M. (2001), "Self-compacting concrete incorporating high volumes of class F fly ash – Preliminary results", *Cement and Concrete Research*, 31 (3), pp. 413–420.

BS EN 934-2:2009+A1:2012, „ Admixtures for concrete, mortar and grout, Part 2: Concrete admixtures — Definitions, requirements, conformity, marking and labelling", *British Standard Institution*, 28 p.

BS EN 12390-3:2009, „Testing hardened concrete, Part 3: Compressive strength of test specimens", *British Standard Institution*, 22 p.

BS EN 12504-4:2004, „Testing concrete, Part 4: Determination of ultrasonic pulse velocity", *British Standard Institution*, 18 p.

BS EN 13791:2007, „Assessment of in-situ compressive strength in structures and precast concrete components", *British Standard Institution*, 32 p.

Hamid R., Yusof, K.M., Zain, M.F.M. (2010), "A combined ultrasound method applied to high performance concrete with silica fume", *Construction and Building Materials*, 24 (1), pp. 94–98.

Hearn, N., Hooton, R.D., Mills, R.H. editors (1994) "Pore structure and permeability. Significance of tests and properties of concrete and concrete-making materials", *American Society for Testing and Materials,* ASTM STP 169C*,* Philadelphia, pp. 240-262.

ISO/DIS 17892-3:2014(E) (2014), "Geotechnical investigation and testing - Laboratory testing of soil, Part 3: Determination of particle size density", *British Standard Institution*, 20 p.

Khayat, K.H. (1999)," Workability, Testing, and Performance of Self-Consolidating", *ACI Materials Journal*, V.96, No.3, May-June, pp. 346–354.

Lamond, J. F., Pielert, J. H. editors (2006), "Significance of Tests and Properties of Concrete and Concrete-Making Materials", *American Society for Testing and Materials,* ASTM STP 169D*,* Bridgeport, NJ, 661 p.

Malhotra, V. M. editor (1976), "Testing hardened concrete: non-destructive methods", *ACI Monograph,* No. 9, Detroit, USA

MSZ 4798:2016, "Concrete. Specification, performance, production, conformity, and rules of application of EN 206 in Hungary", *Hungarian Standard Institution*, 172 p. (in Hungarian)

Neville, A.M. (1981), "Properties of concrete", 3rd edition, *Pitman Publishing Ltd, London*

Neville, A. M. (2005), "Properties of concrete", 4th edition, *Pearson Education Ltd, Singapore*

Ravindrarajah R.S. (1992), "Strength evaluation of high-strength concrete by ultrasonic pulse velocity method", *NDT & E International*, 29 (1), January-February, pp. 6-9.

Sahmaran, M., Christianto, H.A., Yaman, I.Ö. (2006): "The effect of chemical admixtures and mineral additives on the properties of self-compacting mortars", *Cement & Concrete Composites*, 28 (5), pp. 432–440.

Skarendahl, A., Petersson, O. (2000)," Self-compacting concrete State-of-the art report of RILEM technical committee 174-SCC, *RILEM Publications S.A.R.L.*, France. Report RILEM TC 174 SCC, pp. 91-92.

Solís-Carcano, R., Moreno, E. I. (2008), "Evaluation of concrete made with crushed limestone aggregate based on ultrasonic pulse velocity", *Construction and Building Materials*, 22 (6), pp. 1225–1231.

Trägardh, J. (1999), "Microstructural features and related properties of self-compacting concrete" In: Skarendhal, A., Petersson, Ö. editors (1999) "Proceedings of 1st international RILEM symposium on self-compacting concrete", Sweden, Stockholm, pp. 175–186.

Whitehurst, E. A. (1951), "Soniscope tests concrete structures", *Journal of American Concrete Institute*, Vol. 47, pp. 443–444.

Zhu, J., Kee, S., Han, D., Tsai, Y. (2011), "Effects of air voids on ultrasonic wave propagation in early age cement pastes", *Cement and Concrete Research*, 41 (8), pp. 872–881.

Zhu, W., Bartos, P. J. M. (2005), "Microstructure and properties of interfacial transition zone in SCC". In: Yu, Z., Shi, C., Khayat, K.H., Xie, Y. editors (2005), "Proceedings of 1st international symposium on design, performance and use of selfconsolidating concrete", China, Changsha, pp. 319–327.

Abdulkader El Mir (1990) civil engineer (MSc), PhD candidate at the Department of Construction Materials and Technologies, Budapest University of Technology and Economics. *Main fields of interest:* non-destructive testing, High performance concretes, Supplementary cementitious materials.

Salem G. Nehme (1963) civil engineer (MSc), PhD, associate professor at the Department of Construction Materials and Technologies, Budapest University of Technology and Economics. *Main fields of interest:* concrete technology, mass concrete, self-compacting concrete, fibre reinforced concrete, quality control of building materials, non-destructive testing, reinforced concrete structures, recycling of building materials.

EXPERIMENTAL STUDY ON THE BEHAVIOUR OF ANCHORS IN LIGHTWEIGTH AGGREGATE CONCRETE



Viktor Hlavička - Éva Lublóy – László Jancsó

Our research mainly focuses on the behaviour of post-installed anchors in lightweight concrete mixtures. In our tests three types of lightweight-aggregate (Liapor 8F, Liapor 5N, crushed brick) were used in the lightweight concrete together with three different anchoring systems (headed studs, undercut anchor, torque-controlled expansion anchors). Load bearing capacity results were evaluated and compared to the values given by the producers for normal concretes.

Keywords: lightweight aggregate concrete, fastening systems, pull-out test, splitting failure, concrete cone failure

1. INTRODUCTION

1.1 Overview of tensioned anchors in concrete

1.1.1 Fastening systems

Nowadays in the industrial applications mainly two types of anchors are used in fastenings: cast-in-place and post-installed anchors.

There are also several types of anchors available with different way of load-transfer. The commercially available fastenings can transfer the load to the host material via the following mechanisms: mechanical interlock, friction or bond *(Fig. 1)*. In case of cast-in-place anchors the load is transferred by mechanical interlock. Post-installed anchors can transfer the load by all the three types of mechanism. Mechanical interlock is the load-transfer mechanism is case of undercut anchors. In case of expansion anchors the load is transferred by friction: an expansion sleeve is expanded by an exact displacement or torque applied on the anchor head during the installation process. The chemical fastenings are anchored by bond. In addition, bonded anchors can be divided into two subgroups: capsule or injection systems. The bond material can be either organic, inorganic or a mixture of them. The loads are transferred from the steel (normally a threaded rod, rebar) into the bonding material and are anchored by bond between the bonding material and the sides of the drilled holes (*Eligehausen, Hofacker, Lettow, 2001; Eligehausen, Mallée, Silva, 2006; Fuchs, 2001)*.

1.1.2 The load bearing capacity of anchors

Load bearing of fastenings can be determined by taking the minimum of ultimate loads corresponding to different failure modes. In case of tensioned anchors steel failure, concrete cone failure, pull-out failure and splitting can occur *(Fig 2)*.

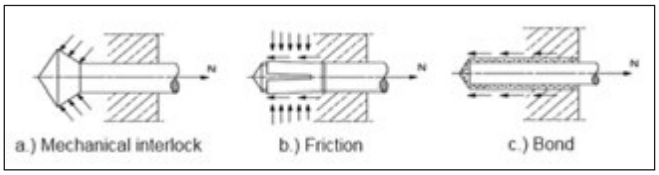

Fig. 1: Fastening methods in concrete (Fuchs, 2001)

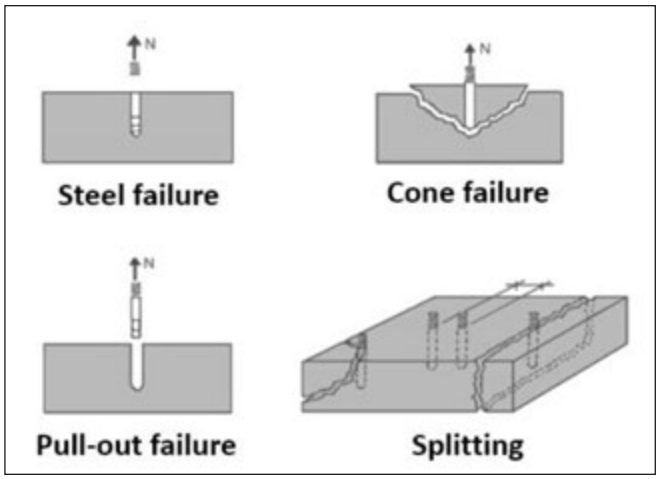

Fig. 2: Failure modes (Eligehausen, Hofacker, Lettow 2001)

Steel failure depends on the tensile strength of the steel rod. Steel capacity can be calculated from the ultimate steel strength and the cross-sectional area *(Eligehausen, Hofacker, Lettow 2001; fib MC 2010)*.

Properties of concrete cone failure mostly depend on the embedment depth (h_{ef}) and the concrete strength ($f_{cc,200}$). Cone failure is the optimal failure type, because concrete strength is completely utilized. Ultimate tensile force corresponding to full cone failure can be calculated as:

$$N_{u,c}^{0} = k * \sqrt{f_{cc,200}} * h_{ef}^{1,5} \quad (1)$$

where coefficient k shows the anchor type (in non-cracked concrete in case of expansion anchors: k = 13.5, in case of

headed stud: k = 15.5) *(Eligehausen, Mallée, Silva, 2006)*.

Pull-out failure has to be discussed separately for bonded and expansion anchors. Pull-out failure of mortar bonded anchors means bond failure between mortar and concrete, while pull-out failure excluding mortar means bond failure between the steel fastening and the bonding material. The bond strength depends on the certain product, but its value is included in the corresponding approvals.

Splitting failure is caused by the critical member thickness and spacing distances. In case of a single anchor in non-reinforced concrete this failure mode depends on the member thickness (h) and the embedment depth (h_{ef}). The load bearing capacity can be calculated as *(Eligehausen, Mallée, Silva, 2006)*:

$$N_{u,sp} = \Psi_{h,sp} * N^0_{u,c} \quad (2)$$

where:

$$\Psi_{h,sp} = (\frac{h}{2*h_{ef}})^{2/3} \leq 1.0 \quad (3)$$

It means that if $h \geq 2h_{ef}$ then splitting does not occur.

1.2 Lightweight aggregate concrete

Lightweight concrete is the concrete type with density less than 2000 kg/m^3. The smaller density can be achieved by using lightweight aggregates, or by increasing the porosity.

The load-bearing mechanism is different in case of the lightweight-aggregates concrete. In normal concretes the quartz aggregates have the higher strength, therefore the aggregates bear the major part of the load (*Fig. 3a*). In lightweight-aggregate concrete the aggregate has lower strengths, so in this case the cement bears the major part of the load (*Fig. 3b*) *(Romić, Lazić, 1985)*.

In case of lightweight-aggregate concrete the different load-bearing mechanism can determine the tensile resistance of the anchors. The bond strength is influenced not only by the compressive strength, but also by the structure of concrete *(Nemes, 2007)*.

2. MATERIALS

2.1 Tested anchors

In our experimental program one type of undercut anchor, one type torque-controlled expansion anchor and one type of headed stud system were tested (*Fig. 4*). All post-installed anchors were installed according to the MPII (Manufacturer`s Printed Installation Instructions). The embedment depth was

Fig. 3: Load bearing mechanism in normal concrete (a.) and in light-weight aggregate concrete (Romić, Lazić, 1985)

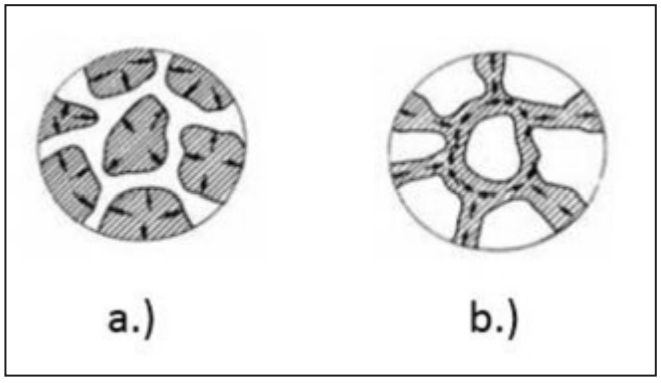

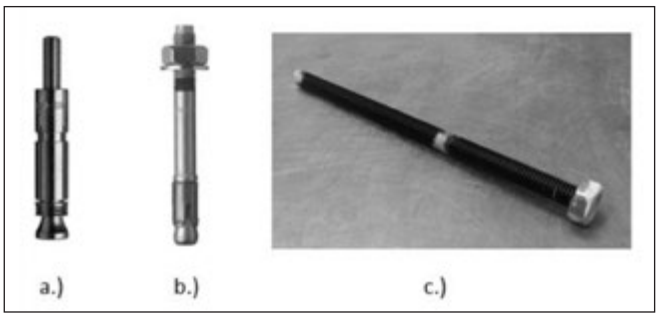

Fig. 4: Tested anchors: undercut anchor + M8 threaded rod (a), torque controlled expansion anchor (b), headed stud with M8 threaded rod (c)

h_{ef}=50 mm (~6d, where d is the diameter of the anchor) in all cases, and the diameter of the anchors and threaded rods was 8 mm, the strength class of threaded rods was 10.9 while material quality of the expansion anchors was 8.8.

2.2 Concrete mixtures

The composition of the tested concrete mixtures is shown in *Table 1*. The mixtures were made with Portland cement (CEM I 42.5 N or CEM I 52.5). The 0/4 mm aggregates were natural quartz sand in all cases, while the 4/8 and the 8/16 mm aggregates were lightweight aggregates. In mix C1 and C2 the lightweight aggregates were expanded clay aggregates with different strength class (Liapor 5N, Liapor 8F). In case of mix B1 the lightweight-aggregates were crushed brick aggregates. Superplasticiser BASF Glenium C323 was also applied. The specimens used for pull-out, compressive strength and flexural tests were held under water for 7 days and then kept at laboratory temperature (20 ˚C) for additional 21 days.

Compressive strength properties of each mixture were tested on 3 cubes of 150x150x150 mm. Flexural strength properties of each mixture were tested on 3 specimens with dimensions of 70x70x250 mm. The dimensions of concrete specimens for pull-out tests were the minimum dimensions that allowed the occurrence of all potential failure modes during the tests. The minimum required sizes could be calculated as a function of the embedment depth.

3. PULL-OUT TESTS

Our unconfined test setup is shown in *Fig. 5*. The size of the specimens was 300x300x100 mm. We have tested 4 specimens from C1 and C2 mixtures and 3 specimens from B1 mixture. The loading device was a displacement controlled, which allowed the recording of residual stresses after the failure. This setup enabled the formation of all possible failure modes, the results were not affected by the geometry of the investigated samples (thickness of the test member, critical edge, placing). The measurement setup was capable to measure, record and show the applied load and related displacement of the anchors in real-time. The perpendicular pin-joints ensured the centrality of the load. The displacement was measured by two electronic transducers (LVDTs). Three additional independent displacement transducers were used to record the deformation of the surface. The load was measured by a calibrated load cell. The tests were carried out in accordance with the instructions given in ETAG 001 Annex A. The support distance was higher than 4 h_{ef} *(ETAG 2006; ETAG 2008)*.

Table 1: Composition of concrete mixtures

Samples	Lightweight aggregate type	Quartz aggregate	Lightweight aggregate [kg/m³]		Cement		Water	Superplasticizer
		0/4 mm	4/8 mm	8/16 mm	CEM I 52.5 [kg/m³]	CEM I 42.5 [kg/m³]	[kg/m³]	[kg/m³]
C1	Liapor 8F	621	680		460		175	1.15
C2	Liapor 5N	307	169			390	104	1.70
B1	crushed brick	490	404	404		460	160	1.15

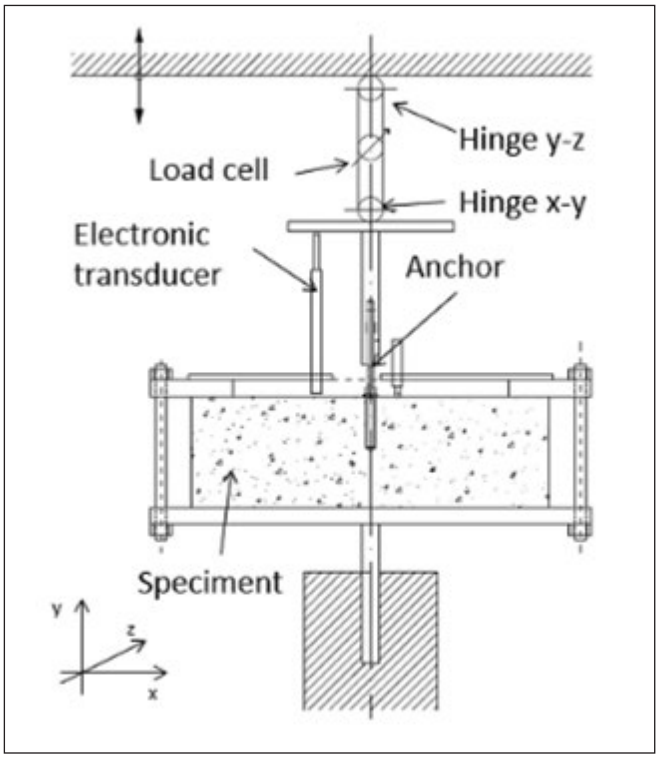

Fig. 5: Arrangement of pull-out tests

4. RESULTS

4.1 Concrete strengths

Compressive strength is the primary parameter for the determination of the capacity of anchors. Uniaxial compressive strength tests were carried out on concrete cubes (150x150x150 mm) 28 days after casting. The results were evaluated in accordance with EN 12390 -3:2009.

The determination of flexural strength under bending was carried out on 3 samples (70x70x250 mm) taken from each concrete mixture. The tensile resistance was calculated. The results were obtained and evaluated according to EN 12390-5:2009.

The strength values of the tested concrete mixtures are shown in *Fig. 6*.

Fig. 6: Compressive and flexural strength values of the tested concrete mixtures

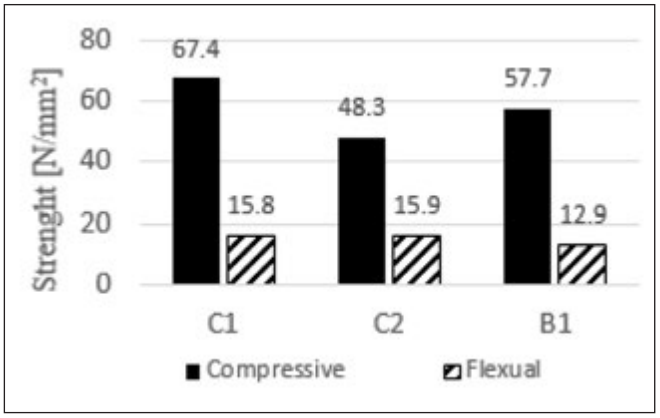

4.2 Failure modes

In our tests three types of anchoring system were tested. Failure modes and ultimate tensile force values of anchors are summarized in *Table 2*.

Based on Table 2 it is visible that splitting failure and cone failure were typical in our tests. Resistance of the anchors can be calculated by Eq. (1) and (2) as a function of the compressive strength of concrete and geometry of the tested specimen. In our case, because of the dimensions ((h=100 mm; h_{ef}=50 mm), reduction factor ($\Psi_{h,sp}$) had not to be applied therefore the resistance can be calculated from the formula for cone failure. On the contrary 54% of our specimens failed by splitting failure that contradicts to the standards applied for conventional concretes.

4.3 Relationship between the tensile resistance and the compressive strength of concrete

Fig 7, *Fig 8* and *Fig 9* represent the compressive strength-load bearing capacity functions of different anchors. Each point of the diagram represents one measurement. The dashed line represents the resistance value as a function of concrete compressive strength calculated according to Eq. (1).

Fig. 7 shows the tensile resistance values of headed stud anchors as a function of concrete compressive strength, in case of mixtures C1, C2 and B1. It is visible that resistance values of the headed studs are lower than the calculated resistances. Load bearing capacity of mixture C1 is only 36.33% of the calculated value. Both splitting and cone failure occurred twice. In case of mixture C2 measured resistance is 46.91% of the calculated value and failure of three specimens was cone failure, while splitting only occurred once. All specimens of mixture B1 failed by splitting and resistance were 49.49% of the calculated value.

Fig. 8 shows the tensile strength values of torque-controlled expansion anchors as a function of concrete compressive strength, in case the three applied concrete mixtures. The figure shows that measured resistance values also lower than the calculated ones. In case of mixture C1 one specimen suffered splitting, while cone failure occurred three times. Resistance values of specimens were 41.06% of the calculated resistance. This ratio is 38.08% in case of mixture C2, where cone failure did not occur. Two specimens casted from mixture B2 failed by splitting and one by cone failure, measured resistance were 44.15% of the calculated value.

Fig. 9 shows the tensile resistance values of undercut anchors as a function of concrete compressive strength, in case of the three different concrete mixtures. Measured

Table 2: *Failure modes and tensile resistances of bonded anchors*

Anchor type	Concrete mixture	Failure mode	Tensile resistance [kN]
Headed studs	C1	Splitting	16.55
	C1	Splitting	17.60
	C1	Concrete cone	14.74
	C1	Concrete cone	18.43
	C2	Splitting	17.56
	C2	Splitting	19.83
	C2	Splitting	19.75
	C2	Concrete cone	16.40
	B1	Splitting	21.15
	B1	Splitting	20.54
	B1	Splitting	22.07
Expansion anchor	C1	Concrete cone	16.93
	C1	Concrete cone	19.11
	C1	Concrete cone	16.89
	C1	Splitting	13.33
	C2	Splitting	12.19
	C2	Splitting	13.09
	C2	Pull-out	12.56
	C2	Pull-out	14.16
	B1	Splitting	15.03
	B1	Splitting	18.49
	B1	Concrete cone	15.92
Undercut anchor	C1	Concrete cone	21.72
	C1	Concrete cone	21.18
	C1	Concrete cone	19.53
	C1	Splitting	21.69
	C2	Splitting	18.03
	C2	Splitting	21.45
	C2	Splitting	19.44
	C2	Splitting	19.14
	B1	Concrete cone	22.24
	B1	Concrete cone	23.61
	B1	Concrete cone	25.36

resistances are also lower in this case, the measured values reached 52.12% (Mix. C1), 57.17% (Mix. C2) and 63.59% (Mix. B1) of the calculated values. Ratios of splitting and cone failures are 1:3 (Mix. C1), 4:0 (Mix. C2) and 0:3 (Mix. B1).

5. CONCLUSIONS

The research focused on the behaviour of post-installed anchors in lightweight concrete mixtures. Three types of lightweight aggregate (Liapor 8F, Liapor 5N, crushed brick) were used in concrete together with three different anchoring systems (headed stud, undercut anchor, torque-controlled

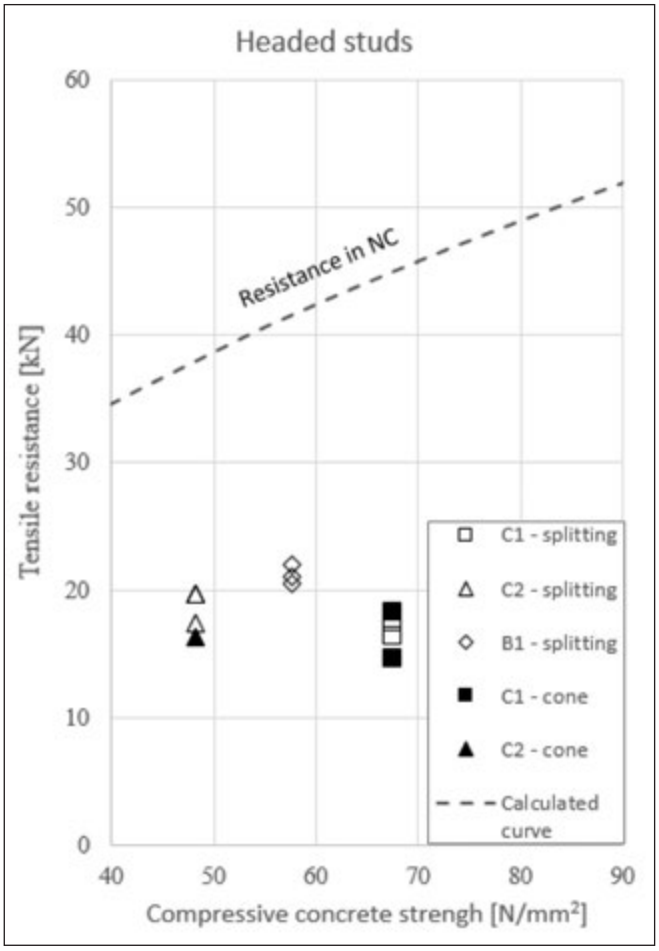

Fig. 7: *Headed studs - relationship between the tensile resistance and the compressive strength of concrete (in some cases symbols overlap)*

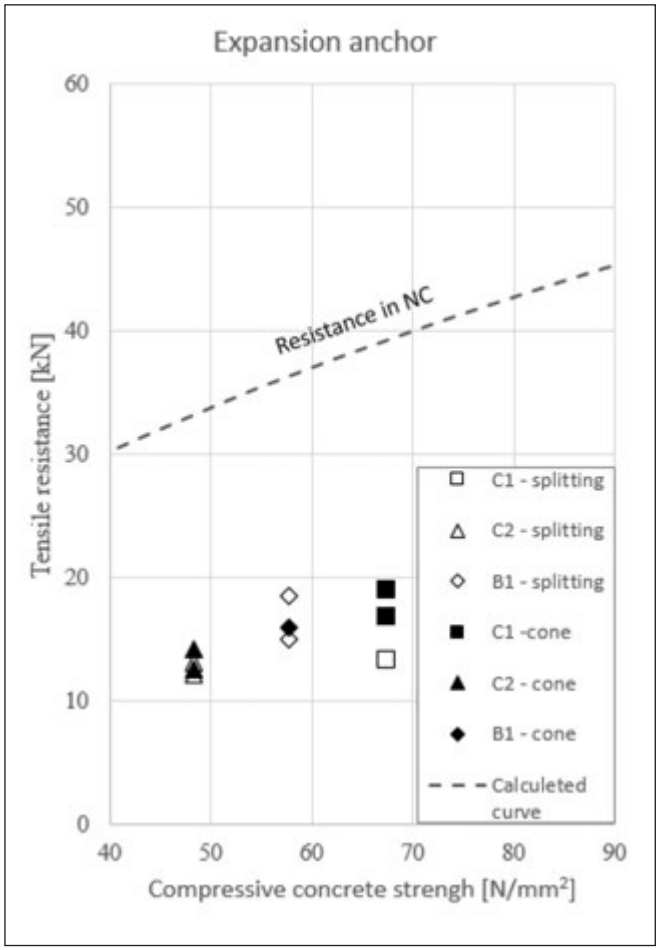

Fig. 8: *Torque-controlled expansion anchors - relationship between the tensile resistance and the compressive strength of concrete (in some cases symbols overlap)*

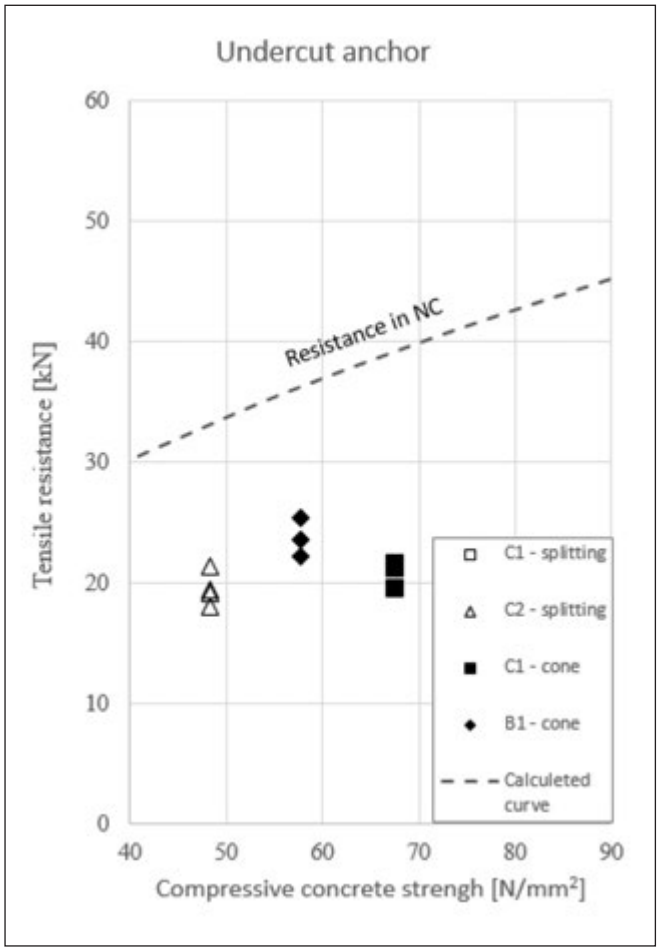

Fig. 9: Undercut anchors - relationship between the tensile resistance and the compressive strength of concrete (in some cases symbols overlap)

expansion anchor). Results of pull-out tests were evaluated and ultimate load values were compared to the values given by the producers for normal concretes.

In 54% of our tests splitting was the typical failure mode, which is contradictory to the literature data. Splitting can be caused by the low flexural strength of lightweight aggregate concretes. Based on our test results it can be stated that resistance and failure of anchors installed in lightweight concrete can be different from the behaviour of anchors installed in normal concrete.

Based on the above study conclusions are the following:

- *Headed studs*: measured loadbearing capacity values were 36.33% (Mix. C1), 46.91% (Mix. C2) and 49.59% (Mix. B1) of the values determined by the standards.
- *Torque controlled expansion anchors*: measured load bearing capacity values were 41.06% (Mix. C1), 38.08% (Mix. C2) and 44.15% (Mix. B1) of the values determined by the standards.
- *Undercut anchors*: measured load bearing capacity values were 52.12% (Mix. C1), 57.17% (Mix. C2) and 63.59% (Mix. B1) of the values determined by the standards.

A possible explanation for the low load bearing capacity of the anchors can be found in the load bearing mechanism of lightweight aggregate, they can crush more easily. Their strength is lower therefore they only take part in the load bearing mechanism, loads are mainly carried by the cement.

6. REFERENCES

Eligehausen R., Mallee R., Silva J. F. (2006): "Anchorage in Concrete Construction", First edition, *Ernst&Sohn* , ISBN: 978-3-433-01143-0

Eligehausen, R., Fuchs, W., Sippel, T. (2000): „Anchorage to Concrete", *TARTÓK 2000,* Budapest, pp. 261–270. ISBN: 963-420-640-9

Eligehausen, R., Hofacker, I., Lettow, S. (2001): „Fastening technique – current status and future trends", *International Symposium on Connections between Steel and Concrete*, Volume One, pp. 11-27.

ETAG 001. „Guideline for European Technical Approval of Metal Anchors for use in concrete", Annex A: *Details of test*. November. (2006).

ETAG 001. „Guideline for European Technical Approval of Metal Anchors for use in concrete", Part 5**:** *Bonded anchors.* November. (2008).

fib MODEL CODE 2010. *Concrete to steel*. Volume One. 282-285. ISBN: 978-3433-03061-5

Fuchs, W. (2001): „Evolution of fastening design methods", *Proceedings of International Symposium on Connections between Steel and Concrete* (Eds.: Eligehausen, R.), Volume One, Stuttgart, Germany, pp. 45-60.

Nemes R. (2007): "Expansion and bonded anchors in expanded clay aggregate concrete", *2nd International Symposium on Connections between Steel and Concrete*, Volume 2, pp. 955-962

Romić, S., Lazić M. (1985): „Armirani lakoagregatni beton" *IRO Gradevinska knjiga,* Beograd

Viktor Hlavička (1987) structural engineer (MSc), PhD student of Department of Construction Materials and Technology at the Budapest University of Technology and Economics. His main fields of interest are: fastening to concrete, fastening systems, finite element modelling. Member of the Hungarian Group of ***fib***.

Éva Lublóy (1976), PhD, Senior lecturer in structural engineering, at the Budapest University of Technology and Economics. Her main fields of interest are: fire design, behaviour of constructions materials at elevated temperature. Member of the Hungarian Group of ***fib***.

László Jancsó (1990), structural engineer (MSc), His main fields of interest are design of reinforced concrete and timber building structures, design of fastening to concrete.

SIZE EFFECT ON CYLINDER AND CUBE STRENGTH OF CONCRETE


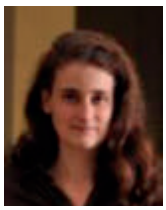

Zoltán Gyurkó – Rita Nemes

The aim of the present study was to investigate the size effect on compressive strength of concrete. To accomplish that a series of laboratory experiments were conducted in which the compressive strength of normal concrete was measured on cylinder and cube specimens of different size. Normal, in the industry every day used concrete mixes of three different strength classes were investigated: C20/25; C30/37; C35/45. For every mix three cubes and three cylinders of different sizes were casted and for each size at least three specimens were tested. The results of the experiments were evaluated and compared to the specifications of the MSZ EN 4798:2016 and the MSZ EN 4798-1:2004 standards. In addition, it was also investigated whether the size has an effect on the ratio of compressive strengths measured on cylinder and cube specimens.

Keywords: Normal strength concrete, size effect, compressive strength, cylinder-cube ratio.

1. INTRODUCTION AND LITERATURE REVIEW

The sizes and shapes of the standard uniaxial compression test samples for concrete are different in many areas of the world (Tokyay, 1997). Cube is the most commonly used in the European countries, while in the USA cylinder is the standardized shape for compressive strength test. The size of the used specimen can be different as well for instance due to the easy handling of the samples or due to the maximum capacity of the testing machine.

Size effect on concrete was a widely studied area by many researchers, however still uncovered areas can be found on that interesting field of research. The topic was investigated widely by Bažant in his many researches (Bažant, 1976, 1998, 1999). Size effect on concrete depends on many influencing factors (aggregate size, aggregate distribution, mix proportion, etc.) making it to a complex material science problem (Li *et al*., 2016). It has a large influence on the results of uniaxial compression test. It was observed in the literature that the compressive strength of concrete depends on the shape of the test specimen, what was built in into the standards as well (del Viso, 2008). Besides that, it was shown that with the increase of the size of the investigated specimen the compressive strength of the material is decreasing, if no other influencing factors are changed (Balázs, 1983).

However, some researchers reported different results:

- the compressive strength of concrete does not depend on the size, if wet curing (specimen kept under water until the day of the compressive strength test) is applied (Zsigovics, 1984).
- the specimen with larger volume has the higher strength in range of very small size specimens (under 50 mm edge length) (Sangha, 1972).

In the book of Balázs (1983) it is also clearly showed that with the increase of the height of a specimen the measured compressive strength is decreasing. It can be explained with the increase of the area of free deformation compared to the area of constrained deformation. On the boundaries of these two areas has the highest shear stresses in the sample. If this boundary is longer then the failure of the structure happens at lower stresses. Theoretically the phenomenon of size effect could generally be explained as a macroscopic phenomenon resulted by the internal microscopic failures of the material. Such defects as microcracks are hard or, in most cases, even impossible to be avoided (Tanigawa, 1978). Most theories, which are trying to explain the size effect, are assuming that the material strength is related to the number of defects in the sample, which is related to the size of the specimen. It is also worth to mention that the shape of the test specimen is an important influencing factor as well.

In our research it was aimed to investigate the size effect on compressive strength of normal strength concrete. The variables of the experiments were the shape of the specimen (cube or cylinder), the size of the specimen and the strength of the concrete (but all in the range of normal strength concrete). In this research the samples were mix cured (based on the recommendation of the Hungarian *MSZ EN 4798-1:2004* standard).

2. DESCRIPTION OF THE EXPERIMENTS

To investigate the size effect on compressive strength of concrete a series of laboratory experiments were conducted. In the first step concrete mixes were designed. It was aimed at the concrete mix design to produce specimens, which have the strength that is frequently applied in industry. Therefore, three different mixes were designed: C20/25; C30/37; C35/45. The class of the concrete was determined based on the recommendation of MSZ 4798:2016 standard. It was derived in the literature that the characteristic strength of concrete can be determined from the mean strength of a 150 mm edge length cube specimen in the following way (Kausay, Simon, 2007):

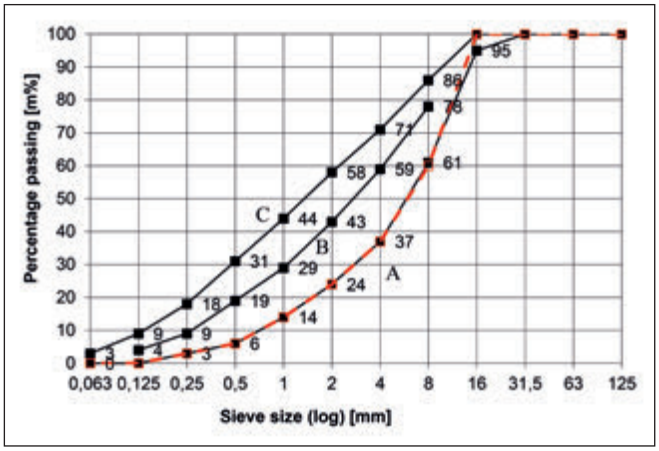

Fig. 1: *Aggregate size distribution of Mixture 1*

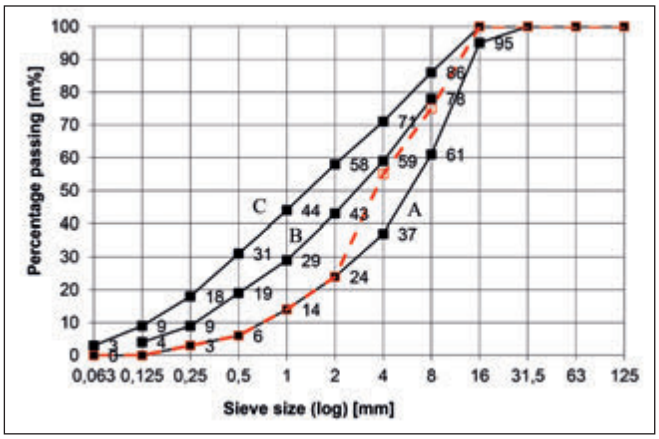

Fig. 2: *Aggregate size distribution of Mixture 2*

$$f_{ck,cube,H} = f_{cm,cube,H} - 11.1\ [N/mm^2]. \quad (1)$$

This expression is true for mix cured specimens, which have the strength class under C50/60. Later in this study for the easier identification the different mixes are referred by the following way: C35/45 as *Mixture 1*; C30/37 as *Mixture 2* and C20/25 as *Mixture 3*. In all cases the maximum aggregate size (d_{max}) was 16 mm. Mixture 1 and 2 were similar to each other, the main difference was the aggregate size distribution of the mixes. Mixture 1 contained more from the fine aggregate (0-4 mm), while Mixture 2 had more from the 8-16 mm aggregate (See *Fig. 1 and 2*). However, in all cases the aggregate size distribution of the mixes was between the standard A and B aggregate size distribution curves.

In our research it was aimed to investigate the size effect of concrete on both cylinder and cube specimens. Due to that three different size cube specimens were casted as well as three different size cylinder specimens. The following specimens were used:

Table 1: *The applied cylinder and cube sizes (standard is marked with grey background colour)*

Cylinder [diameter × height in mm]	Cube [edge length in mm]
60×120	-
100×200	100
150×300	150
-	200

From every size at least three identical specimens were casted.

Fig. 3: *Cylinder specimens for every tested sizes ready for testing*

Fig. 4: *Uniaxial compressive strength test of a concrete cylinder*

The specimens were stored first under water for seven days and after that for another seven days on air. On the age of 14 days the specimens were tested for compressive strength by uniaxial compressive strength test. Before testing the dimensions and mass of the specimens were measured.

3. EVALUATION OF THE RESULTS

The following table contains the result of the compressive strength tests.

Table 2: Results of the compressive strength tests

	Mixture	Dimensions [mm]	Average Volume [l]	Average Compressive Strength [N/mm²]
Cube	Mixture 1	200x200x200	8.035	54.3
		150x150x150	3.423	57.8
		100x100x100	1.023	60.8
	Mixture 2	200x200x200	8.095	50.1
		150x150x150	3.405	55.1
		100x100x100	1.019	58.5
	Mixture 3	200x200x200	8.15	35.9
		150x150x150	3.402	40.2
		100x100x100	1.026	44.6
Cylinder	Mixture 1	150x300	5.243	51.5
		100x200	1.553	54.3
		60x120	0.326	57.5
	Mixture 2	150x300	5.332	48.8
		100x200	1.548	52.3
		60x120	0.335	56.7
	Mixture 3	150x300	5.394	30.0
		100x200	1.584	34.7
		60x120	0.342	36.9

In *Table 2.* it can be seen that with the increase of the volume the compressive strength of the concrete decreases as it can be found in the literature (Tanigawa, 1978).

Based on the results of *Table 2.* an expression for the relationship of the volume and the compressive strength can be drawn and based on that expression the results can be extrapolated for smaller volumes. This expression was determined for cubes and for cylinders as well based on the measurement data. As a lower boundary of this extrapolation 0.2 liter was used, which belongs to a 60×60×60 mm edge length size cube that is still possible to have in laboratory practice for this type of concrete with d_{max}=16 mm.

Table 3. shows the results of this extrapolation in case of Mixture 1.

Table 3: The extrapolated data for cubes and cylinders as well as their ratio

Mixture 1 - Volume [l]	Compressive strength [N/mm²] Cube	Compressive strength [N/mm²] Cylinder	Ratio of the comp. Stresses: Cyl/Cube [-]
0.2	66.60	58.70	0.881
1	61.09	55.08	0.902
2	58.86	53.59	0.910
3	57.59	52.73	0.916
4	56.71	52.14	0.919
5	56.03	51.68	0.922
6	55.49	51.31	0.925
8	54.63	50.73	0.929

Table 3 shows the compressive strength belonging to a given volume for cubes and cylinders as well. Besides that, the ratio of compressive strength measured on cylinder and cube can be seen in this table. *Figure 4* and *5* are showing these results for Mixture 1 and Mixture 3 respectively. In case of Mixture 1 and 2 the results were very similar within the meaning of the cylinder-cube ratio of compressive strength. As it can be seen on the figures with the increase of the volume the ratio of compressive strengths is increasing as well, but the slope of the function is continuously decreasing and the values start to tend to an asymptote. This behaviour was observable in case of all mixtures. The difference in the values in case of small and larger values is about five to ten percent; it is higher in case of the lower strength material. Despite of all the similarities, if one sees the exact values of the ratios a significant difference can be observed between the higher (Mixture 1 and 2) and the lower (Mixture 3) strength concretes. In case of Mixture 1 and 2 the maximum of the ratio of compressive strengths is around 0.93, while in case of Mixture 3 this value is only around 0.82, which means a 10 % difference. Based on that it can be assumed that the size effect is dependent on the strength of the material as well.

4. COMPARISON WITH STANDARDS

Most of the standards have some kind of regulation, which deals with the size effect on concrete. In the MSZ EN 4798:2016 standard for every strength class two values are given:

- the first is the characteristic strength of concrete measured on a cylinder (150×300 mm)
- the second is the characteristic strength of concrete measured on a cube (150×150×150 mm).

The ratio of those values shows the size effect of concrete

Fig. 5: Cylinder-cube ratio of compressive strength of concrete (Mixture 1)

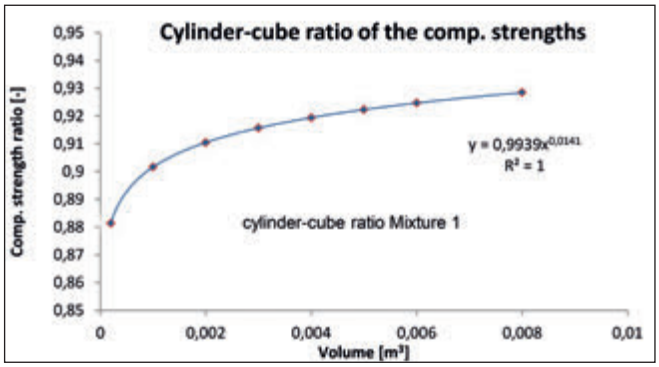

Fig. 6: Cylinder-cube ratio of compressive strength of concrete (Mixture 3)

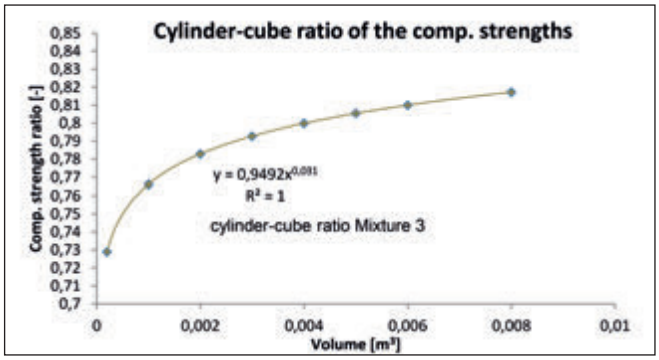

(the standard cube has the dimensions of 150×150×150 mm, while the standard cylinder has 150 mm diameter and 300 mm height, meaning the volume of the standard cylinder is 1.5 times much as the volume of the standard cube.

This ratio is not a constant number for every strength class (due to practical reasons), but it is varying around 0.8 for every value. This previous comment belongs to concrete, which compressive strength measurement was done at 28 days old age and they were wet cured. In our case the samples were mix cured. Based on the recommendations of the standard these values can be determined for mix cured samples as well:

$$f_{ck,cyl,H} = \frac{f_{ck,cyl}}{0.97}; \quad (2)$$

$$f_{ck,cube,H} = \frac{f_{ck,cube}}{0.92} \quad (3)$$

where $f_{ck,cyl,H}$ and $f_{ck,cube,H}$ are the mix cured samples, while $f_{ck,cyl}$ and $f_{ck,cube}$ are the wet cured. These expressions are true if one has a concrete of C50/60 strength class or lower.

For the concretes used in this study these values are the following:

If these values are compared to the results of our experiments, it can be seen that in case of Mixture 3 (C20/25) the result is very close to the value of the standard, however in case of the other two mixtures significant difference can be found. In case of Mixture 2 this difference is 11 %, while in case of Mixture 1 this value is 15 % if we compare them to the wet cured standard values. If one compares the mix cured standard values to the experimental results, then in case of Mixture 1 and 2 an even larger difference can be seen (15 and 19 % respectively). This results may lead us to the conclusion that the $f_{ck,cyl}/f_{ck,cube}$ ratio is dependent on the compressive strength of the concrete and it is not a constant value, not even in case of normal strength concretes. It is also important to note that the standard overestimates the real values, thus it is on the safe side. Meaning, if the value of $f_{ck,cyl}$ is calculated from the $f_{ck,cube}$ based on the suggestion of the standard, the result will be likely smaller than the real value.

MSZ EN 4798-1:2004 contains other expressions regarding the size effect. Based on these suggestions from the compressive strength of cubes or cylinders of various sizes and curing modes, it is possible to determine the strength of a specimen with different parameters. For example, from the results of the 200 mm edge length cube the standard (150×300 mm) cylinder's compressive strength can be determined, based on the following expression.

$$f_{ck,cyl,H} = 0.85 \times f_{ck,cube,H,200} \quad (4)$$

In our experiment the compressive strength of the standard cylinder was measured and calculated from equation (4) as well and the results were compared. Similar approach was proceeded for all the following expressions, which can be found in the standard.

Wet cured standard size cylinder compressive strength calculated from the mix cured standard size cube measurements:

$$f_{ck,cyl} = 0.75 \times f_{ck,cube,H} \quad (5)$$

Wet cured standard size cylinder compressive strength calculated from mix cured 200 mm edge length cube:

$$f_{ck,cyl} = 0.76 \times f_{ck,cube,H,200} \quad (6)$$

The results coming from the above expressions and from the laboratory experiments can be seen in the 5. table:

In Table 5. it can be seen that in case of Mixture 1 and 2 significant differences (more than 10 %) can be found between the measured and based on the standard calculated results. However, in case of Mixture 3, which had the smallest compressive strength, the measurements are fairly close to the calculated values.

It is also important to note that in case of the large differences always the measured results were higher, so the standard is on the safe side from design point of view.

5. CONCLUSIONS

The aim of our laboratory experiments was to analyse the size effect on concrete compressive strength measure on specimens with different shapes and dimensions. The investigations have shown that the earlier findings for the decrease of compressive strength with the increase of the volume can be considered as correct for various size cubes and cylinders as well. Based on the data evaluation of the experimental results it can be seen that the ratio of compressive strength measured on cylinder and cube is increasing with the volume. The figures showed an asymptotic behaviour. It was also shown that in case of concrete with less strength (Mixture 3) the compressive strength ratio is smaller than in case of concrete mixes with higher strength (Mixture 1 and 2). The results were compared to the recommendations of the MSZ EN 4798:2016 standard and it could be seen that in case of Mixture 1 and 2 the ratio of compressive strength measured on cylinder and cube is higher than it is stated in the standard. In case of Mixture 3 the results of the experiments were close to the recommended values. In addition to that, the recommendations of MSZ EN 4798-1:2004 were also analysed to see that how accurate the suggestions of this standard are. In that case significant differences were found in case of the two higher strength concrete, while Mixture 3 was close to the standard recommendations. Based on the results of the present research it would be worth to consider the increase of the $f_{ck,cyl}/f_{ck,cube}$ ratio for concretes with higher strength class than C25/30. However, the topic requires more experiments to accurately determine the value of the increase.

6. FUTURE WORK

Present study is the first step of our research project, where the size effect on normal concrete is investigated. Later part

Table 4: *The applied strength classes and the corresponding cylinder over cube ratios based on the EN 206-1 and MSZ EN 4798:2016 standards*

Strength class	$f_{ck,cyl}$	$f_{ck,cube}$	$f_{ck,cyl}/f_{ck,cube}$ Wet cured (EN 206-1 standard)	$f_{ck,cyl,H}/f_{ck,cube,H}$ Mix cured (MSZ EN 4798:2016 standard)	$f_{ck,cyl,H}/f_{ck,cube,H}$ measurements
C20/25	20	25	**0.80**	**0.76**	**0.82**
C30/37	30	37	**0.81**	**0.77**	**0.92**
C35/45	35	45	**0.78**	**0.74**	**0.93**

Table 5: Comparison of experimental results with standards

Eq. (4): $f_{ck,cyl,H}=0.85\times_{fck,cube,H,200}$	Mixture	$f_{ck,cyl,H}$ measured	$f_{ck,cyl,H}$ calculated	Difference [%]
	1	51.53	46.14	**10.45**
	2	48.83	42.54	**12.88**
	3	30.01	30.55	**1.79**
Eq. (5): $f_{ck,cyl}=0.75\times f_{ck,cube,H}$	**Mixture**	**$f_{ck,cyl}$ measured**	**$f_{ck,cyl}$ calculated**	**Difference [%]**
	1	49.98	43.37	**13.23**
	2	47.36	41.29	**12.82**
	3	29.11	30.15	**3.56**
Eq. (6): $f_{ck,cyl}=0.76\times f_{ck,cube,H,200}$	**Mixture**	**$f_{ck,cyl}$ measured**	**$f_{ck,cyl}$ calculated**	**Difference [%]**
	1	49.98	41.26	**17.46**
	2	47.36	38.04	**19.69**
	3	29.11	27.31	**6.18**

of the research the numerical modelling of size effect will be carried out by using Discrete Element Method. With the modelling our target is the deeper understanding of the processes inside the material in different size samples.

7. ACKNOWLEDGEMENT

Authors are grateful to the Hungarian Scientific Research Fund (OTKA) for the financial support of the OTKA K 109233 research project,

8. REFERENCES

Balázs, G. (1983), "Construction materials and Chemistry", (in Hungarian). *Tankönyvkiadó Vállalat*, Budapest.

Bažant, Z. P. (1976), "Instability, ductility, and size effect in strain-softening concrete", *J. Eng. Mech. Div., Am. Soc. Civil Engrs.*, 102, EM2, 331-344; disc. 103, 357-358, 775-777, 104, 501-502.

Bažant, Z. P. (1998), "Size effect in tensile and compression fracture of concrete structures: computational modeling and design", In: Mihashi, H.; Rokugo, K.: (eds.) *Fracture Mechanics of Concrete Structures. 3rd Int. Conf., FraMCoS-3(Gifu, Japan)*, pp. 1905-1922.

Bažant, Z. P. (1999), "Size effect on structural strength: a review", *Archive of Applied Mechanics*, Vol. 69 pp. 703-725.

del Viso, J. R., Carmona, J. R., Ruiz, G. (2008), "Shape and size effects on the compressive strength of high-strength concrete", *Cement and Concrete Research*, Vol. 38 pp. 386-395.

Kausay, T., Simon, T. K. (2007), "Acceptance of concrete compressive strength", *Concrete Structures*, Vol. 8. pp. 54-63.

Li, D., Jin, L., Du, X., Fu, J., Lu, A. (2016), "Size effect tests of normal-strength and high-strength RC columns subjected to axial compressive loading", *Engineering Structures*, Vol. 109 pp 43-60.

MSZ EN 4798-1:2004 Concrete Part 1. Technical requirements, fulfilment, production and conformity, and the Hungarian NAD for MSZ EN 206-1 (Beton. 1. rész Műszaki feltételek, teljesítőképesség, készítés és megfelelőség, valamint az MSZ EN 206-1 alkalmazási feltételei Magyarországon) Hungarian standard.

MSZ EN 4798:2016 Concrete. Specification, performance, production, conformity, and rules of application of EN 206 in Hungary.

Sangha, C. M., Dhir, R. K. (1972), "Strength and deformation of rock subject to multiaxial compressive stresses", Matériaux et Constructions, Vol. 5 pp. 361-373.

Tokyay, M., Özdemir, M. (1997). "Specimen shape and size effect on the compressive strength, of higher strength concrete", *Cement and Concrete Research*, Vol. 27 pp. 1281-1289.

Tanigawa, Y., Yamada, K. (1978), "Size effect in compressive strength of concrete", *Cement and Concrete Research*, Vol. 8 pp. 181-190

Zsigovics, I. (1984) A próbatest alak és méret hatása a beton nyomószilárdságára (in Hungarian), *Doctoral Thesis*. Budapest University of Technology ~~and Economics.~~

Zoltán Gyurkó (1989) civil engineer (MSc), PhD candidate at the Department of Construction Materials and Technologies, Budapest University of Technology. *Main fields of interest:* non-destructive testing of concrete and porous building materials, Discrete Element Modelling, numerical modelling of porous materials.

Rita Nemes (1978) civil engineer (MSc), postgraduate diploma in concrete technology, PhD, associate professor at the Department of Construction Materials and Technologies, Budapest University of Technology and Economics. *Main fields of interest:* non-destructive testing of concrete, supplementary cementing materials for concrete, bond in concrete, fibre reinforced concrete, lightweight concrete, shrinkage of concrete, durability measurement, waste materials as aggregates. Member of the Hungarian Group of ***fib*** and the Scientific Society of Silicate Industry.

INFLUENCE OF MIXING TIME TO THE PROPERTIES OF STEEL FIBRES AND STEEL FIBRE REINFORCED CONCRETE


Olivér Czoboly – György L. Balázs

Properties of fibre reinforced concrete (FRC) are mainly influenced by type and amount of fibres. Fibre properties are defined by the fibre producers. However, the properties of hardened FRC are influenced by the properties of fibres after mixing. Fibres are often added to the concrete in the concrete plant during mixing or immediately after the concrete was added into the mixer so the fibres participate in the mixing process for 0.5 up to 1.5 hours long in concrete before concreting in the workplace.

According to our earlier experimental studies macro polymer fibres can deteriorate as a consequence of long mixing in concrete (Czoboly, Balázs, 2015-1). Hence, the post-cracking residual flexural strength of FRC beams with macro polymer fibres in three-point bending can also decrease with a longer mixing time (Czoboly, Balázs, 2015-2, Czoboly, Balázs, 2016). Important question is whether the properties of steel fibres and steel fibre reinforced concretes (SFRC) are significantly influenced by the longer mixing time than the minimum? Our research was directed to the possible influences of mixing time on the pull out behaviour of steel fibre and flexural properties of SFRC.

Keywords: SFRC, steel fibre, mixing time, pull out behaviour, residual flexural strength

1. INTRODUCTION

Favourable experiences with fibre reinforced concrete (FRC) resulted in its increasing application. Fibres are used to improve properties of fresh or hardened concrete, respectively. Toughness and residual strength after cracking of concrete can be significantly increased by application of fibres. Nowadays residual tensile strength of FRC is one of the most important parameter both for design and for practice *(Erdélyi, 1993)*. The mechanical properties of FRC depend on the material properties of fibres (e.g. strength, stiffness, and Poisson's ratio), fibre geometry and surface, amount of fibres, matrix properties (e.g. strength, stiffness, Poisson's ratio), interface properties (adhesion, frictional and mechanical bond) and loading condition *(Naaman, Najm, 1991; Kim, Naaman, El-Tawil, 2008; Aydın, 2013; Felekoglu, 2014)*. Testing and modelling of bond behaviour of fibres are important to realize the favourable uses of FRC *(Kovács, Balázs, 2003, 2004; Zhao, Verstrynge, di Prisco, Vandewalle, 2012; Balázs, 2012; Halvax, Lublóy, 2013-1; Halvax, Lublóy, 2013; Zile, Zile, 2013; Breitenbücher, Meschke, Song, Zhan, 2014)*.

Application of fibres can be effective in hardened concrete until the fibres fail or are pulled out. Typically steel fibres are pulled out in cross-section of failure. Therefore, pull out tests of steel fibres with different mixing times and fibre shapes were carried out.

In addition to above parameters, mixing operation is of high importance. The manufacturers of the fibres determine the minimum mixing time after addition of fibres into the concrete. Based on the guidance of European Ready Mixed Concrete Organization *(ERMCO, 2012)* one hundred turns of the mixer are required to ensure good fibre distribution, but in practice it is difficult to exactly monitor. Therefore, a minimum mixing time of five minutes (or minimum 1 minute per m^3) at the maximum speed of the drum is required. Many ready mixed concrete supplier as well as some national regulations (e.g. in Germany) do not allow fibres to add at the construction site.

Fibres are often added to the concrete in the concrete plant during mixing or immediately after the concrete was added into the mixer so the fibres can be homogenously dispersed in concrete. As a result, the fibres participate in the mixing process for 0.5 up to 1.5 hours long in concrete with different rates.

Important question is whether the properties of steel fibres are significantly influenced by the longer mixing time than the minimum? On the other hand, can it significantly influence the final properties of SFRC?

Main purpose of our research was to study the possible influences of mixing time on the flexural properties of SFRC.

2. EXPERIMENTAL PROGRAMME

Our mix compositions are presented in *(Tab. 1)*. In our experimental programme two types of steel fibres (S1: steel fibre without coating and S2: steel fibre with brass-coating) were tested *(Fig. 1)*. The properties and amount of fibres are presented in *Tab. 2*.

Before adding fibres the mixing process of concrete was 5 minutes with pan type mixer. (The pan type mixer was used

Table 1: Concrete compositions

Material	Type	Amount [kg/m^3]
Aggregate	sand (45%): quartz (0/4 mm fraction)	824
	coarse aggregate (55%): quartz (4/16 mm fraction)	1008
Cement	CEM I 42.5 N	380
Fibres	S1 or S2 type steel fibre amount: 0.3., 0.5 V%	
Water	m_w/m_c=0.43	163
Admixture	Glenium C300 (max 0.7 m_c%)	max 2.66

Table 2: Properties of tested fibres

Sign	Material	Length [mm]	Equi-valent diame-ter [μm]	Tensile strength [N/mm^2]	Density [kg/m^3]
S1	Steel	50	1000	1000-1200	7850
S2	Steel (brass-coated)	13	200	3000	7850

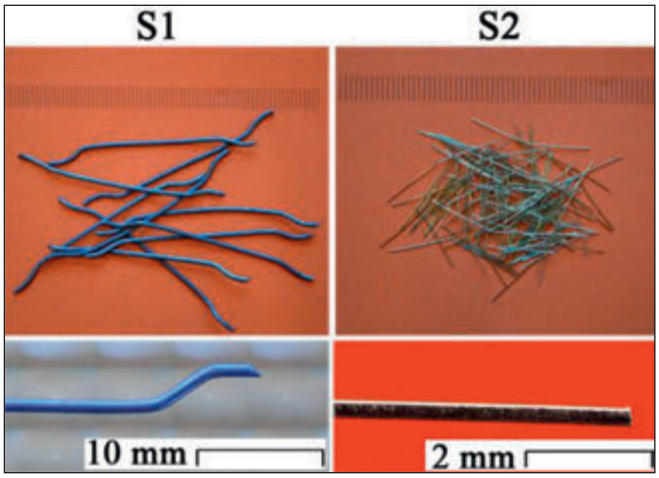

Fig. 1: Image and optical microscope image of the steel fibres before mixing in concrete

every time with activator). The consistence of fresh concrete was checked every 5 minutes and if necessary Glenium C300 type plasticizer admixture was added to the concrete to keep the flow class F4 (to *EN 206:2013*). Fibres were isolated from the fresh concrete *(Fig. 2)*. Separated fibres were analysed with optical microscope.

Pull out tests of S1 type (hooked end) steel fibres (initial shape) with different anchorage length (15 mm or 25 mm) and of steel fibre with shape deformation were carried out *(Fig. 3)*. FRC beams with S1 type steel fibre (fibre content: 0.5 V%) were used for pull out tests *(Fig. 4)*. Loading rate was 10 mm/min.

From each steel fibre reinforced concrete mixture 3 pieces of SFRC beams were cast after 5 or 30 minutes mixing in pan type mixer. Three-point bending tests were carried out in crack mouth opening displacement (CMOD) control on notched SFRC beams (28 days old specimens with sizes of 150×150×600 mm) according to *EN 14651:2005+A1:2007 (Fig. 5)*. The span of the beam was 500 mm. The distance between the tip of the notch and the top of the test specimens in the mid-span section (h_{sp}) was 125 mm. We studied how the mixing time of concrete of additional 5 or 30 minutes influences the properties of SFRC. The tested beams were also subjected to compression tests. Compression tests of 90 days old cubes (dimensions: 150 mm) were carried out that were cut from the undamaged parts of the beams.

3. TEST RESULTS

3.1. Type of deterioration of fibres

Shape deformations were observed for S1 type steel fibres during mixing in concrete *(Fig. 6-a)*. However, abrasion of coating was realized by S2 type steel fibre *(Fig. 6-b)*. Modification of surface colour (from yellow to grey) was clearly visible for the coated steel fibres.

3.2. Pull out behaviour of steel fibre with initial shape and after shape deformation

Fig. 7 represent the average of pull out force vs. displacement diagrams for 5 pieces of S1 type (hooked end) steel fibres with 15 mm or 25 mm anchorage length. The pull out tests were carried out on FRC beams with 0.5 V% S1 type steel fibre content. The maximum average pull out force and the residual average pull out force increase as the anchorage length increases.

Shape deformations were observed for S1 type steel fibres during mixing in concrete *(Fig. 6-a)*. Our tests indicated that the deformation of steel fibres could be observed after 5 minutes long mixing in concrete and the number of deformed fibres and the degree of deformation slightly increased as mixing time increased. Probably the shape

Fig. 2: Isolation of steel fibres from fresh concrete and analysing with optical microscope

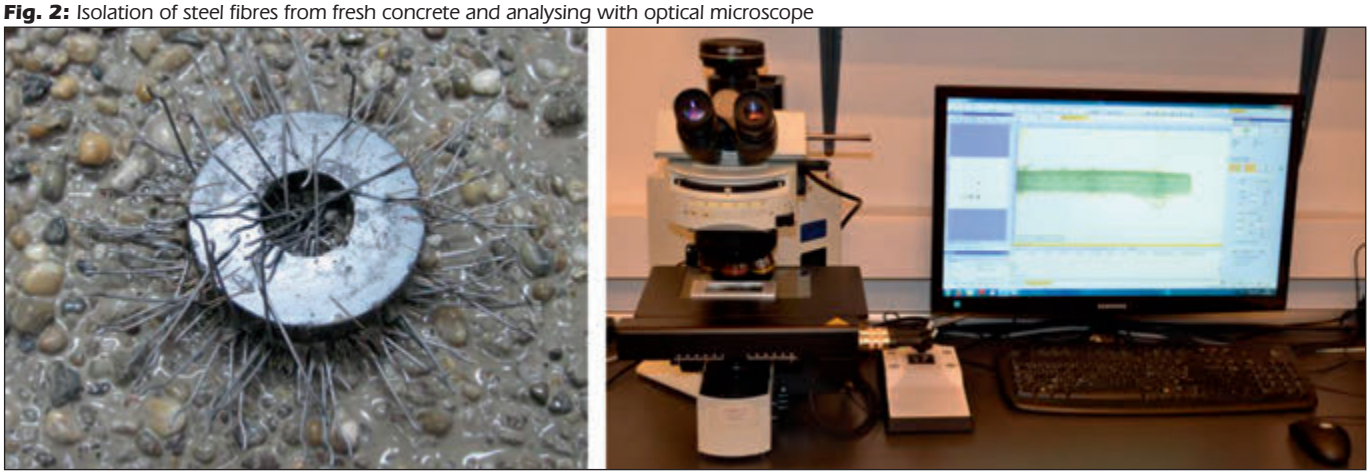

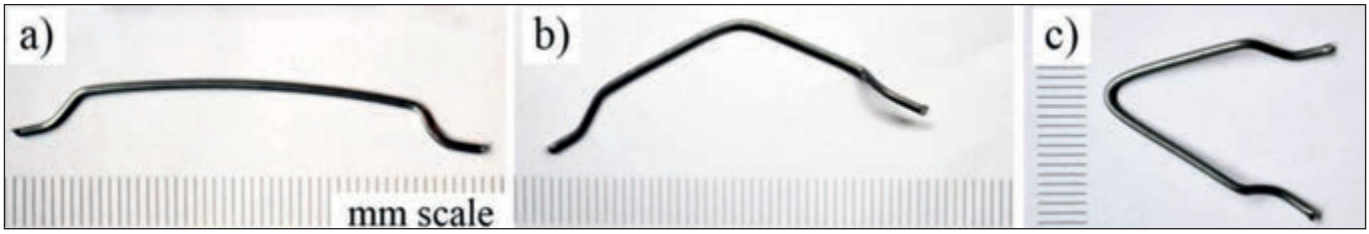

Fig. 3: S1 type steel fibres prepared to pull out test a) initial shape, b) deformed shape, c) U shape

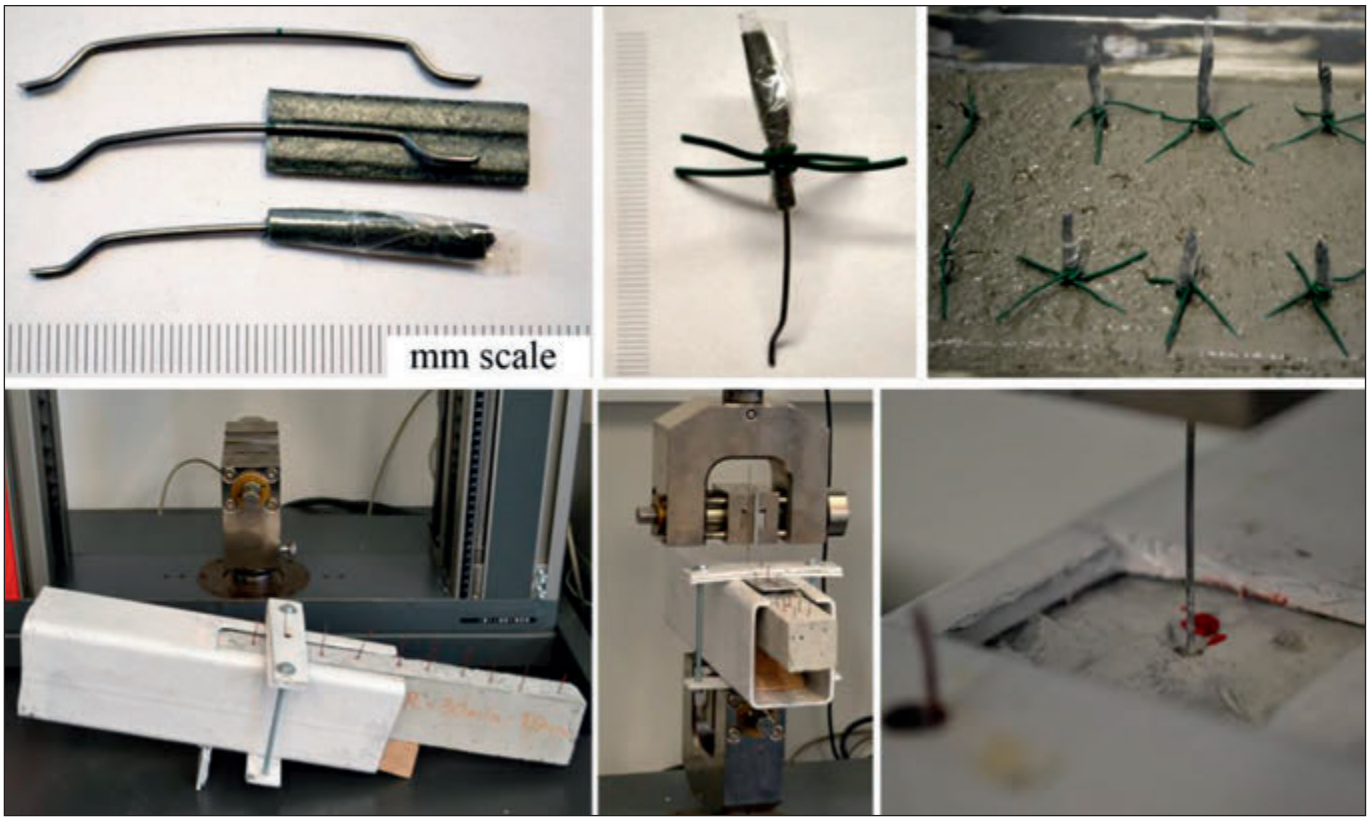

Fig. 4: Preparation of S1 type steel fibres and pull out tests

deformation could slightly improve the anchorage capacity of steel fibres. Therefore pull out tests were carried out on steel fibres after shape deformation (Fig. 8). The continuous line in *Fig. 8* shows the average pull out force of the simultaneously tested 5 pieces of steel fibres (with initial shape), the other curves indicate individual measurements of a single fibre (with shape deformation).

According to our tests the maximum pull out force was higher in case of fibres with shape deformation than in case of fibres with initial shape. One of the tested fibres with shape deformation (see the dotted curve) had higher residual pull out force than those of steel fibre with initial shape. The other tested fibres with shape deformation (see the dashed curve) were broken during the test. (The pull out force was greater than the load bearing capacity of the steel fibre.)

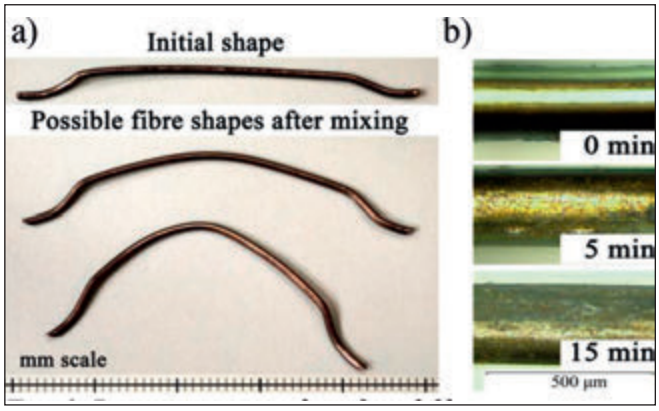

Fig. 6: Deterioration modes of steel fibres, a) shape deformation of S1 type steel fibre b) abrasion of coating of S2 type steel fibre

Fig. 5: Three-point bending tests on notched FRC beam

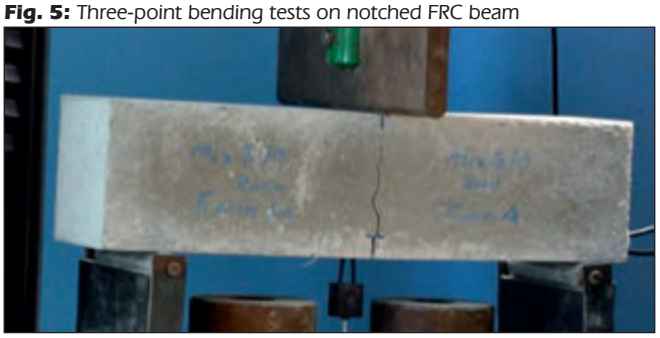

We observed a steel fibre with significantly deformed shape in the failed cross-section of a 30 minutes mixed SFRC beam by three-point bending test. In this case both ends of the fibre were bonded in the same side of the concrete beam *(Fig. 9)*. The fibre could not pull out so the concrete crashed around the fibre. In order to analyse such behaviour, pull out tests were carried out on steel fibres with U shape.

The pull out force vs. displacement curve of U shape fibres with concrete crash failure is presented by dashed curve *(Fig. 10)*. The dashed curve in *Fig. 11* represents the results of one steel fibre with U shape by one side of the U was broken and the fibre pulled out into the other side. According to our

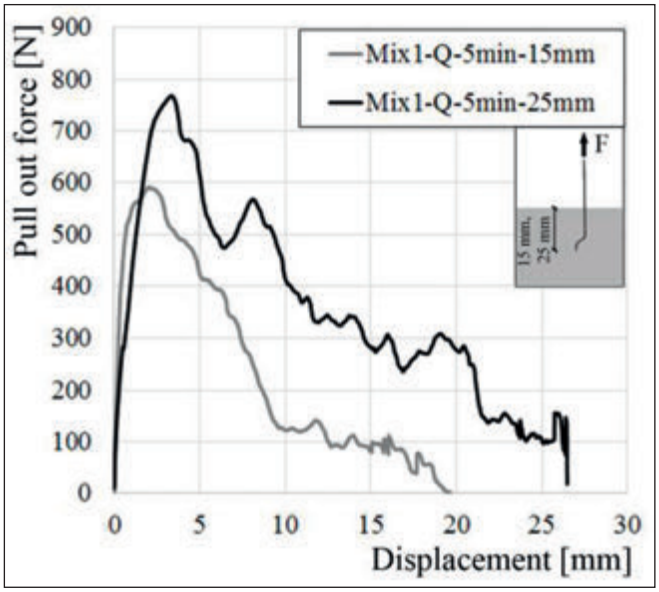

Fig. 7: Pull out force vs. displacement curves of S1 type steel fibres (with initial shape - hooked end)

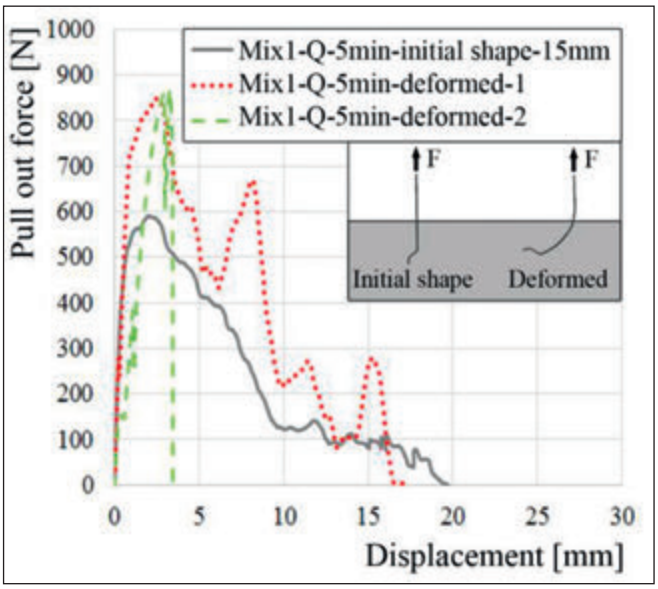

Fig. 8: Pull out force vs. displacement curves of S1 type steel fibres (with initial shape and with shape deformation)

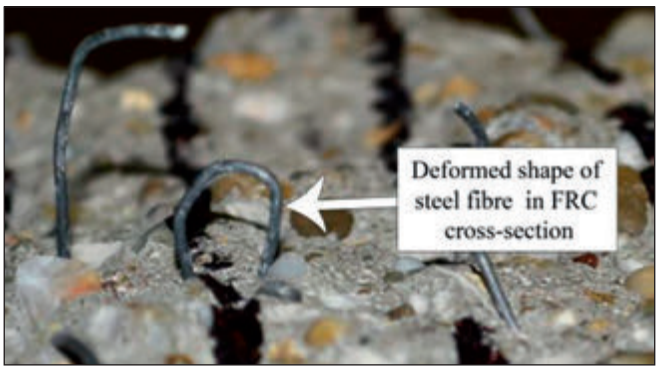

Fig. 9: Deformed shape of steel fibre in cross-section of beam by the 30 min mixed SFRC

tests the maximum pull out force was higher in case of U shape steel fibres than in case of steel fibres with initial shape.

3.3. Compressive strength of FRC with different mixing times

From each steel fibre reinforced concrete mixture 3 pieces of FRC beams were cast after 5 or 30 minutes mixing with fibres in pan type mixer. The tested beams were subjected

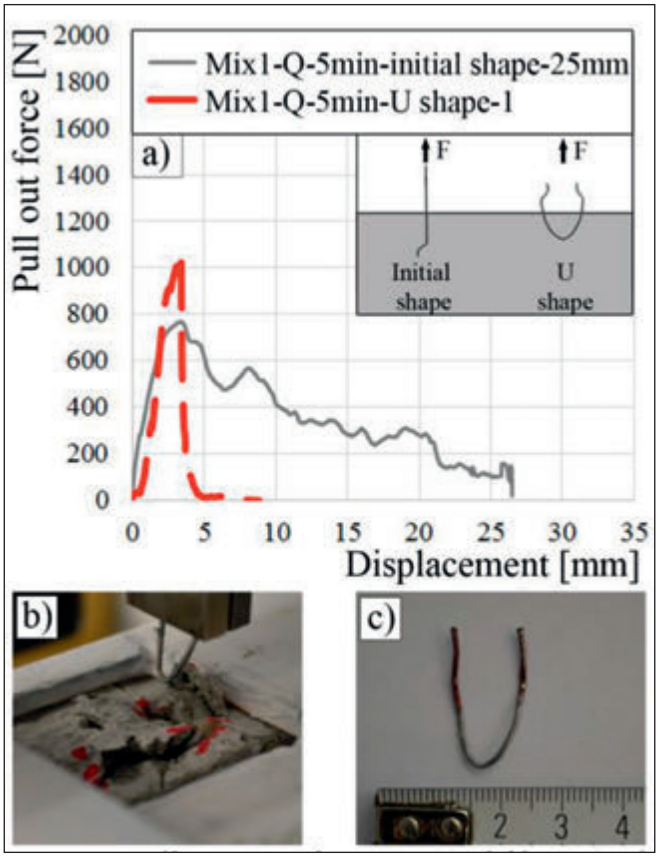

Fig. 10: Pull out test of S1 type steel fibres (with initial shape and with U shape) a) force vs. displacement curves, b)-c) images of tested fibre with U shape

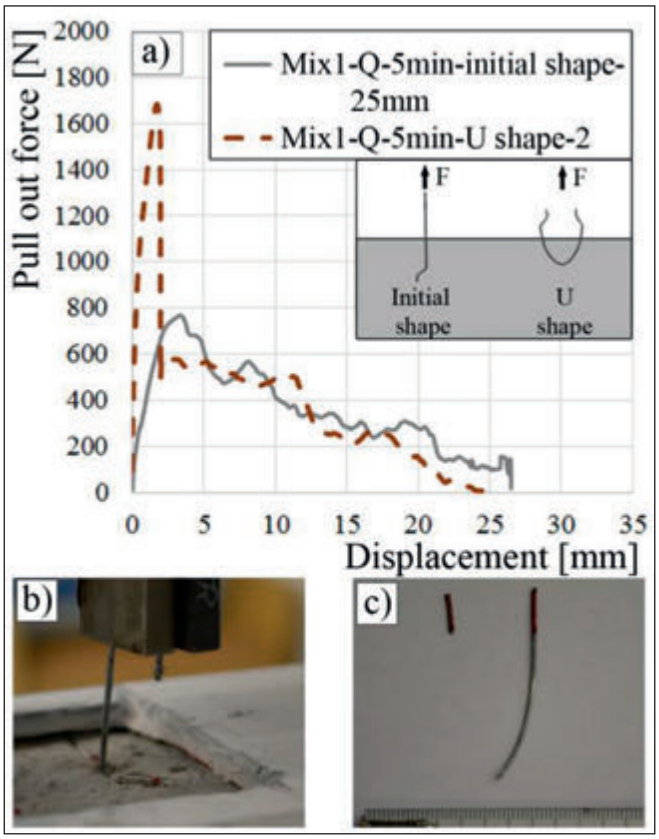

Fig. 11: Pull out test of S1 type steel fibres (with initial shape and with U shape) a) force vs. displacement curves, b)-c) images of tested fibre with U shape

to compression tests. Compression tests were carried out on 90 days old cubes specimens of 150 mm sides cut out of the undamaged parts of the beams. The porosity of the specimens was calculated from the density and the bulk density with the applied fibre content.

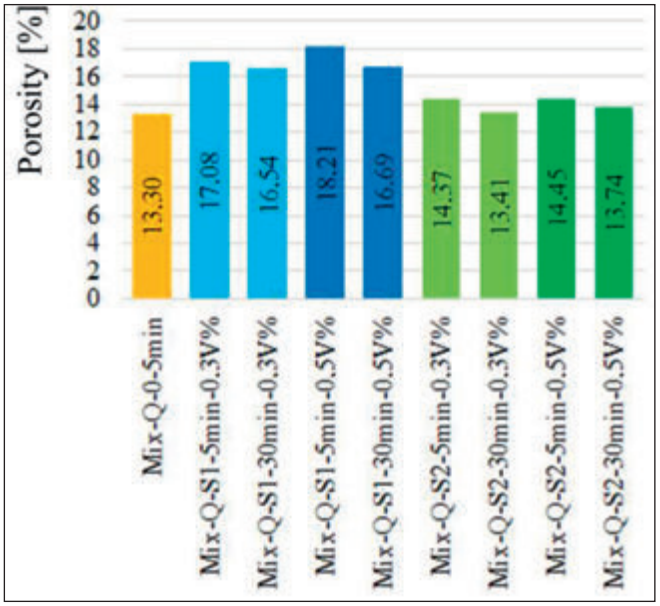

Fig. 12: Porosity of specimens with or without S1 or S2 type steel fibres

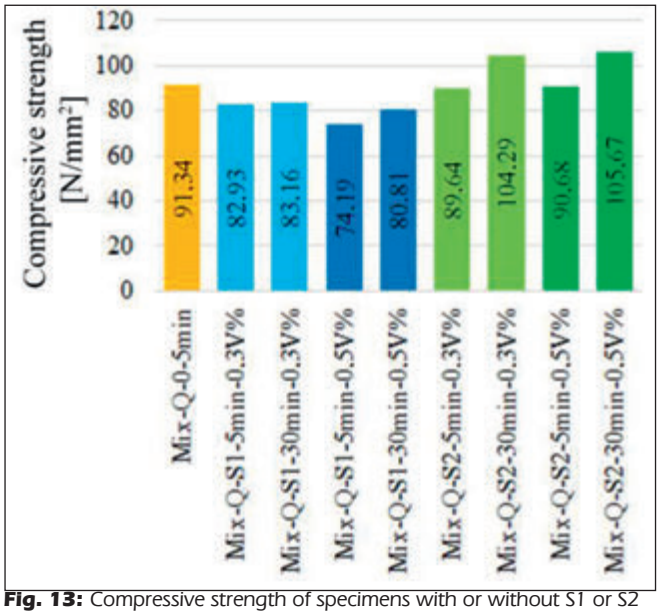

Fig. 13: Compressive strength of specimens with or without S1 or S2 type steel fibres

Legends in *Fig. 12* and *Fig. 13* indicate the fibre type (0: no fibre, S1 or S2: steel fibres), the mixing time (5 or 30 min) after addition of fibres and the fibre dosage in volume fraction (0.3 or 0.5 V%). Each column shows the average of 3 measurements.

The porosity of the FRC specimens with steel fibres decreases as mixing time increases *(Fig. 12)*. However, the compressive strength of the FRC specimens with steel fibres increases as the mixing time increases *(Fig. 13)*.

3.4. Test results of FRC beams with different mixing times

Post cracking residual flexural strength of FRC is one of the most important parameter both for design as well as for practice. Present part of our research was directed to study the possible influence of the mixing time on the post-cracking residual flexural strength of FRC beams with S1 type steel fibres *(Fig. 14)* or with S2 type steel fibres *(Fig. 15)*. The SFRC beams were prepared with two different mixing times (an additional 5 or 30 minutes mixing of concrete after adding the fibres into the concrete).

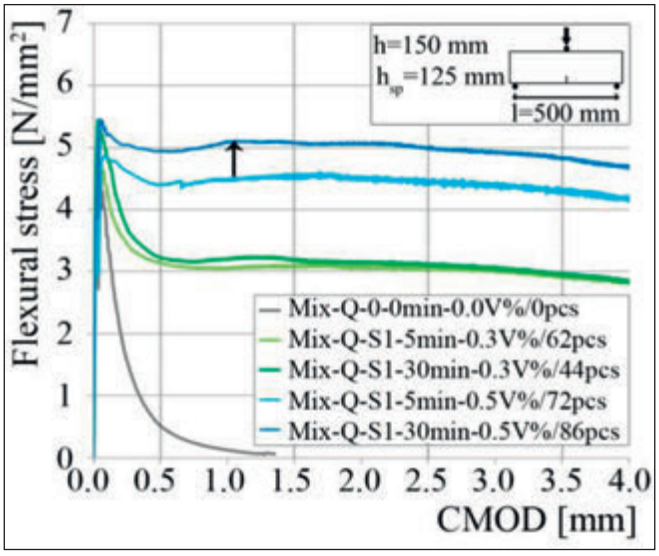

Fig. 14: Flexural stress-CMOD curves of three-point bending tests of SFRC beams with S1 type steel fibres

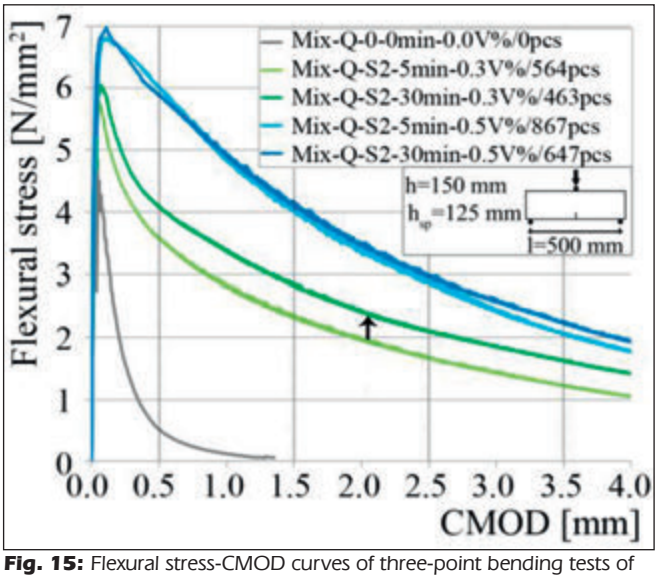

Fig. 15: Flexural stress-CMOD curves of three-point bending tests of SFRC beams with S2 type steel fibres

In the legends of *Fig. 14* and *Fig. 15* the applied fibre type (0 → without fibre, S1 → S1 type steel fibre, S2 → S21 type steel fibre), the mixing time after adding of fibre (5 or 30 min), the planed fibre content in volume fraction (0.3 or 0.5 V%) and the number of fibres counted in the failed cross-section (… pcs) are represented, respectively.

Fig. 14 and *Fig. 15* indicate flexural stress vs. CMOD of SFRC (steel fibre reinforced concrete) with quartz aggregate. Longer mixing times resulted in a slight increase of the post-cracking residual flexural strength of FRC beams containing steel fibres.

4. CONCLUSIONS

Main purpose of our experimental study was to determine the effect of mixing time (from 5 to 30 min) on the properties of steel fibres and SFRC, respectively. We tested two types of steel fibres (without coating or with brass-coating). Results of our experimental study indicated the following:

1. Pull out test were carried out on hooked end steel fibres with initial shape and with shape deformation. According to our tests the maximum pull out force was higher in case of fibres with shape deformation than in case of fibres with initial shape.

2. The compressive strength of the FRC specimens with steel fibres increases as mixing time increases. On the other hand the porosity of the SFRC decreases with the increase of the mixing time.
3. Longer mixing times resulted in a slight increase of the post-cracking residual flexural strength of FRC beams containing steel fibres. The main reason for this was the increased compressive strength and increased number of the deformed steel fibres as the mixing time increased.

5. ACKNOWLEDGEMENT

The authors gratefully acknowledge the possibility of using the digital microscope and the pull out test machine at the Department of Polymer Engineering (BME - Budapest University of Technology and Economics). We acknowledge specifically to dr. Bálint Morlin, dr. Salem G. Nehme, dr. Katalin Kopecskó, dr. Éva Lublóy, Viktor Hlavička, Sándor Sólyom and Lili Laczák for their help and advices.

6. REFERENCES

Aydın S. (2013): "Effects of fiber strength on fracture characteristics of normal and high strength concrete" Periodica Polytechnica Civil Engineering, Vol. 57, No. 2, pp. 191-200, DOI 10.3311/PPci.7174.

Balázs, G. L. (2012): "Fibres in Concrete Structures", "Section of the book: "Innovative Materials and Techniques in Concrete Construction" (Ed. Fardis, M. N.), Springer-Science+Business Media, Dordrecht, Heidelberg, London, New York, 2012, ISBN 978-94-007-1996-5, pp. 153-165. http://www.springer.com/us/book/9789400719965

Breitenbücher R., Meschke G., Song F., Zhan Y. (2014): "Experimental, analytical and numerical analysis of the pullout behaviour of steel fibres considering different fibre types, inclinations and concrete strengths", Structural Concrete, Vol. 15, No. 1, pp. 126–135.

Czoboly O., Balázs L. Gy. (2015-1): „Possible mechanical deterioration of fibres influenced by mixing in concrete", CONCRETE STRUCTURES, HU ISSN 2062-7904, online ISSN: 1586-0361, Vol. 16., pp. 18-23. (http://www.fib.bme.hu/folyoirat/cs/cs2015.pdf)

Czoboly O., Balázs L. Gy. (2015-2): „Can too long mixing time negatively influence properties of FRC?", Keynote presentation, 11 th Central European Congress on Concrete Engineering, (CCC2015), Innovative Concrete Technology in Practice, ISBN 978-3-9502387-2-3, Austria, Hainburg, 2015. 10. 01-02., (363p.), pp. 33-36.

Czoboly O., Balázs L. Gy. (2016): „Keverési idő hatása a szálerősítésű beton jellemzőire", XX. Nemzetközi Építéstudományi Konferencia, ÉPKO 2016, Erdélyi Magyar Műszaki Tudományos Társaság, ISSN 1843-2123, Csíksomlyó, 2016. 06. 01-05., pp. 40-43.

EN 14651:2005+A1:2007: Test method for metallic fibre concrete – Measuring the flexural tensile strength (limit of proportionality (LOP), residual), European Committee for Standardization, 17 p.

ERMCO (2012): „Guidance to fibre concrete, Properties Spetification and Practice in Europe", European Ready Mixed Concrete Organization, pp. 1-39.

Erdélyi A. (1993): "The toughness of steel fibre reinforced concretes", Periodica Polytechnica Civil Engineering. Vol. 37, No. 4, pp. 329–344.

Felekoglu B. (2014): "Effects of loading conditions and specimen thickness on the flexural behavior of fiber-reinforced cementitious composites", Periodica Polytechnica Civil Engineering, Vol. 58, No. 3, pp. 279–291, DOI: 10.3311/PPci.7486

Halvax K., Lublóy É. (2013-1): "Pull-out behaviour of steel fibres", Fibre Concrete 2013, Prague, Czech Republic, Sep. 12-13, 2013, pp. 1-10.

Halvax K., Lublóy É. (2013-2): "Investigation of steel fibers bond strength in mortar matrix", Pollack Periodica, Vol. 8, No. 3, pp. 101-110.

Kim D. J., Naaman A. E., El-Tawil S (2008): "Comparative flexural behavior of four fiber reinforced cementitious composites", Cement and Concrete Composites, Vol. 30, No. 10, pp. 917–928. DOI 10.1016/j.cemconcomp.2008.08.002.

Kovács, I., Balázs, G. L.,(2003): "Structural behaviour of steel fibre reinforced concrete", Journal of Structural Concrete, 2003/2, pp. 57-63.

Kovács, I., Balázs, G. L.,(2004): "Structural performance of steel fibre reinforced concrete", Book, Publ. Comp. of Budapest University of Technology and Economics, 2004, ISBN 963 410 822 3, 233 p http://fib.bme.hu/konyvek/steel-fiber-.pdf

Naaman A. E., Najm H. (1991): "Bond-Slip Mechanism of Steel Fibers in Concrete", ACI Materials Journal, March-April 1991, pp. 135-145.

Zhao G., Verstrynge E., di Prisco M., Vandewalle L. (2012): "Investigation on single fiber pullout and interfacial debonding mechanisms with acoustic emission techniques", 8th RILEM International Symposium on Fiber Reinforced Concrete: challenges and opportunities (BEFIB 2012), pp. 369-380.

Zile E., Zile O. (2013): "Effect of the fiber geometry on the pullout response of mechanically deformed steel fibers", Cement and Concrete Research, Vol. 44, No. 1, pp. 18-24.

Olivér Attila Czoboly (1988) Civil Engineer, PhD student (Department of Construction Materials and Technologies, Budapest University of Technology and Economics). His main fields of activities are experimental investigation and modelling of FRC structures, HPC, structural diagnostics, reconstruction of structures, fire resistance of concrete. He is member of ***fib*** and Hungarian Group of ***fib.*** He is the secretary of ***fib*** Commission 9 „Dissemination of knowledge".

György L. Balázs (1958), Civil Engineer, PhD, Dr.-habil., professor of structural engineering, head of Department of Construction Materials and Technologies. His main fields of activities are FRC, HSC, HPC, durability, sustainability and fire resistance. He is chairman of several commissions and task groups of ***fib***, like Com 9 Dissemination of knowledge, Honorary President of ***fib*** (he was President of ***fib*** for the period of 2011-2012). He is president of Hungarian Group of ***fib***, Editor-in-chief of the Journal "Concrete Structures".

SAND COATED CFRP REBARS – MODELLING OF BOND


Sándor Sólyom – György L. Balázs

In order to perform numerical or analytical analyses of reinforced concrete members including the interaction between concrete and reinforcement to determine for example the anchorage length, the bond stress-slip constitutive law is necessary.

Existing stress-slip laws of FRP (Fibre Reinforced Polymer) reinforcements are based on limited number of parameters only. Present study includes the description of an extensive experimental work, as well as an analytical part for modelling the bond behaviour of FRP rebars in plain and in fibre-reinforced concrete. Experimental parameters consisted of: (1) concrete strength, (2) type of fibres in concrete mixes (no fibres, steel, synthetic micro or synthetic macro polymer fibres), resulting 72 pull-out tests. Conclusions are drawn on bond behaviour and modelling by using the experimental parameters.

Keywords: FRP (Fibre Reinforced Polymer), carbon, sand coating, FRC, short fibres, bond behaviour, modelling of bond

1. INTRODUCTION

In recent years, FRP materials have become as an acceptable construction material for both new constructions and for the rehabilitation and strengthening of existing structures. FRPs offer better resistance to environmental agents as well as high stiffness-to-weight and strength-to-weight ratios when compared to conventional construction materials [Balázs and Borosnyói (2001a); Balázs and Borosnyói (2001b); Borosnyói and Balázs (2002); Borosnyói and Balázs (2003); Borosnyói and Balázs (2008); Balázs (2008); Benmokrane, Ali and Mohamed (2016)] . One of the main advantages of FRP reinforcing materials is their excellent corrosion resistance (Baena, Torres, Turon and Barris (2009); Lublóy, Balázs, Borosnyói and Nehme (2005)).

Numerous studies can be found in literature underlining the significance of the bond behaviour of reinforcement in concrete. Yet, in case of FRP rebars there are still open issues owing to the high number of parameters which affect the bond.

Recently, various experimental studies have been conducted to investigate the bond strength of FRP rebars in concrete. The influence of a variety of parameters is investigated, such as embedment length, concrete strength, rebar diameter, concrete cover, surface treatment, etc. on the bond behaviour of FRP rebars [Balázs and Borosnyói (2000); Guadagnini, Pilakoutas, Waldron and Achillides (2005); Pilakoutas, Guadagnini, Neocleous and Taerwe (2007); Weber (2005); Gudonis, Kacianauskas, Gribniak, Weber, et al. (2014); Haffke, Veljkovic, Carvelli and Pahn (2015); Veljkovic, Haffke, Carvelli and Pahn (2016)] . On the other hand, less attention was payed to determine analytically the bond stress-slip constitutive law for FRP rebars, which is essential for finite element analysis of FRP reinforced concrete structures (Sólyom and Balázs 2016).

Effect of short fibres, mixed into the concrete matrix, is still an open issue with contradictory results reported in literature Belarbi and Wang (2004); Won, Park, Kim, Lee, et al. (2008); Wang and Belarbi (2010); Mak (2011); Ametrano (2011); Mazaheripour, Barros, Sena-Cruz, Pepe, et al. (2013); Ding, Ning, Zhang, Pacheco-Torgal, et al. (2014); Yoo, Kwon, Park and Yoon (2015). It can be concluded from the cited papers, that there are still inconsistencies in the available results and further research is needed.

Mixing short fibres into the concrete matrix represents a possible way to confine the concrete in compression zone and provide it with additional strain capacity. Available studies show that FRC has improved tensile strength, strain capacity and ductility over normal concrete (Czoboly and Balázs 2015).

In this paper two bond stress-slip models will be assessed. They show how the parameters of the models change according to the studied bond influencing factors, namely: short fibre type and concrete compressive strength.

2. EXPERIMENTAL PROCEDURE

The paper aims to present analytical approaches to the bond stress-slip behaviour, however basic information about the experimental work is given also for better understanding, more details are in Ref. Sólyom, Balázs and Nehme (2016).

Pull-out specimens with cubic shape and 150 mm size were prepared using metallic moulds. The bars were vertically placed in the centre of the moulds with the prepared 5Ø bond length (Ø – nominal rebar diameter).

Concrete specimens (*Fig.1*, right) were demoulded one day after concrete pouring, kept under laboratory ambient conditions. The concrete cubes, marked and placed under water for 6 days. After this period of time the concrete specimens were taken out of water and kept in laboratory air until testing (mixed curing was applied).

Specimens were tested at age of 28 days. Pull-out specimens were placed into a metallic frame and the FRP rebars were gripped by the test machine (*Fig.1*, left). The gripped side is

considered as the loaded end of the test specimen. Relative displacement between the FRP rebar and concrete was measured with three Linear Variable Differential Transducers (LVDT) at the loaded end. At the other end, usually referred to as unloaded or free end, the slip was measured by one LVDT. Displacement controlled test was selected on the loading machine (Instron 600 kN) to capture post-peak behaviour. The load was applied to the rebar at a rate of 1 mm/min and measured with the electronic load cell of the testing equipment. An automatic data acquisition system was used to record the data transmitted by LVDTs. For each configuration three nominally identical specimens were tested.

Six different concrete grades were used (mean values of concrete compressive strength ranging between 27.7 and 91.9 N/mm^2 measured on 150 mm cubic specimens, mean values of three nominally identical specimens) to study the influence of concrete strength on bond development between FRP bars and concrete. Three different type of FRP bars were used: carbon, glass and basalt. However, in this paper the focus is only given to the sand coated CFRP rebars with diameter of 9.5 mm (*Fig.1*, middle). Three different short fibres were added to the concrete matrix: steel, synthetic micro and synthetic macro polymer fibres.

The symbols of concrete mixes consist of 3 characters, the first C or S stands for traditional and self-compacting concrete (SCC), respectively. The second character represents the concrete strength, the higher the value of the character, the higher the concrete strength is. The third character mix refers to the type of short fibres in concrete, namely: 1 represents that no short fibres are mixed to concrete, while 2 refers to synthetic macro, 3 to steel and 4 to synthetic micro fibres. For example C21 represents traditional concrete prepared according to composition C2 without any short fibres, while S13 stands for self-compacting concrete prepared according to composition S1 with steel fibres.

Concrete mixes were prepared using quartz sand (0/4 mm fraction) and coarse aggregate (4/8 and 8/16 mm fractions). CEM II/B-S 42.5 N cement was used for all mixes. The only change in concrete mixt design in case of traditional concrete (C0 to C3) consist of the amount of cement used: 250, 300, 350 and 400 kg/m^3, respectively. In case of SCC (S1 and S2), limestone was added additionally. Cement dosage was 400 and 420 kg/ m^3, respectively.

Fig.1: Left: pull-out test setup; middle: sand coated CFRP with 5Ø bond length (Ø - rebar diameter); right: pull-out specimens before demolding

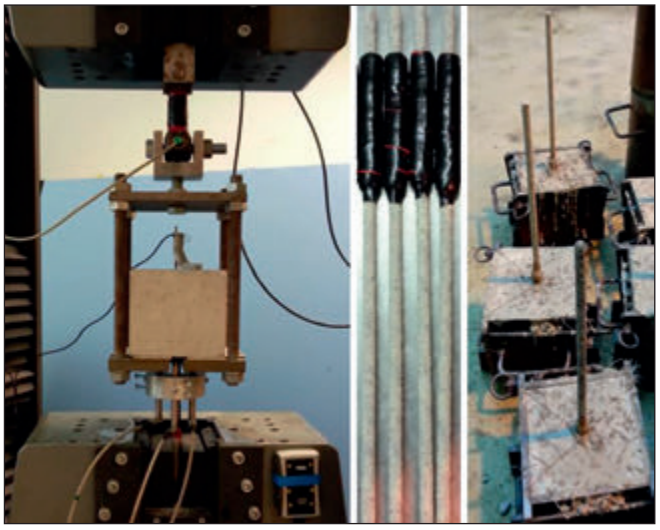

Table 1: Symbols of concrete mixes (with or without fibres)

Concrete type	No fibres	Synthetic macro fibres	Steel fibres	Synthetic micro fibres
Conventional concrete	C01	C02	C03	C04
	C11	C12	C13	C14
	C21	C22	C23	C24
	C31	C32	C33	C34
Self-compacting concrete	S11	S12	S13	S14
	S21	S22	S23	S24

3. MODELLING OF BOND

3.1. Bond stress and slip relationship

Bond between reinforcement and concrete is typically described, when modelling it analytically, by means of a constitutive bond stress-slip (τ_b - s) relationship. Bond stress is an average value of the shear stress acting along the surface of the bar-concrete interface while the slip is the relative displacement between rebar and concrete. The bond stress-slip diagram is usually compounded of two branches, ascending and descending, also referred as pre-peak and post-peak phases, where the peak is the point where the highest bond stress is observed *(Fig. 2)*.

At the beginning of ascending part the stresses are transferred between concrete and FRP rebars through chemical adhesion (slip is null). After adhesion breaks down, the bond stresses are transferred by mechanical interlock and friction. Depending on the surface characteristics of the rebars, the above mentioned phases of the bond stress transfer can vary. Furthermore, they can even become negligible for some special surface types. In case of FRP rebars with sand coated surfaces, owing to the brittle nature of the bond failure (by shearing off of the rebar surface), usually the bond behaviour can be analytically describe by only the first (ascending) part of the bond stress-slip diagram (*Fig. 2*).

Constitutive bond stress-slip (τ_b - s) relationship that can be introduced in the solution of problems, such as the calculation of the development length, crack widths and spacing (Cosenza, Manfredi and Realfonzo 2002) are still not defined in the available literature, even though high effort has been put by numerous researcher groups to propose an appropriate formulae.

The available formulae that do exist for FRP rebars are intended to establish a general law, which is validated by determining its parameters by curve fitting (Ametrano 2011).

In the following subsections two of the most often used bond stress-slip relationships will be presented.

Fig. 2: Typical bond stress-slip relationship for FRP bars (after Vint, 2012)

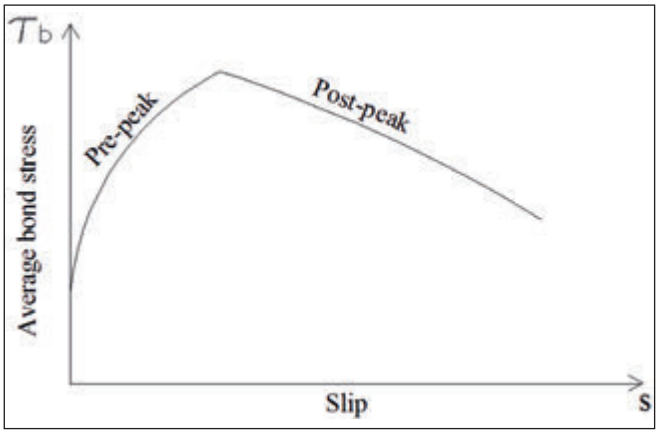

3.2. Modified Bertero, Popov and Eligehausen model (mBPE model)

One of the most commonly used model is the mBPE. It is based on the well-known bond stress-slip analytical law for deformed steel bars failing by rebar pull-out proposed by Eligehausen et al. (1983). Modification consist of omitting the second branch of the diagram (constant bond strength plateau), since it was observed that it is not present (*Fig. 3*) in case of FRP rebar [Cosenza, Manfredi and Realfonzo (1995); Cosenza, Manfredi and Realfonzo (1997); Focacci, Nanni and Bakis (2000); Pecce, Manfredi, Realfonzo and Cosenza (2001)]. The mBPE model has the following formulae (Eqs. 1, 2 and 3) for the different branches:

• ascending branch ($0 \le s \le s_m$, where s_m is the slip corresponding to the maximum bond stress $\tau_{b,max}$)

$$\tau_b = \tau_{b,max}\left(\frac{s}{s_m}\right)^{\alpha} \quad (1)$$

• descending branch ($s_m \le s \le s_3$)

$$\tau_b = \tau_{b,max}\left[1 - p\left(\frac{s}{s_m} - 1\right)\right] \quad (2)$$

• third branch ($s_3 \le s$)

$$\tau_b = \tau_{b,3} \quad (3)$$

where α and *p* are experimental parameters.
The third branch ($s_3 \le s$) is horizontal and has a value representing the friction component (residual bond strength) τ_3. The modified BPE model appears to be more suitable for FRP rebars than the original BPE model (*Fig. 3*).

3.3. Cosenza, Manfredi and Realfonzo model (CMR model)

Given that most of the structural problems are to be dealt in serviceability limit state, modelling of the bond stress-slip curve can be done by a formulae for the ascending branch only. Furthermore, in case of some surfaces types (i.e.: sand coated) of FRP rebars, owing to the brittle bond failure mode, the ascending branch is able to model the whole bond behaviour up to failure. The studied rebar type in this paper possesses a surface type which usually cause brittle bond failure (*Fig. 4*).

A new model has been proposed by Cosenza, Manfredi and Realfonzo (1995) for the ascending branch of the stress-slip diagram. This model represents an alternative to the mBPE model and is defined by the following equation (Eq. 4):

Fig. 3: *Modified BPE (mBPE) model*

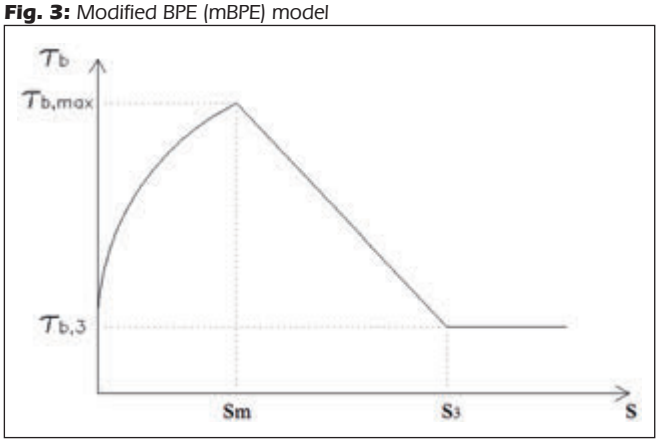

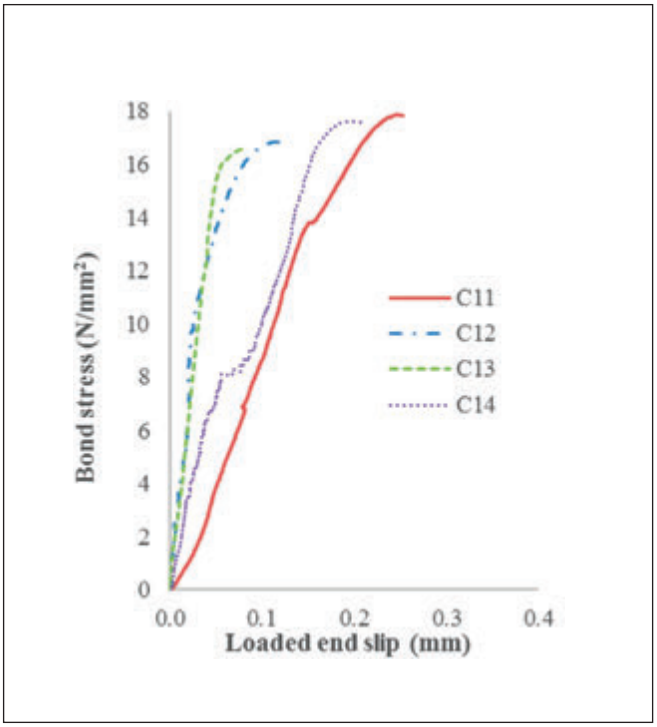

Fig. 4: *Experimental bond stress-slip curves for sand coated CFRP rebars, C1 concrete composition (for symbols of concrete mixes see Table 1)*

$$\frac{\tau_b}{\tau_{b,max}} = \left(1 - e^{-\frac{s}{s_r}}\right)^{\beta} \quad (4)$$

Where $\tau_{b,max}$ is peak bond stress while s_r and β are experimental parameters.

3.4. Calculating the bond strength and adherent slip

There are numerous standards, guidelines or papers which contain formulae for bond strengths including, but not limited to: ACI 440.1R (2015), CAN/CSA-S806-02 (2002); CAN/CSA-S6-06 (2006) and papers Ehsani, Saadatmanesh and Tao (1996); Tighiouart, Benmokrane and Gao (1998); Lee, Kim, Kim, Yi, et al. (2008); Ametrano (2011); Lee, Kim, Kim, Lee, et al. (2013); Pour, Alam and Milani (2016); Yan, Lin and Yang (2016).

In this paper only two formulae will be presented, which most agree with the experimental results, namely: ACI 440.1R (Eq. 5) and CSA-S806 (Eq. 6).

$$\frac{\tau_{b,max}}{0.083\sqrt{f_c}} = 4.0 + 0.3\frac{c}{\phi} + 100\frac{\phi}{l_b} \quad (5)$$

where *c* is the lesser of the cover to centre of the bar or one-half of the centre-on-centre spacing of the bars being developed (mm), Ø is the nominal rebar diameter (mm), l_b the embedment length (mm) and f_c is the concrete compressive strength (N/mm²).

CSA-S806 gives the following formula (Eq. 6):

$$\tau_{b,max} = \frac{c\sqrt{f_c}}{1.15(K_1K_2K_3K_4K_5)\pi\phi} \quad (6)$$

where c = smallest of the distance from the closest concrete surface to the centre of the bar being developed or two-thirds the centre-on-centre spacing of the bars being developed (mm), $c \le Ø$; f_c is the compressive strength of concrete (N/mm²);

K_1 = bar location factor (1.3 for horizontal reinforcement placed so that more than 300 mm of fresh concrete is cast below the bar; 1.0 for all other cases); K_2 = concrete density factor (1.3 for structural low-density concrete; 1.2 for structural semi-low-density concrete; 1.0 for normal density concrete); K_3 = bar size factor (0.8 for $A_b \leq 300$ mm^2; 1.0 otherwise); K_4 = bar fibre factor (1.0 for CFRP and GFRP; 1.25 for AFRP); K_5 = bar surface profile factor (1.0 for surface roughened or sand coated or braided surfaces; 1.05 for spiral pattern surfaces or ribbed surfaces; 1.8 for indented surfaces).

In *Table 2* along with the bond strength values calculated according to ACI 440.1R and CSA S806 (columns 5 and 8) experimental bond strength (column 2) and slip values measured both at loaded (column 3) and free ends (column 4) are also presented.

It can be observed by looking at *Table 2* that the calculated bond strength values are in reasonable correlation with the experimental results. To provide better comparison between experimental and calculated bond strength, the ratio of them (columns 6 and 9) are formed. Furthermore, to be able to draw a general conclusion about the agreement of the bond strength values calculated with various equations, the absolute value of differences are also created in columns 7 and 10 of *Table 2*. The averages of these differences are presented in the last row of *Table 2*.

Slip values could be calculated also (see i.e.: Quayyum 2010), however this is not addressed in current paper. When defining the s_m values for mBPE model the experimental results will be used.

4. RESULTS AND DISCUSSION

In this paragraph the attention is given to the results of analytical modelling of bond behaviour, more specifically curve fitting of parameters of two already available analytical models: modified BPE (mBPE) (Cosenza, Manfredi and Realfonzo 1996) and CMR (Cosenza et al., 1995) models. More information about the experimental procedure and results can be found in authors' previous paper [Sólyom and Balázs (2016)], furthermore a similar study on modelling of helically wrapped BFRP rebars was also published [Sólyom, Balázs and Nehme (2016)].

Table 3 shows the results of curve fitting procedure for the selected two analytical models in case of sand coated CFRP rebars. The agreement between the experimental ($\tau_{b,exp}$) and the corresponding analytical predictions (τ_b) for each analytical model was evaluated by calculating the difference (standard er-

Table 2: *Experimental and calculated results for bond strength and slip values*

Mix	Experimental results			Calculated results based on Eqs. 5 and 6					
	Average bond strength	Loaded end slip at $\tau_{b,max}$	Free end slip at $\tau_{b,max}$	$\tau_{b,max}$ (ACI)	$\tau_{b,exp}$ / $\tau_{b,ACI}$	$\lvert \tau_{b,exp}-\tau_{b,ACI} \rvert$	$\tau_{b,max}$ CSA S806-02	$\tau_{b,exp}$ / $\tau_{b,CSA\ S806}$	$\lvert \tau_{b,exp}-\tau_{b,S806} \rvert$
	(N/mm^2)	(mm)	(mm)	(N/mm^2)	(-)	(N/mm^2)	(N/mm^2)	(-)	(N/mm^2)
1	2	3	4	5	6	7	8	9	10
C01	14.92	0.16	0.10	11.45	1.30	3.47	14.34	1.04	0.57
C02	16.10	0.43	0.16	12.49	1.29	3.62	15.65	1.03	0.45
C03	13.84	0.19	0.08	11.60	1.19	2.24	14.53	0.95	0.70
C04	12.22	0.20	0.10	12.44	0.98	0.22	15.59	0.78	3.37
C11	19.31	0.23	0.10	13.82	1.40	5.49	17.32	1.12	1.99
C12	16.13	0.24	0.07	14.91	1.08	1.22	18.69	0.86	2.56
C13	16.56	0.14	0.05	14.18	1.17	2.38	17.77	0.93	1.21
C14	18.24	0.19	0.08	13.77	1.32	4.47	17.26	1.06	0.98
C21	15.57	0.26	0.05	14.96	1.04	0.62	18.75	0.83	3.17
C22	16.01	0.20	0.01	14.92	1.07	1.10	18.69	0.86	2.68
C23	16.95	0.14	0.06	14.80	1.15	2.16	18.54	0.91	1.59
C24	17.21	0.36	0.06	15.07	1.14	2.14	18.89	0.91	1.67
C31	15.95	0.19	0.05	15.52	1.03	0.43	19.45	0.82	3.50
C32	16.57	0.29	0.00	16.58	1.00	0.01	20.78	0.80	4.21
C33	18.39	0.21	0.04	17.39	1.06	1.00	21.80	0.84	3.40
C34	17.82	0.42	0.05	17.23	1.03	0.59	21.59	0.83	3.77
S11	16.30	0.26	0.04	17.83	0.91	1.54	22.35	0.73	6.05
S12	19.29	0.48	0.05	18.43	1.05	0.85	23.10	0.83	3.81
S13	16.14	0.32	0.06	17.49	0.92	1.35	21.91	0.74	5.77
S14	14.49	0.66	0.05	17.68	0.82	3.19	22.16	0.65	7.66
S21	15.19	0.15	0.04	20.87	0.73	5.68	26.15	0.58	10.96
S22	16.35	0.23	0.04	20.96	0.78	4.61	26.27	0.62	9.92
S23	16.38	0.15	0.05	21.07	0.78	4.69	26.41	0.62	10.03
S24	16.40	0.24	0.05	20.59	0.80	4.18	25.80	0.64	9.39
					Average:	*2.38*		*Average:*	*4.14*

ror) for each registered slip values (s) by using equation (Eq. 7), and are presented in columns 5 and 12:

$$SE = \sqrt{\frac{\sum_{i=1}^{n}\left(\tau_{b,i}-\tau_{b,exp,i}\right)^2}{n}} \quad (7)$$

where *n* is the number of experimental values registered during the pull-out test in case of one specimen, while τ_b is calculated according to the assessed analytical model.

Three specimens were tested for each concrete mix, the average of these values are presented in *Table 3* columns 2, 6 and 9. In columns 4, 8 and 11 the standard deviation of the three values are presented calculated by the following formula (Eq. 8):

$$SD = \sqrt{\frac{\sum_{i=1}^{n}\left(\alpha-\alpha_{avg}\right)^2}{n-1}} \quad (8)$$

To observe the effect of concrete strength on the curve fitting parameters, the mean values for each concrete composition are calculated and presented in columns 3, 7 and 10.

Analysing *Table 3* and *Fig. 5-7* the following observations can be made:

mBPE model (ascending branch), parameter α:

- Slightly increases with the addition of short fibres (some exceptions apply, i.e.: S2 concrete composition), which in turn represents a less stiff bond stress-slip diagram. As α increases the ascending part of the diagram is approaching to a linear function.
- The highest increase of α is in case of synthetic micro and steel fibres, *Table 3*, column 2.
- Slightly increases with the increase of the strength of concrete, which in turn represents a less stiff bond stress-slip curve, *Fig. 5* and *Table 3*, columns 2 and 3.

CMR model, parameter β:

- Slightly increases with the increase of the concrete strength (outlier: S2), which represents a stiffness decrease of the bond stress-slip curve, *Fig. 6* and *Table 3*, columns 6 and 7. This observation is in agreement with the findings for mBPE model. However, there are no clear tendencies which fibres provide the highest increase of β.
- No clear tendency for the effect of short fibres can be observed in *Fig. 6* and *Table 3*, column 6.

CMR model, parameter s_r:

- If not taking into consideration the results which seem outliers, than the concrete strength increase has no considerable effect on this parameter (*Fig. 7* and *Table 3*, column 14).
- In most cases increases with the addition of short fibres, which represents a less stiff bond stress-slip curve and lower bond strength values. The highest increase is achieved with synthetic macro fibres, *Fig. 7* and *Table 3*, column 9.

5. PROPOSSED PARAMETERS FOR BOND STRESS-SLIP MODELS

In this section the aim is to define relationships among the studied parameters (α, β and s_r) and concrete compressive strength as well as the type of short fibres. Concrete compressive strength is chosen instead of the tensile strength, as parameter.

Table 3: Results of parameter fitting of modified BPE and CMR models

Mix	mBPE model				CMR model						
	α	α (Avg.)	SD	SE	β	β (Avg.)	SD	s_r	s_r (Avg.)	SD	SE
1	2	3	4	5	6	7	8	9	10	11	12
C01	0.39	0.57	0.09	1.02	0.73	1.29	0.25	0.07	0.07	0.03	0.87
C02	0.63		0.14	0.94	1.80		0.76	0.12		0.05	0.63
C03	0.59		0.09	0.53	1.05		0.14	0.06		0.03	0.38
C04	0.67		0.01	1.31	1.59		0.00	0.04		0.00	0.44
C11	0.55	0.57	0.10	0.38	1.01	1.31	0.28	0.09	0.10	0.02	0.25
C12	0.57		0.02	1.14	1.71		0.05	0.06		0.03	0.47
C13	0.57		0.12	0.68	1.35		0.68	0.11		0.03	0.38
C14	0.60		0.04	0.65	1.16		0.10	0.15		0.05	0.33
C21	0.83	0.88	0.09	0.90	2.46	2.60	1.08	0.08	0.09	0.04	0.65
C22	1.00		0.00	1.67	2.49		1.27	0.12		0.03	1.93
C23	0.77		0.21	0.79	2.11		0.87	0.05		0.00	0.43
C24	0.93		0.08	0.99	3.36		2.07	0.12		0.03	0.85
C31	0.84	0.89	0.14	0.96	2.13	2.77	1.14	0.06	0.08	0.03	0.87
C32	0.92		0.08	1.24	1.91		0.47	0.12		0.01	1.28
C33	0.81		0.04	1.15	2.42		0.15	0.06		0.01	0.59
C34	1.00		0.00	1.50	4.61		0.53	0.09		0.02	0.87
S11	0.87	0.91	0.07	1.20	3.16	2.89	0.60	0.07	0.16	0.03	0.64
S12	0.90		0.01	0.63	1.56		0.42	0.30		0.10	0.95
S13	0.93		0.10	0.77	3.84		1.64	0.09		0.01	0.61
S14	0.94		0.09	0.72	2.99		1.09	0.18		0.01	0.64
S21	0.95	0.87	0.05	1.26	3.56	2.35	0.17	0.04	0.08	0.01	0.65
S22	0.92		0.07	0.87	2.67		0.01	0.13		0.04	0.86
S23	0.65		0.01	0.54	1.33		0.20	0.07		0.01	0.61
S24	0.95		0.05	1.07	1.84		0.27	0.07		0.01	0.63
Ave.	*0.78*				*2.20*			*0.10*			

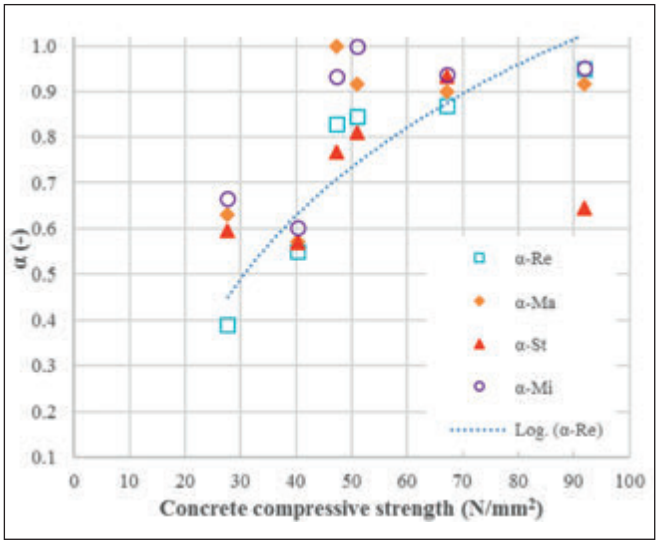

Fig. 5: Parameter α for mBPE model (each symbol represents an average value of three specimens). Re – reference concrete (no short fibres) and concrete with synthetic macro (Ma), steel (St) or synthetic micro (Mi) fibres

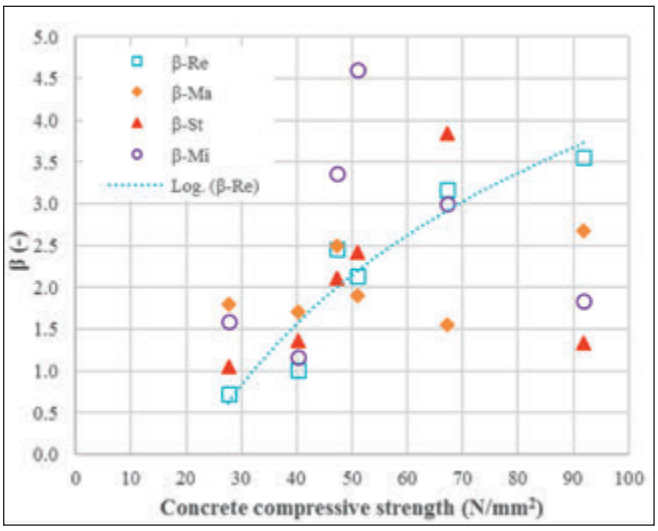

Fig. 6: Parameter β for CMR model (each symbol represents an average value of three specimens). Re – reference concrete (no short fibres) and concrete with synthetic macro (Ma), steel (St) or synthetic micro (Mi) fibres

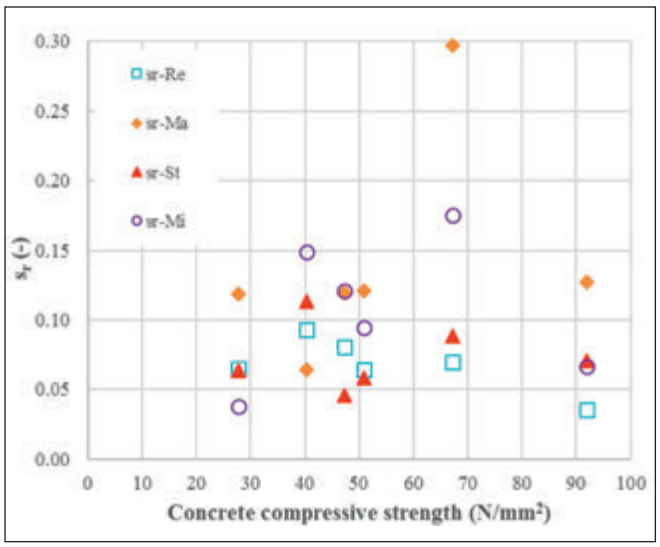

Fig. 7: Parameter s_r for CMR model (each symbol represents an average value of three specimens). Re – reference concrete (no short fibres) and concrete with synthetic macro (Ma), steel (St) or synthetic micro (Mi) fibres

The authors are aware of the papers available in literature stating that the (compressive) strength of concrete should not affect the bond strength of FRP rebars as long as the failure happens due to failure of the surface of the rebar (i.e.: Muñoz 2010). Even though, during the experiments in all of the cut specimens (after failure) shearing off of the rebar surface was observed, increase in bond strength was achieved by increasing the concrete strength.

Analysing the curve fitting parameters presented in *Table 3* the following relationships can be given:

$$\propto = 0.5\,ln(f_c) - 1.15 \quad (9)$$

$$\beta = 2.60\,ln(f_c) - 8.0 \quad (10)$$

$$s_r = -0.001 f_c + 0.126 \quad (11)$$

where f_c is the compressive strength of concrete (N/mm²) (mean value in experiments).

The effect of short fibres on the studied parameters can be observed in *Table 4*. In columns 3, 5 and 7 the ratio between the values of parameters for reference (plain) concrete to fibre reinforced concrete are presented. For example: α increases with 11% and 15% when using synthetic macro and synthetic micro fibres respectively, while addition of steel fibres have no considerable effect on parameter α. Addition of short fibres to concrete has no considerable effect on parameter β.

It is important to mention, that owing to the different natures (in many mechanical and physical properties) of FRP rebars these recommendations are only valid for the given materials used. Care should be taken before directly applying the above conclusions to other rebars or short fibres.

Table 4: Average values of parameters after curve fitting of modified BPE and CMR models (see Eqs. 1 and 4)

Type of fibres added to concrete matrix	α	$\alpha_{plain}/\alpha_{fibres}$	β	$\beta_{plain}/\beta_{fibres}$	s_r	$s_{r,plain}/s_{r,fibres}$
1	2	3	4	5	6	7
Plain concrete (no fibres)	0.74	1.0	2.12	1.0	0.07	1.0
Synthetic macro fibres	0.82	1.113	2.12	0.998	0.11	1.478
Steel fibres	0.73	0.994	2.15	1.015	0.08	1.055
Synthetic micro fibres	0.85	1.148	2.19	1.032	0.11	1.439

In *Fig. 8* a comparison of experimental to analytical result, both for mBPE and CMR models, are presented for the C2 concrete composition. The analytical bond stress-slip curves are defined using the above formulae (Eqs. 1 and 4). Parameters were calculated using the mean concrete compressive strength for C2 concrete composition, 47.2 N/mm², α=0.77 (Eq. 9), β=2.02 (Eq. 10) and s_r=0.12 (Eq.11). Bond strength, necessary for models, was calculated using Eq. 5, while the slip corresponding to the bond strength was taken from experimental data. The effect of short fibres mixed to concrete on the curve fitting parameter can be accounted with the help of *Table 4*. A relatively good agreement between the experimental, mBPE and CMR models can be observed.

6. CONCLUSIONS

In the present paper the interfacial bond behaviour between sand coated CFRP rebars and six different concrete compositions have been analysed. Since the experimental results have been presented in a previous paper, herein the focus was given to analytical modelling, more specifically parameter fitting of two already available analytical models, namely: modified

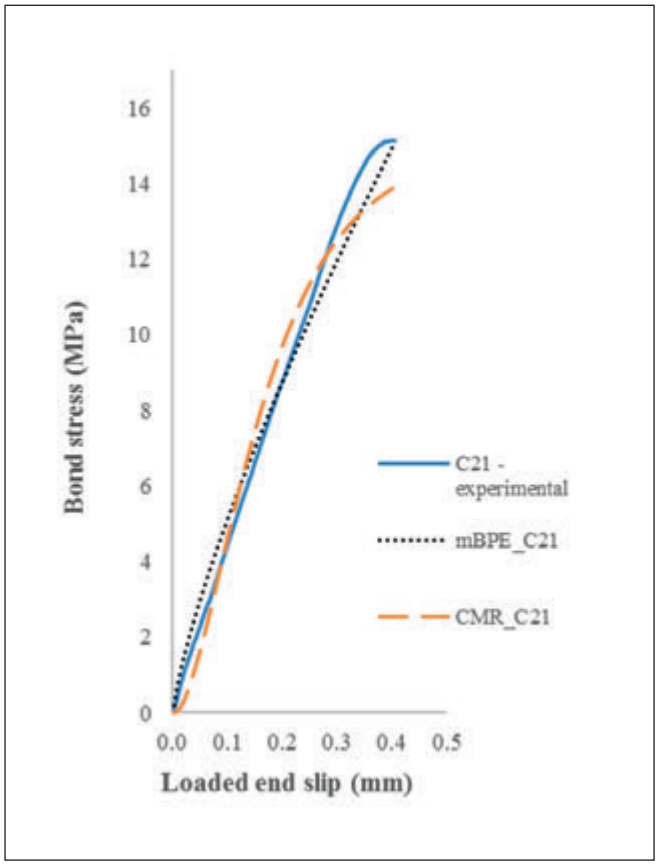

Fig. 8: Comparison of experimental and analytical bond stress-slip curves

BPE (Bertero, Popov and Eligehausen) and CMR (Cosenza, Manfredi and Realfonzo) models. Results of 24 mixes (72 pull-out tests) were considered. Studied parameters: concrete compressive strength and short fibre type. Based on the results of the presented study the conclusions are the following.

Parameter α (mBPE model, Eq. 1) increases with the increase of the compressive strength of concrete and with the addition of short fibres. The highest increase is in case of synthetic macro and micro fibres, while in case of steel fibres there is no considerable effect. Increase of α represents a less stiff bond stress-slip curve.

Similarly, parameter β (CMR model, Eq. 4) slightly increases with the increase of the compressive strength. Observations for the assessed two models are in agreement.

Values for the parameters (α, β and s_r) were proposed depending on the concrete compressive strength and short fibre type.

Care should be taken before directly applying the above conclusions to other rebars or short fibres owing to different natures (in many mechanical and physical properties) of FRP rebars available on market. The presented values for curve fitting parameters are only valid for the materials used in this research.

7. ACKNOWLEDGEMENTS

The authors gratefully acknowledge the financial support of European Network for Durable Reinforcement and Rehabilitation Solutions (endure), Networks for Initial Training (ITN), Seventh Framework Programme of the European Union (Grant: PITN-GA-2013-607851). Help and advices are also acknowledged from Dr. Salem Georges Nehme, Olivér Attila Czoboly and András Jakab.

8. REFERENCES

ACI Committee 440,(2015), "*Guide for the Design and Construction of Structural Concrete Reinforced with FRP Bars (ACI 440.1R-15)*", Farmington Hills, MI.

Ametrano, D.,(2011), "*Bond characteristics of glass fibre reinforced polymer bars embedded in high performance and ultra-high performance concrete*". Ryerson University.

Baena, M., Torres, L., Turon, A. & Barris, C.,(2009), "Experimental study of bond behaviour between concrete and FRP bars using a pull-out test". *Composites Part B: Engineering*, 40(8), pp.784–797. Available at: http://dx.doi.org/10.1016/j.compositesb.2009.07.003.

Balázs, G.L.,(2008),"Innovative materials and technologies for concrete stuctures".In *Betontag*. Wien: 24-25 April 2008, pp. 183–186.

Balázs, G.L. & Borosnyói, A.,(2001a),"Long-term behavior of FRP".In *ASCE Proceedings of the Int. Workshop Composites in Construction A Reality*. Capri, Italy: 20-21 July 2001, pp. 84–91.

Balázs, G.L. & Borosnyói, A.,(2001b),"New construction materials in bridges". In I. Fi, L. Gáspár, & G. L. Balázs, eds. *"Roads and Bridges in Europe", 8th Int. Road Conference*. Budapest-Esztergom: 21-23 May 2001.

Balázs, G.L. & Borosnyói, A.,(2000), "Non-metallic (FRP) reinforcement for bridge construction (in Hungarian)". *Vasbetonépítés*, 2, pp.45–52. Available at: http://fib.bme.hu/kiadvanyok.html.

Belarbi, A. & Wang, H.,(2004),"Bond-slip response of FRP reinforcing bars in fiber reinforced concrete under direct pullout".In *Int. Conf. on Fiber Comp., High Performance Concretes and Smart Materials*. pp. 1–10. Available at: http://transportation.mst.edu/media/research/transportation/documents/c7.pdf.

Benmokrane, B., Ali, A.H. & Mohamed, H.M.,(2016),"Mechanical and durability characteristics of Glass-FRP bars with different types or resins".In *7th International Conference on Advanced Composite Materials in Bridges and Structures*. Vancouver.

Borosnyói, A.,(2014), "Use of corrosion resistant Fibre Reinforced Polymer (FRP) reinforcements for the substitution of steel bars in concrete.". *Korróziósfigyelő*, 54(1), pp.3–15.

Borosnyói, A. & Balázs, G.L.,(2002), "Bond of Non-mettallic (FRP) reinforcements (in Hungarian)". *Vasbetonépítés*, IV.(4), pp.114–112. Available at: http://fib.bme.hu/kiadvanyok.html.

Borosnyói, A. & Balázs, G.L.,(2003), "Bond on non-metallic (FRP) reinforcement in cocnrete". *Concrete Structures*, 4, pp.76–83. Available at: http://fib.bme.hu/concrete-structures.html.

Borosnyói, A. & Balázs, G.L.,(2008),"Precast Girders Prestressed with CFRP Wires – Hungarian Experiences".In *ACI Special Publication, SP-245—5*. pp. 73–94.

CAN/CSA-S6-06,(2006), "*Canadian Highway Bridge Design Code*", Mississauga, Ontario, Canada.

CAN/CSA-S806-02,(2002), "*Design and construction of building components with fiber reinforced polymers.*", Toronto: Canadian Standard Association.

Cosenza, E., Manfredi, G. & Realfonzo, R.,(1995),"Analytical modelling of bond between FRP reinforcing bars and concrete".In L. Taerwe, ed. *Non-metalic (FRP) reinforcement for concrete structurestalic (FRP) reinforcement for concrete structures*. London: E & FN Spon, pp. 164–171.

Cosenza, E., Manfredi, G. & Realfonzo, R.,(1997), "Behavior and Modeling of Bond of FRP Rebars to Concrete". *Journal of Composites for Construction*, (May), pp.40–51.

Cosenza, E., Manfredi, G. & Realfonzo, R.,(1996),"Bond character- istics and anchorage length of FRP rebars".In M. EI-Badry, ed. *Proc., 2nd Int. Cant on Advanced Compos. Mat. in Bridge Struct.*

Cosenza, E., Manfredi, G. & Realfonzo, R.,(2002), "Development length of FRP straight rebars". *Composites Part B: Engineering*, 33(7), pp.493–504.

Czoboly, O. & Balázs, G.L.,(2015),"Can too long mixing time negatively influence properties of FRC?".In *11th CCC Conference*. Hainburg, Austria.

Ding, Y., Ning, X., Zhang, Y., Pacheco-Torgal, F., et al.,(2014), "Fibres for enhancing of the bond capacity between GFRP rebar and concrete". *Construction and Building Materials*, 51, pp.303–312. Available at: http://dx.doi.org/10.1016/j.conbuildmat.2013.10.089.

Ehsani, M.R., Saadatmanesh, H. & Tao, S.,(1996), "Design Recommendations For Bond Of GFRP Rebars To Concrete". *Journal of Structural Engineering*, pp.247–254.

Focacci, F., Nanni, A. & Bakis, C.E.,(2000), "Local bond-slip relationship for FRP reinforcement in concrete". *Journal of Composites for Construction*, (February), pp.24–31.

Guadagnini, M., Pilakoutas, K., Waldron, P. & Achillides, Z.,(2005), "Tests for the evaluation of bond properties of FRP bars in concrete". , pp.343–350.

Gudonis, E., Kacianauskas, R., Gribniak, V., Weber, A., et al.,(2014), "Mechanical Properties of the Bond Between GFRP Reinforcing Bars and Concrete". *Mechanics of Composite Materials*, 50(4), pp.457–466. Available at: http://link.springer.com/10.1007/s11029-014-9432-0.

Haffke, M.M., Veljkovic, A., Carvelli, V. & Pahn, M.,(2015),"Experimental investigation of the static bond of GFRP rebar and concrete".In *SMAR 2015 - The Third Conference on Smart Monitoring, Assessment and Rehabilitation of Structures*. Antalya, Turkey, pp. 1–8.

Lee, J.Y., Kim, T.Y., Kim, T.J., Yi, C.K., et al.,(2008), "Interfacial bond strength of glass fiber reinforced polymer bars in high-strength concrete". *Composites Part B: Engineering*, 39(2), pp.258–270.

Lee, Y.H., Kim, M.S., Kim, H., Lee, J., et al.,(2013), "Experimental study on bond strength of fiber reinforced polymer rebars in normal strength concrete". *Journal of Adhesion Science and Technology*, 27(5–6), pp.508–522. Available at: http://www.tandfonline.com/doi/abs/10.1080/01694243.2012.687554.

Lublóy, É., Balázs, G.L., Borosnyói, A. & Nehme, S.G.,(2005),"Bond of CFRP wires under elevated temperature".In *Bond Behaviour of FRP in Structures*. 7-9 Dec. 2005, pp. 163–167. Available at: http://www.iifc-hq.org/proceedings/BBFS_2005/Basic Bond Mechanisms/Bond of CFRP Wires Under Evaluated Temperature.pdf.

Mak, C.,(2011), "*Experimental and Theoretical Investigation of Glass Fibre Reinforced Polymer Tension Lap Splices in Ultra High Performance Concrete*". Ryerson University.

Mazaheripour, H., Barros, J.A.O., Sena-Cruz, J.M., Pepe, M., et al.,(2013), "Experimental study on bond performance of GFRP bars in self-compacting steel fiber reinforced concrete". *Composite Structures*, 95, pp.202–212. Available at: http://dx.doi.org/10.1016/j.compstruct.2012.07.009.

Muñoz, M.B.,(2010), "*Study of bond behaviour between FRP reinforcement and concrete*". University of Girona. Available at: http://www.tdx.cat/handle/10803/7771.

Pecce, M., Manfredi, G., Realfonzo, R. & Cosenza, E.,(2001), "Experimental and analytical evaluation of bond properties of GFRP bars". *Journal of Materials in Civil Engineering*, (July/August), pp.282–290.

Pilakoutas, K., Guadagnini, M., Neocleous, K. & Taerwe, L.,(2007),"Design guidelines for FRP reinforced concrete structures.pdf".In *ACIC 07, Advanced Composites in Construction*. Bath, UK, pp. 31–39.

Pour, S.M., Alam, M.S. & Milani, A.S.,(2016), "Improved Bond Equations for Fiber-Reinforced Polymer Bars in Concrete". *materials*, 9(737), pp.1–14.

Quayyum, S.,(2010), "*Bond behaviour of Fibre Reinforced Polymer (FRP) rebars in concrete*". The University of British Columbia.

Sólyom, S. & Balázs, G.L.,(2016),"Influence of FRC on bond characteristics of FRP reinforcement".In *11th fib International PhD Symposium in Civil Engineering*. Tokyo, J, pp. 271–278.

Sólyom, S., Balázs, G.L. & Nehme, S.G.,(2016),"Bond modelling of FRP rebars in FRC".In *CICE 2016 - 8th International Conference on Fibre-Reinforced Polymer (FRP) Composites in Civil Engineering - paper accepted for publishing*. Hong Kong.

Tighiouart, B., Benmokrane, B. & Gao, D.,(1998), "Investigation of bond in concrete member with fibre reinforced polymer (FRP) bars". *Construction and Building Materials*, 12(8), pp.453–462.

Veljkovic, A., Haffke, M.M., Carvelli, V. & Pahn, M.,(2016),"Experimental investigation of the static bond of GFRP rebar and concrete".In *11th fib International PhD Symposium in Civil Engineering*. Tokyo, Japan, pp. 527–534.

Vint, L.M.,(2012), "*Investigation of Bond Properties of Glass Fibre Reinforced Polymer (GFRP) Bars in Concrete under Direct Tension*". University of Toronto. Available at: https://tspace.library.utoronto.ca/handle/1807/33573.

Wang, H. & Belarbi, A.,(2010), "Static and Fatigue Bond Characteristics of FRP Rebars Embedded in Fiber-reinforced Concrete". *Journal of Composite Materials*, 44(13), pp.1605–1622. Available at: http://jcm.sagepub.com/cgi/doi/10.1177/0021998309355845.

Weber, A.,(2005),"Bond Properties of a Newly Developed Composite Rebar". In *International Symposium on Bond Behaviour of FRP in Structures - BBFS 2005*. pp. 379–384.

Won, J.P., Park, C.G., Kim, H.H., Lee, S.W., et al.,(2008), "Effect of fibers on the bonds between FRP reinforcing bars and high-strength concrete". *Composites Part B: Engineering*, 39(5), pp.747–755.

Yan, F., Lin, Z. & Yang, M.,(2016), "Bond mechanism and bond strength of GFRP bars to concrete: A review". *Composites Part B: Engineering*, 98, pp.56–69. Available at: http://linkinghub.elsevier.com/retrieve/pii/S1359836816305200.

Yoo, D.Y., Kwon, K.Y., Park, J.J. & Yoon, Y.S.,(2015), "Local bond-slip response of GFRP rebar in ultra-high-performance fiber-reinforced concrete". *Composite Structures*, 120, pp.53–64. Available at: http://dx.doi.org/10.1016/j.compstruct.2014.09.055.

Sándor Sólyom (1984) Civil Engineer, PhD student and Marie Curie Early Stage Researcher at Budapest University of Technology and Economics (BME). Main fields of interest: application possibilities of Fibre Reinforced Polymer (FRP) rebars in reinforced concrete structures, bond in concrete, strengthening with advanced composites. Member of the fib T5.1 "FRP (Fibre Reinforced Polymer) reinforcement for concrete structures" and the Hungarian Group of ***fib***. Research fellow in endure (European Network for Durable Reinforcement and Rehabilitation Solutions).

György L. Balázs (1958), Civil Engineer, PhD, Dr.-habil., professor of structural engineering, head of Department of Construction Materials and Technologies. His main fields of activities are bond, cracking, FRC, HSC, HPC, durability, sustainability and fire resistance. He is chairman of several commissions and task groups of ***fib***, like Com 9 Dissemination of knowledge, Honorary President of ***fib*** (he was President of ***fib*** for the period of 2011-2012). He is president of Hungarian Group of ***fib***, Editor-in-chief of the Journal "Concrete Structures".

SHEAR BEHAVIOUR OF CONCRETE BEAMS REINFORCED WITH FRP BARS

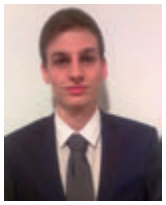


Péter SCHAUL – György L. BALÁZS

Synthetic reinforcements in concrete structures, such as macro synthetic fibres and fibre reinforced polymer bars become more popular nowadays, because of their most important advantage: the resistance against electrochemical corrosion. The fibre reinforced polymer (FRP) bars can increase the flexural capacity, and the macro synthetic fibres can increase the shear capacity of the concrete structures. At the moment there is no standard for this kind of reinforcements, that is why the calculation should be carefully carried out.

Keywords: FRP, fibre reinforced concrete, shear, finite element analysis

1. INTRODUCTION

FRP rebar has become considered more and more as reinforcement in concrete structures, due to its main advantage of being free from electrolythical corrosion. These bars are made of high strength continuous fibres embedded in a matrix, which is usually a polymeric resin. The fibres (which are usually glass basalt or carbon) carry the load and the matrix has the function of binding together the fibres and transferring the load to the fibres. The resin also protects the fibres from mechanical degradation.

The FRP bars are manufactured with the procedure called pultrusion. During the manufacturing process the matrix which is usually a thermoset resin gets heated and the bars reach the final form. This is one of the most significant disadvantage of using of the FRP bars, because the forming of the bars such as for stirrups, for bent-up bars, or for hooks can be difficult and uneconomical. Also these elements cannot be modified on the site, which makes the design and the manufacturing more risky.

Based on previous publications (Kovács and Juhász 2013; 2014) the fibre reinforcement could be alternative for shear reinforcement in concrete structures. In order to maintain the non-corrosive nature of the composite material synthetic fibre should be used in this case. These fibres are made from modified olefin and their surface is optimised to make good bond with concrete. With proper mixing these fibres are distributed equally in concrete and after the first cracks they will make the crack propagation slower by bridging the cracks.

Combining the FRP bars as bending reinforcements and synthetic fibres as shear reinforcement a completely corrosion-free structure could be developed, where the price and time of labour is optimised.

2. SHEAR MECHANISM OF RC BEAMS

One of the most dangerous mode of failures in concrete structures is the shear failure due to its rigidity. In this case inclined cracks are appearing along the shear span of the concrete beam, and the upper and the lower parts of the structure start to be separated.

Because of the above mentioned reasons it is really important to have a proper and accurate shear design. The currently used standards and guidelines always make a separated chapter for the shear designs which show the calculation method, and sometimes also make a numerical example too. However the physical and mechanical background of these standards and guidelines are different.

The shear capacity of a reinforced concrete beam contains the contributions of the concrete and also of the actually used steel stirrups. According to Wight and MacGregor (2012) the shear capacity contains the following contributions: the compressed concrete zone (V_c), the aggregate interlock (V_A), the dowel effect (V_s) and the load bearing capacity of the steel stirrups (V_w) (*Fig. 1*).

The efficiency of these components is continuously changing during the loading procedure. In the first part of the loading, the shear stress is carried by the tensile strength of the concrete. The maximal stress is on the bottom surface during the three point bending test, and at the loading point the shear stress is zero. After when the first inclined crack has appeared, the shear stress is carried by the compressed concrete zone, the stirrups, the dowel effect and along the appeared crack there is a friction which is caused by the aggregate interlock.. However there are many recent studies which show that the effect of the aggregate interlock is not significant, the nowadays used standards take this component into account for shear capacity too. After if the crack width of the inclined crack is quite large there is a part on the bottom of the crack where is no aggregate interlock effect anymore.

Fig. 1: Shear components in reinforced concrete beams

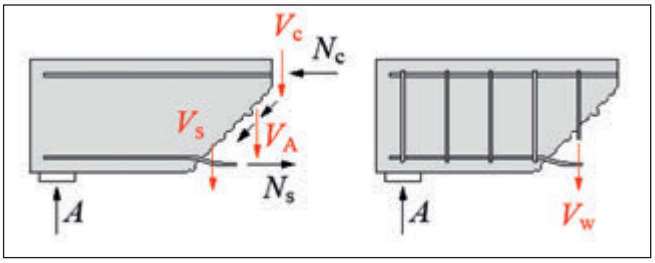

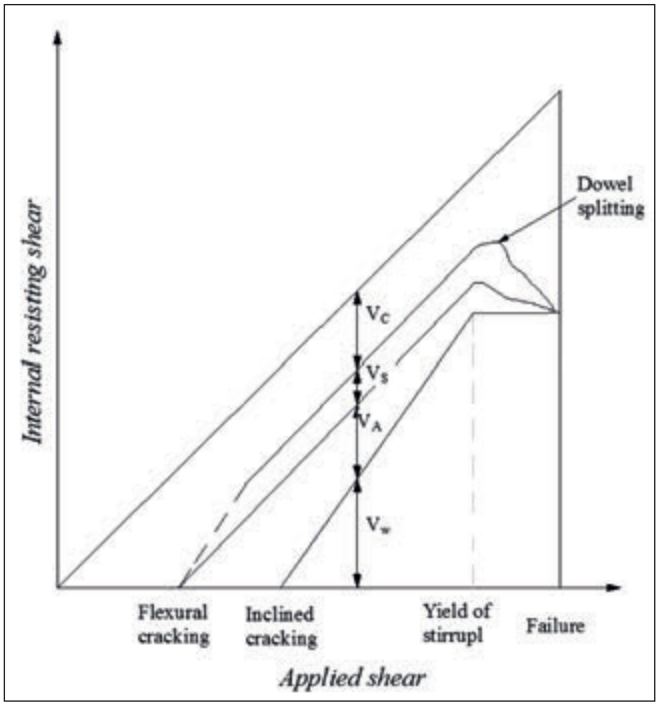

Fig. 2: Efficiency of the shear components during loading (Wight and MacGregor, 2012)

The shear failure of the structure becomes because of the crushing of the compressed zone or the yielding of the steel stirrups. The effect of the different shear components according to Wight and MacGregor (2012) can be seen in *Fig. 2.*

Due to the different physical and mechanical backgrounds of the shear capacity, the calculated results according to the different codes show differences, too. To compare the results a shear capacity calculation according to nowadays used guidelines, standards has been carried out. The beam considered was 160 mm high, 100 mm wide with 1.0 m span. The concrete strength class was C30/37, and the used steel was 3Ø12 B500 tensile bars and 8/200 stirrups with the same material properties. In the calculation the effect of the concrete and the effect of the steel stirrups were calculated separately and were summarized in the *Fig 3*. The material parameters were always represented by characteristic values, none of them contains any safety factor.

The calculation was carried out according to the ACI (ACI 2015), the Japanese JSCE (JSCE 2007), the *fib* Model Code 2010 (*fib* 2013) and the Eurocode (European Com. for Stand. 2004). The results are summarized in *Fig. 3*.

To verify the results a virtual laboratory beam has been numerically tested by using ATENA STUDIO 5 finite element software specialized for concrete structures. The software uses a combined failure criteria to model the different behaviours of the concrete for tension and for compression. For

Fig. 3: Shear capacity according to different standards and guidelines

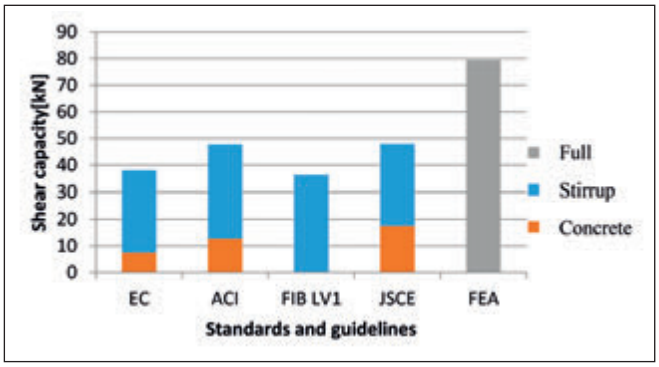

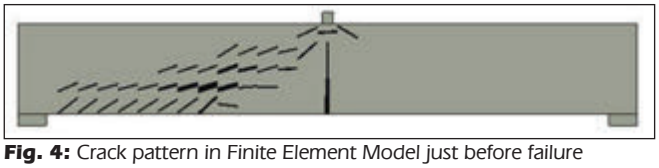

Fig. 4: Crack pattern in Finite Element Model just before failure

tension it calculates with the Rankin failure criteria (Rankin 1857) and for compression it uses the Menétrey-William failure surface (Cervenka and Papanikolaou, 2008). After the cracking the software uses the characteristic length to transform the stress-strain diagram to a stress-crack width relationship, which makes possible the nonlinear calculation of the concrete structure and the visualization of the crack width and the crack propagation.

The model was made with beam geometry and material mentioned above. The steel bars and stirrups were modelled with discrete link elements. These 1D elements are in the concrete, and behave like a link. The connection between the concrete and the steel bars were made according to the recommendation of the ***fib***. The virtual test was controlled by the displacement, so with this the diagram after the peak point could be investigated too. The results of the Finite Element Calculation are shown in the *Fig*. 3 and the crack propagation can be seen in the *Fig* 4.

The studied beam failed in shear, the inclined crack goes from the loading point to the bottom surface, close to the support. *Fig*. 3 indicates that standards calculate the shear capacity quite conservative, all of them are on the safe side of the design. The Model Code which uses the Modified Compression Field Theory (Vecchio and Collins, 1986) for calculating shear capacity contains the highest safety, and the semi-empirical Japanese formulas are the closest to the numerical values of the studied beam. Future work is required to define the required safety of different formulas.

3. SHEAR MECHANISM OF FRP REINFORCED CONCRETE BEAMS

There are some standards of calculation methods for concrete beams reinforced with FRP bars, such as *fib* Model Code 2010 (*fib* 2013) or ACI 440 (ACI 2015), ***fib*** defines the different types of FRP (or non-metallic) reinforcements and describes the important material behaviours, such as stress-strain diagram, fatigue and creep. The ACI 440 gives semi-empirical calculation methods, but it has many criteria to the geometry of the structures and it can only be used for non - prestressed elements. The use for non - rectangular or prestressed structures is also possible according to this guideline but it must be validated with real scale tests.

More accurate and general calculation methods could be done with Finite Element Analysis. The advantage of this analysis is to model the real behaviour of the structure at any stage, such as crack propagation and crack width at any time. The difficulties of this type of calculation are to choose the proper material laws and to model the connection between the rebar and the concrete properly.

The shear behaviour of FRP reinforced concrete structure is really similar to the traditionally reinforced concrete structures; however there is some difference in the shear components. The FRP bars are from a linear elastic material which means before rupture there is no yielding. Because of this property the dowel effect of the FRP bars cannot be as effec-

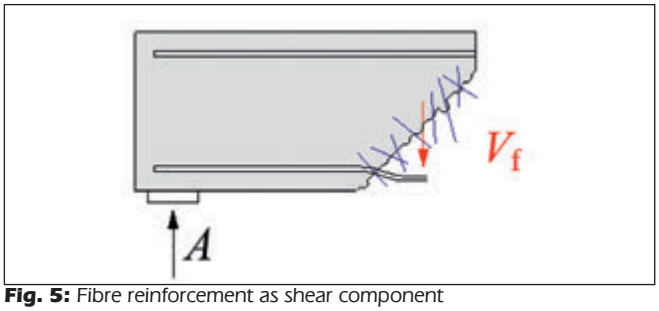

Fig. 5: Fibre reinforcement as shear component

tive as the steel bars, the more rigid material will cause the bar rupture or the failure of the concrete cover much sooner like in case of the traditionally reinforced concrete structure. In this structures it is also a serious danger that the connection between the concrete and the bars are not as well as in case of steel bars. Due to this the slip of the bars has a higher risk for FRP reinforced structures.

According to many recent studies the fibre reinforcement can be used for shear strengthening in concrete structures. The effect of the fibres represented mostly in the increase of the fracture energy of the plain concrete (G_f), giving to the concrete a serious ductility after the first cracks. The effect of the fibre on the compression or cracking strength of the concrete is negligible, however it raise the residual strength of the concrete, which makes the structure more ductile.

There are many recommendations on how the effect of the fibres could be calculated in case of shear load (Kovács and Juhász, 2014). These codes take the fibres into account similar to stirrups: calculating the residual strength of the fibres and the area of the cracked surface (*Fig 5.*) However, there are many more advantages from the use of the fibres. Generally, fibres decrease the distances between the cracks thanks to the increased fracture energy, due to this the crack widths will also be smaller. The function of aggregate interlock determined by Kolmar (Kolmar, 1986) shows a precipitous slope during crack opening. These were researched by using large specimen tests by Kovács and Juhász.

4. FINITE ELEMENT MODELLING OF FRP REINFORCED FRC BEAMS

The modelling of the FRP bar reinforced fibre reinforced concrete structures is a compound method, because the different reinforcement has its own modelling specialities.

In case of modelling FRP bars, it is indispensable to define a proper material model which follows the elastic linear behaviour and the rupture of the bars. It is also necessary to define the bond slip law of the bars. This parameter defines the failure method of the connection between the concrete matrix and the bars without this factor the modelling leads to an inappropriate result (*Fig.* 7).

There are two accepted and used methods to model the fibre reinforcement in concrete structures however both of them needs advanced finite element software.

The easiest and the most time-saving way to model the fibre reinforced concrete is the Modified Fracture Energy Method (Juhász, 2013), where the fracture energy of the concrete is raised with the fibres added fracture energy (G_{ff}). The added fracture energy of the fibres could be derived from the inverse analysis of the three points bending beam tests. With this data the Hordjik (Cervenka and Papanikolaou, 2008)

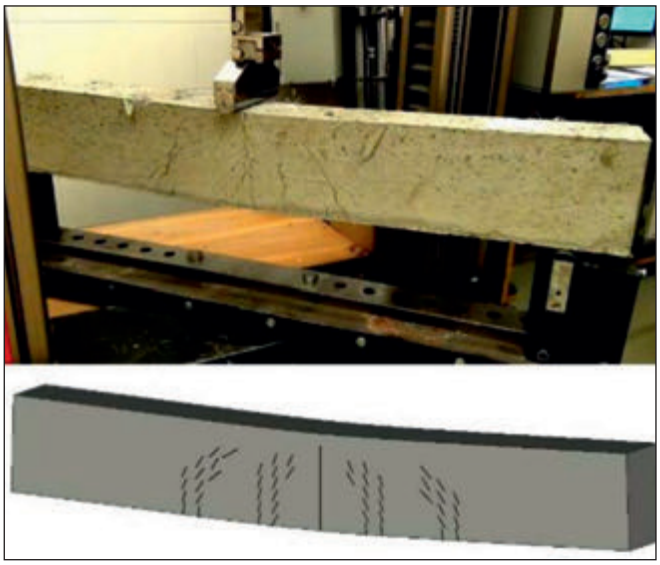
Fig. 6: Crack propagation in experiment and FEA

curve which defines the concrete's tension law, can be modified with the effect of the fibres. These method represent the reality well, the crack propagation and also the shear capacity of the structures can be calculated rather properly with acceptable accuracy.

The other method to model the fibre reinforced concrete is to add the fibres discretely. With this method a more accurate result may be obtained, however it needs more input data and the calculation time and energy is also higher. In this method the location of the discrete fibres is generated randomly with taking into consideration the wall effect which means that the fibres close to the formwork start to be orientated. It is also important to define a bond-slip law for the fibres which can get from pull out tests. It is necessary to make for a single beam more models with new and different fibre dispersion to get a proper and safe result.

5. LABORATORY EXPERIMENTS

In 2015 an FRP reinforced concrete beam test series was cast at Budapest University of Technology and Economics (Juhász and Schaul, 2015). The geometry of the beam was similar to the above mentioned beams. The beams contained 2 pieces of 6 mm diameter FRP bars made of basalt or glass as tensile reinforcement. The beams were made without steel stirrups. To determine the shear capacity of the synthetic fibres beams with 5 kg/m^3 BarChip 48 fibre dosage and without any fibres were casted, too. The tests were displacement controlled with three point loading. To verify the results a finite element model was made, too with using ATENA.

All of the beams during the experiment performed shear failure, however the beam's capacity with fibre reinforcement was higher with almost 35% in case of basalt and 25% in case of glass FRP bars.

Before the failure the slip values of the basalt FRPs were significant, it caused a horizontal crack on the side of the beam (*Fig.* 7).

6. CONCLUSIONS

FRP rebars are more and more frequently used as reinforcement in concrete structures, due their electrolytic corrosion-free behaviour. However, FRP bars can be bent only at the manufacturing stage and not on site, which makes the pro-

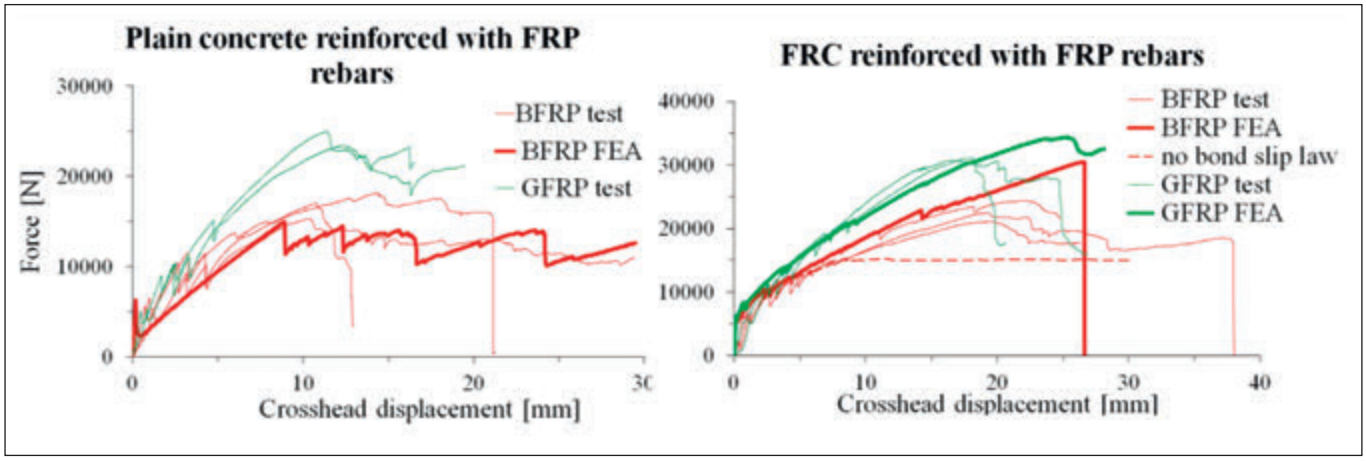

Fig 7. Results of the laboratory experiments

duction of items such as shear stirrups difficult and uneconomical. As an alternative shear reinforcement bars could be replaced by fibres mixed into the concrete. Beam tests were carried out to study the shear behaviour of these fully non-corrosive reinforced concrete beams.

The shear modelling is still one of the most actual topic in engineering and researches because of the complex and rigid failure mode. The currently used standards and guidelines provide for the shear capacity conservative methods, however with advanced finite element analysis provides reasonable solutions. With using synthetic macro fibres it is possible to raise the shear capacity of the FRP reinforced concrete beams. Three point bending beam tests were carried out to investigate the effect of fibre reinforcement to shear capacity and mechanism in FRP bar reinforced concrete beams. In a preliminary experiment almost 35% raising was noticed with adding 5 kg/m^3 macro synthetic fibre reinforcement to the concrete with basalt FRP bars and 25% with using glass fibre reinforced polymer rebars. The modelling of the fibre reinforcement with advanced finite element software is an important field of researches; however, the modelled behaviour of beams were really close to the results of experiments.

7. REFERENCES

ACI (2015): ACI 440.1R-15: Guide for the Design and Construction of Structural Concrete Reinforced with Fiber-Reinforced Polymer (FRP) Bars, ISBN: 978-1-942727-10-1

Advisory Committee on Technical Recommendations for Construction (2006): "CNR-DT 204/2006: Guide for the Design and Construction of Fibre-Reinforced Concrete Structures"

Balázs, G. L. (2010), „A historical review of shear", in *fib* Bulletin 57 "Shear and punching shear in RC and FRC elements", ISBN 978-2-88394-097-0, pp. 1-10

Bank, L.C. (2006): "Composites for Construction – Structural Design with FRP Materials", John Wiley & Sons Inc.

Cervenka, J. and Papanikolaou, V.K. (2008), "Three dimensional combined fracture-plastic material model for concrete" International Journal of Plasticity (24): 2192-2220

European Com for Stand.: (2004)" Eurocode 1992-3: Design of Concrete Structures – Part 3" 6.2. Shear

fib (2013), "*fib* Model Code for Concrete Structures 2010", Ernst & Sohn Wiley, ISBN 978-3-433-03061-5

ITAtech Activity Group Support (2015): "ITAtech Design Guidance For Precast Fibre Reinforced Concrete Segments" ITAtech Report n7, draft

JSCE Guidelines for Concrete No.15. (2007), "Standard specifications for Concrete Structures". pp. 154-156.

Juhász, K.P. (2013), "Modified fracture energy method for fibre reinforced concrete", in: Proceedings of Fibre Concrete 2013: Technology, Design, Application. Prague, Czech Republic 2013, pp. 89-90.

Juhász, K.P, Schaul, P. (2015), "Shear behaviour of synthetic fibre reinforced concrete beams reinforced with FRP rebars" Proceedings of 11th CCC Congress, Hainburg, 2015, pp.42-46.

Kolmar, W. (1986), "Beschreibung der Kraftübertragung über Risse in nichtlinearen Finite-Element-Berechnungen von Stahlbetontragwerken", Dissertation, T.H. (In German)

Kovács, G. and Juhász, K.P. (2013), "Precast, prestressed grandstand of PFRC in Stadium, Hungary", in: Proceedings of CCC 2013, Concrete Structures in Urban Areas

Kovács G. and Juhász K.P. (2014), "Synthetic and steel fibres in prestressed, precast long span beams", in: Proceedings of CCC 2014, "Concrete Offers for Period of Economic Recovery", Liberec, Czech Rep. 2014.

Österreichische Vereinigung für Beton- und Bautechnik (2008): "Richtlinie Faserbeton." Österreichische Vereinigung für Beton- und Bautechnik (In German)

Nanni, A., De Luca, A. and Zadeh, H.J. (2014), "Reinforced Concrete with FRP Bars – Mechanics and Design", CRC Press

Rankine, W. (1857), "On the stability of loose earth", Philosophical Transactions of the Royal Society of London, Vol. 147.

Vecchio, F.J. and Collins, M.P. (1986): "The Modified Compression-Field Theory for Reinforced Concrete Elements Subjected to Shear" ACI Journal, Title no.83-22.

Wight, J.K., and Macgregor, J.G. (2012), "Reinforced concrete: mechanics and design - 6th edition", ISBN-13: 978-0-13-217652-1

Péter Schaul (1989), Civil Engineer, PhD student (Department of Construction Materials and Technologies, Budapest University of Technology and Economics). His main fields of activities are experimental investigation and modelling of FRC and FRP structures, finite element modelling of concrete structures. Structural engineer at JKP Static Ltd.

György L. Balázs (1958), Civil Engineer, PhD, Dr.-habil., professor of structural engineering, head of Department of Construction Materials and Technologies and Deputy Dean of the Civil Engineering Faculty of Budapest University of Technology and Economics (BME). His main fields of activities are experimental investigation and modelling of RC, PC, FRC structures, HSC, fire resistance of concrete. He is chairman of several commissions and task groups of *fib*. He is president of Hungarian Group of *fib*, Editor-in-chief of the Journal "Concrete Structures". He was elected as President of *fib* for the period of 2011-2012.

CRACK CONTROL: AN ADVANCED CALCULATION MODEL – PART I: REVIEW OF CLASSIC TESTS

Dedicated to Prof. Gallus Rehm on the occasion of his 90th birthday

Andor Windisch

Crack control is a fundamental part of dimensioning: in many cases it governs the amount of reinforcement in R/C members. In Part I after the overview of development of calculation methods in international codes since 1989, the data, records and notations of four classical papers with excellently documented tests on tensile members and beams will be studied and evaluated. Secondary cracks get a new interpretation.

Keywords: cracking, Goto-cracks, primary and secondary cracks, bond, concrete cover, cracking model

1. INTRODUCTION

Cracking is an inherent characteristic of structural concrete. Since over 60 years intensive research is made on this topic. National (e.g. ACI, DIN) and international standardization bodies (e.g. CEB, *fib*) direct and summarize the achievements from time to time. Recently the Model Code 2010 (2012) was published. In a paper Balázs et al. (2013) an overview is given about the backgrounds of the design rules for serviceability limit states in MC 2010 and showed calculation examples. The current model assumes that:

- The bond strength is constant and independent of the slip at the crack
- Each rebar in tension is a tensile member within $A_{c,ef}$ around. (Note: according to the definition of $A_{c,ef}$ in the codes, the tensile member is eccentrically loaded.)
- The concrete strain is mentioned in the basic formula but neglected at the calculation
- The influence of the concrete cover is taken into account as extension of the transmission length of bond
- No distinction between RC members in pure tension or in flexure
- No special rules for slabs with remote rebars are given.

In this paper on the contrary

- The effective tension area of concrete, $A_{c,ef}$, presents a fairly different relevance.
- The concrete elongation around the reinforcement is considered directly.
- The influence of concrete cover and rebar distance, resp. are considered in a theoretically correct way
- The difference in crack width of RC members under pure tension or bending is considered in the correct manner.
- The impact of shrinkage on crack width is discussed

In Part I - instead of inscrutable databanks - the data, records and notations of four classical papers with excellently documented tests on tensile members (Broms and Lutz (1965), Goto (1971), Scott and Gill (1987)) and beams (Rüsch and Rehm (1963)) will be studied and evaluated.

In Part II of present article the well-known formula of the design value of crack width gets an advanced interpretation. All influencing factors are taken into consideration at the proper position.

2. DEVELOPMENT OF CALCULATION METHODS SINCE 1989 IN INTERNATIONAL CODES

The calculation method of the (characteristic/design) crack width made the following development during the last 25 years: in Table 1 the main formulas are summarized.

Some comments:

- Comparing the crack width formulas of MC1990 (1993) with EC2 (2003) yields $l_{s,max} = 1.7\ s_{rm}$. The definition of as the distance between the two sections with the point of zero slip is theoretically correct, nevertheless in the figure explaining the stabilized cracking situation = $s_{r,max}$ is depicted: these two distances have no correlation with each other, hence from this point the theoretical correct character of the deduction vanishes. In MC1990 the constant term, 50, does not occur. In MC2010 the position of the $2 * l_{s,max}$ symbol is correct: it refers to the two sides of the crack, nevertheless a) $l_{s,max}$ is only a part of the length over which slip between concrete and steel occurs, the length between the crack and the section without slip is longer, $l_{s,max}$ is supposed to be the load transfer length to cause the cracking of the concrete cross section of A_{ceff} cross section, b) a comparison of the formulas reveals that instead of 1.7*50, in MC2010 $2*c$ occurs, whereas the second term is identical with the $l_{s,max}$ term of MC1990. In the $k*c$ term k is an empirical parameter to take into consideration the influence of the concrete cover. In the background paper (Balázs et al. (2013)) the $k*c$ term refers to the load transfer of bond forces from the rebar surface to the concrete surface. We returned to the ancient problem of the researchers: "ancient" data bank comparisons revealed that the $Ø_s/\rho_{s,ef}$ parameter is weak. Already Ferry Borges (1966) wrote: "It must be emphasized that if the influence of the cover were omitted, a very weak correlation between s and $Ø/A_{ceff}$ would be obtained."

- τ_{bms} τ_{bms} is related to the mean value of the tensile strength. This gives the impression that τ_{bms} τ_{bms} has a strength character, which is not the case.
- EC2 specifies that the calculated crack width refers within a region close to the bonded reinforcement (i.e. within the effective concrete area in tension). Note: as the effective tension area includes the concrete surface hence the calculated crack width seems to be constant across the concrete cover and does not follow the curvature in members in flexure.
- In MC1990 the effective concrete area in tension ($A_{c,ef}$) accounts for the non-uniform normal stress distribution by bond forces into the concrete cross-section at the end of the transmission length. "By means of the method the design crack width within the effective tension area may be calculated. It should be noted that outside this region, larger cracks may occur." This is a correct comment but does not assist the designer.
- The average steel strain terms in MC1990 and MC2010 are identical.
- The $\beta = 0.6$ value is in contradiction with the assumption of the uniform bond stress distribution (the corresponding value would be 0.5).
- The formulas ignore the tensile deformation of the concrete along the $2 * l_{s,max}$ distance. This results in a calculated crack width on the safe side, nevertheless it yields not economical amounts of reinforcement.

The standardization body of the US handles the crack control problem in a different way: The relevant ACI committee publishes reports (2001), (2013), where in addition to the principal causes of cracking- recommended crack-control procedures in flexural members are presented. In a later report performance-based details that can mitigate and control cracking are reviewed. Detailing rules for two-way and one-way slab systems and those of columns are presented.

The legal aspects of cracking are regularly considered in the relevant US literature. The chapter's headings of Coleman (2013) are well representative:

Cracking… Defect or Normal? Part 1: When is concrete cracking a construction defect? Why concrete cracks; Concrete Cracks Occur….; Industry Guidance; When is Cracking Expected? ASCC (American Society of Concrete Contractors) Position Statements; Managing Owner Expectations; Principles and Precedents. Part 2: Case law on concrete cracking; Legal Principles; Cracking is "Normal and Expected".

3. LESSONS FROM CLASSICAL EXPERIMENTS

In this section the records and data of four excellently documented reports are evaluated and discussed. The conclusions serve the understanding of the cracking procedure and the improvement of the crack width formula.

3.1 Tensile specimens of Broms et al.

Broms and Lutz (1965) tested seven ~2.2 m long and six short tensile specimens reinforced with bars in various arrangements. The lengths of the short tensile members were chosen equal to the mean value of primary crack spacings observed for the long members. The dimensions of the specimens with rectangular cross section were 76 x 240 mm, of those of quadratic cross section 135 x 135 mm. T-RC6 specimen was reinforced with one Ø25 (#8) rebar ($f_R = 0.054$, c = 25 mm), whereas the others with four Ø12.7 mm (#4) rebars ($f_R = 0.043$, c = 19 mm), hence the A_s/A_c values were identical. The average compressive strengths measured on 150 x 300 mm concrete cylinders were 30 to 40 N/mm² and the average tensile strengths determined on split cylinder tests were ~3 N/mm². The crack distances and the crack widths were measured on each long side of the cross section along five lines and in the middle of the short side, at three stress levels: 314, 471 and 628 N/mm² (in case of T-RC6 at 593 N/mm²), resp. (Note: the reported max. crack widths are the averages of the two widest relevant cracks!)

Studying the results the development of the cracking process in a member under centric tension can be understood and

Table 1: Calculation formulas of the last 25 years in the international codes

	EC2 [6]	MC1990 [7]	MC2010 [8]
design crack width	$w_k = \beta\, s_{rm}\, \varepsilon_{sm}$ $\beta = 1.7$	$w_k = l_{s,\max}(\varepsilon_{sm} - \varepsilon_{cm} - \varepsilon_{cs})$	$w_d =$ $2\, l_{s,\max}(\varepsilon_{sm} - \varepsilon_{cm} - \varepsilon_{cs})$
average crack spacing for stabilized cracking	s_{rm} $= 50 + 0.25\, k_1\, k_2\, \emptyset/\rho_r$	$l_{s,max} = \frac{\emptyset_s}{3.6\rho_{s,ef}}$	$l_{s,\max} =$ $k \cdot c + \frac{1}{4} \cdot \frac{f_{ctm}}{\tau_{bms}} \cdot \frac{\phi_s}{\rho_{s,ef}}$
for single crack formation		$l_{s,max} =$ $\frac{\sigma_{s2}}{2\tau_{bk}}\, \emptyset_s\, \frac{1}{1 + \alpha_e \rho_{s,ef}}$	
average strain of reinforcement	$\varepsilon_{sm} =$ $\frac{\sigma_s}{E_s}\left(1 - \beta_1 \beta_2 \left(\frac{\sigma_{sr}}{\sigma_s}\right)^2\right)$	$\varepsilon_{sm} - \varepsilon_{cm} = \varepsilon_{s2} - \beta\varepsilon_{sr2}$	$\varepsilon_{sm} - \varepsilon_{cm} - \varepsilon_{cs} =$ $\frac{\sigma_s - \beta \cdot \sigma_{sr}}{E_s} + \eta_r \cdot \varepsilon_{sh}$
β (in EC2 β_2)	0.6	0.6	0.6

explained. *Fig. 1* shows the development of the number of the crack intervals (length of the specimen divided by mean crack spacing).

The test results of specimen T-RC6 indicate that:

- Up to σ_s = 314 N/mm² at positions L3 and R3 three times more crack intervals developed than at position TC (27 vs. 7).
- At position L3: with increasing steel stress the number of crack intervals increased considerably. From 27 pcs. at σ_s = 314 N/mm² to 36 pcs. at σ_s = 604 N/mm², whereas at position TC the number of crack intervals did not change. (Note: at σ_s = 604 N/mm² the calculated tensile stress in the concrete member would be 14.5 N/mm²!) This means that the tensile stresses due to the transfer of bond forces do not reach the fiber as far from the rebar surface.

In case of specimen T-RC5

- At σ_s = 314 N/mm² the number of crack intervals were at positions L3/R3 ~34, whereas at position TC only 7.
- At σ_s = 628 N/mm² at position L3/R3 the number of crack intervals increased to ~44, at position TC to 8 only.

On contrary, in case of specimen T-RC8

- At σ_s = 314 N/mm² at positions L1/L5/R1/R5 25 – 33 crack intervals developed, at TC 38, whereas at positions L3/R3 12 - 16 only.
- Increasing the steel stress to σ_s = 628 N/mm at positions L1/L5/R1/R5 ² the number of crack intervals increased to 33 – 40, at position TC to 54, whereas at positions L3/R3 to 19 – 20 only!

In case of T-RC7 the measuring line L1 is about in the same distance t from the next rebar surface as the line L3. Along line L3 more secondary cracks developed than along L1. Along L3 the tensile stresses due to the bond stresses of two adjacent rebars affected the development of secondary cracks. Note: some authors and codes tackling the slab-like reinforcement pattern proposed a term s/2 in the mean crack distance formula.

At all of these specimens it can be perceived that the number of crack intervals shows a pattern of secondary cracks along eight intervals. The numbers of crack intervals at position TC in case of T-RC5 and T-RC6 reveal that at the contrary to the proposals of Leonhardt (1987) and the codes: rebars can control the crack width within a distance of 7Ø, but (obviously independent of the rebar diameter) less than ~75-100 mm only! Moreover, "control" should mean: to be able to cause concrete elongation, therefore, the affected/controlled area is less than 7Ø around the rebar. (It must be admitted that the crack width formula in MC2010 is valid for structural members with concrete covers of max. 75 mm, in slabs the bar spacing shall not exceed the lesser of 1.2 times the slab thickness and 300 mm. Especially this latter seems to be a bit too big.)

A comparison of the number of crack intervals in case of the quadratic specimens T-RC10 and T-RC11 reveals the sequence of the steps how the crack pattern develops. In principle two processes can be distinguished:

1. Increasing the tensile load primary cracks develop at the weakest cross sections of the R/C member. These primary cracks are "through" cracks and are situated outside the actual transmission lengths of the already developed primary cracks. The transmission lengths increase with the increasing load. Remarkable: at all specimens the occurrence of about seven primary cracks can be observed.
2. Starting from the primary cracks, due to the tensile stresses induced by the bond between the rebar and the concrete around and the high steel strains the well-known Goto-cracks develop. The stress state caused by bond forces is quite symmetric to the bar's axis. Depending on the slip and the local concrete tensile strength the Goto-cracks have different extents. Depending on the distance of the rebar from the concrete surface these Goto-cracks may arrive at the concrete surface and be recognized as secondary cracks and let decrease the crack distances. As a secondary crack does not cross the whole cross section like primary cracks do hence the steel stress in a secondary crack is always less than in the primary crack. As we are interested in the upper 5% fractile value of the crack width, the width of all these secondary cracks are out of our interest (nevertheless, the secondary cracks "perturb" the development of the mean value of the crack distance and the mean rebar elongation!). If the distance of the rebars is less than ~ 2*50 mm and the concrete cover is less than 25 mm then it may occur that the secondary cracks of these rebars "meet" each other and a full crossing crack develops which behaves like a primary crack. Comparing the number of crack intervals at the positions TC of T-RC6 and T-RC5, as well as at positions L3/R3 of the specimens T-RC7 and T-RC8 it can be diagnosed that beyond t ~ 100 mm (in case of Ø25 rebar) and t ~ 75 mm (in case of Ø12.7 rebars) the Goto-cracks cannot cause secondary cracks on the concrete surface, even if the

Fig. 1: – Development of numbers of crack intervals at 314 N/mm², 471 N/mm² and 628 N/mm² steel stresses (in case of T-RC6 at 604 N/mm²; in columns from the left to the right) of Broms and Lutz (1965).

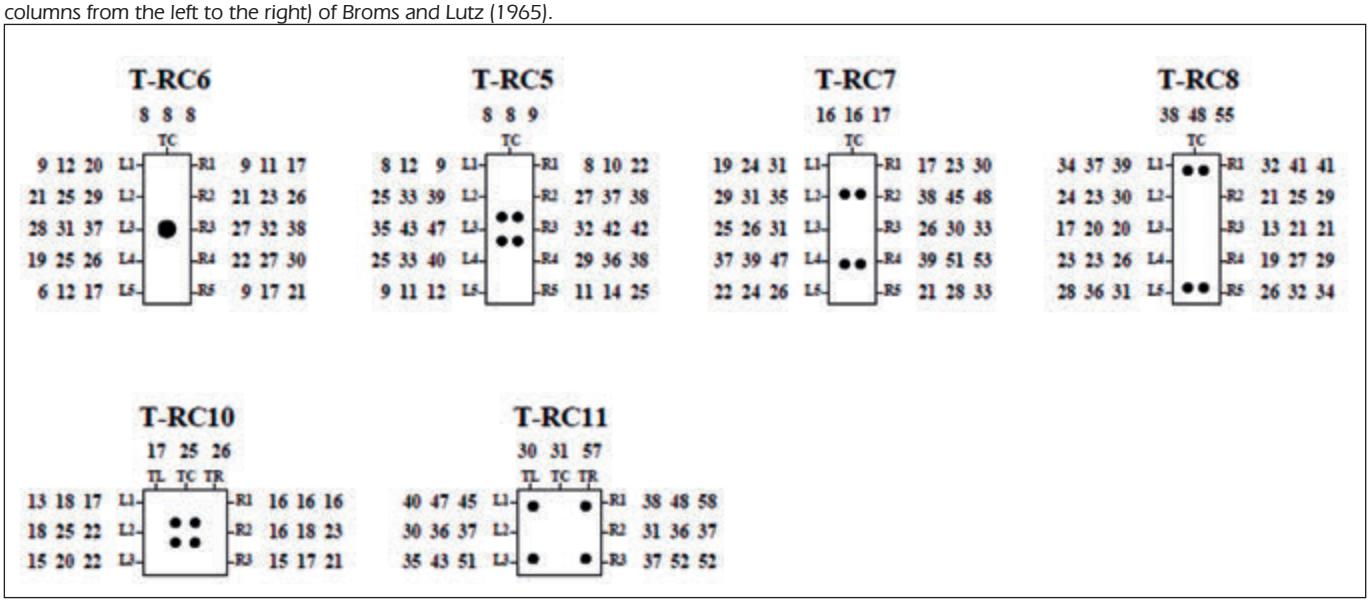

calculated uniformly distributed concrete tensile stress in cross section was 15 N/mm²! This shows that in the cross sections along the transmission lengths full of Goto- and secondary cracks, a quite complicated, not uniform stress state prevails.

After injection and hardening of resin into the short specimens under loading they were sawed. The crack patterns reveal that the secondary cracks around one rebar are not at symmetrical positions, the appearance of the secondary cracks is not imperative. The positions of the Goto- and secondary cracks show no regularity along the transmission lengths and no symmetry to the rebar's axis either. This observation explains the different number of secondary cracks along the measuring lines in identical positions. Near to the primary cracks the Goto-cracks show a ~45° inclination, farther they become steeper.

As preliminary conclusion it can be stated that

- In a tensile member with a given ratio of $Ø/\rho_{ef}$ and given rebar pattern in the cross section very different numbers of crack intervals (i.e. primary cracks) with accordingly very different mean and maximum crack widths develop.
- Secondary cracks with very different distances and widths may occur along a single transmission length of the rebar.

3.2 Goto's fundamental tests

In his fundamental tests Goto (1971) investigated the crack formation by providing narrow holes parallel to reinforcing bars for ink injection in axially loaded specimens. The cylinder compressive strength and the tensile splitting strength of the concrete were about 30 N/mm² and 2.8 N/mm², resp. The side length of quadratic cross sections was 100 mm for Ø19 mm rebars and 120 mm for Ø32 mm rebars. The steel stress at injection was 300 N/mm² (yield strength 390 N/mm²). In each case the maximum crack spacing was assumed approximately to 250 mm. Shallow notches were cut in the specimens beforehand such that primary cracks would first form at spacings of 220, 240, 260 and 280 mm. resp. (The $2 \cdot l_{s,max}$ values as proposed by MC2010 are 247 mm for specimens with Ø32 rebars and 270 mm for Ø19 rebars, resp.) It is a pity that Goto did not report on the development of the crack widths.

Observations, preliminary conclusions:

- The primary cracks – which occur mostly along the regions of the member where still no bond slip occurred and develop from the most tensioned outer fibers of the member according to the Bernoulli-Navier hypothesis – are mostly perpendicular to the member's axis, whereas the secondary cracks – which develop outward from the inner Goto-cracks – are inclined.
- The development of the crack patterns is of random character: A new primary crack and/or secondary cracks need not occur within the longest crack distance i.e. on any side of the widest crack. In case of the specimen with Ø19 mm rebar primary cracks occurred at a steel stress of 150 N/mm² between the cracks in 280 mm distance, at a steel stress of 185 N/mm² between the cracks in 260 mm distance, whereas secondary cracks at 300 N/mm² steel stress between the cracks in 240 mm distance, near to the cracks.
- The secondary cracks developed in case of both rebar diameters from Goto-cracks at a steel strain in the crack of 0.0015, and start from rebar ribs in (3-3.5)Ø distance in case of Ø19 mm rebars and in 2Ø distance in case of Ø32 mm rebars. The secondary cracks have an inclination ~60° to the rebar's axis. This means that their position on the concrete surface differs from that at the rebar surface. Accordingly the corresponding data in the databanks are not correct.
- Internal cracks usually start at a steel stress less than 100 N/mm², shortly after primary cracks are formed. They first develop around ribs near the primary cracks then with increase in steel stress or with repetition of load, at ribs progressively farther from the primary cracks. An adjacent (inclined) internal crack sometimes grows to such an extent that it appears at the inner face of the primary crack.
- Internal cracks need not necessarily occur.
- The width of both, the Goto- and secondary cracks arises not as slip from both sides of the crack but the section between the primary crack and the Goto-crack moves in the direction of the primary crack hence the direction of the slip does not change.

3.3 Tensile members of Scott and Gill (1987)

Short-term longitudinal reinforcement strain distributions in reinforced concrete tension members were measured using electric resistance strain-gauges. The 2.5 mm long gauges were installed at 12.5 mm centers in a 1000 mm long duct milled longitudinally through the center of the rebar. Twelve specimens with square cross-sections ranging from 70 mm x 70 mm up to 200 mm x 200 mm were tested, all reinforced with a single rod positioned centrally in the cross-section. One specimen was of 100 mm x 300 mm dimensions. The rebars were either of 12 mm or 20 mm diameters, both plain mild steel (R) or ribbed high yield (Torbar, T) rods. The strain distributions for five specimens (100T12, 100T20, 200T20, 300/100T20 and 140R20) were published.

Note:

- The measured strains show the steel elongation and the direct concrete contribution hence the slip and crack width values refer to the steel surface, the crack width on the concrete surface is different.
- Due to the milled ducts along the rebars, their longitudinal tensile stiffness is less than in normal cases.

The perceptions are as follow:

- The crack distance and the distance between the two points of no slip on both sides of a crack are not equal. This was theoretically proven by Windisch (1989).
- The rate of concrete contribution increases with increasing crack distance. The tensile stress in the concrete cross-section reaches its max. intensity around the max. fractile value of the tensile strength just before a new crack develops. This means that in case of the mean crack distance the tensile stress in the concrete cross section is definitely (much) less than the f_{ctm} value. Even in case of the characteristic length, $l_{s,max}$, the bond stress to be taken into account is not any bond strength, but depends on the steel stress level in the crack, σ_s. (Note: depending on the dead to live load ratio the steel stress in the primary crack to be taken into account in SLS can be different.)
- In case of a given crack distance the concrete contribution increases with increasing loading (increasing steel stress/slip in the crack). The rate of increase slows down. Nevertheless, when a new crack develops within this crack distance then the contribution drops and the increase begins afresh.
- The course of the steel strains is near to linear (which corresponds to the assumption of uniformly distributed bond stresses along the rebar). Hence the β-value could be taken to 0.5.

- The crack having the design crack width is always an extant primary crack. The development of primary cracks is finished when at every point along the rebar-concrete contact surface slip occurred. The basic length for determining the length $l_{s,max}$ is the transmission length l_0, which occurs when the last primary crack occurred (considered statistically: in the uncracked cross-section the upper fractile value of the concrete tensile strength appears). $l_{s,max}$ can be deduced from this length.
- When the distance of two primary cracks is just $2*l_0$ or more, then increasing the loading a further primary crack will occur between these two cracks. The published strain distributions reveal that when the distance of two primary cracks is max. 1.8 l_0 then an occurrence of a further primary cracks is not probable, i.e. $l_{s,max} \approx 0.9\, l_0$. This relationship is consistent with the well-known relationship: $s_{r,max} \approx 1.7\, s_{r,m}$ (even if crack distance and transmission length are not interrelated at all).

About the distribution of the bond stresses (300/100T20) *(Fig. 2)*:
The bond stresses were calculated from the measured strains as shown in the paper of Scott and Gill. The zig-zag course results from the small deviations from the planned 12.5 mm distances between the strain-gauges. *Fig. 2 top* shows the bond stresses up to the occurrence of the 2nd crack along the gauge-mounted section, whereas *Fig. 2 bottom* of those just before and after the appearance of crack No. 2 there. The legends refer to the steel stresses in the cracks. First the courses shown in *Fig. 2 top* are discussed:

- The course at steel stress of 244 N/mm² reveals that already a crack (No. 0) to the left from the section occurred. Crack No. 1 occurred at about 70 mm distance outside the transmission length of this No. 0 crack. At development of crack No. 1 the slips between the positions ca. -400 mm up to ca. -200 mm change their sign.
- On the right hand side of crack No. 1 the bond stresses show a parabolic course. The max. bond stress is not at the crack where the slip is the maximum but ca. 100 mm away: this shows the development of internal Goto-cracks which makes the bond soften. The actual transmission length ends before the transmission length of a crack being on the right hand side of the gauged-section.
- Increasing the steel stress the bond stresses near to crack No. 1 decrease due to further development of internal Goto-cracks. As equilibrium must be maintained, the transmission length increases, and the bond stresses there increase as well.
- At steel stress of 328 N/mm² the two increasing transmission lengths touch each other. At even small slip values quite high bond stresses act which then remain rather constant.
- For the calculation of the slip values the curved courses of the bond stresses can fairly well substituted with a uniformly distributed course.
- With increasing steel stress and slip in the crack the intensity of the substituting uniformly distributed bond stresses even if slightly, but increases.

Fig. 2 bottom shows the courses of the bond stresses just before and after the occurrence of crack No. 2:

- Crack No. 2 occurs just outside of the transmission length of crack No. 1. This causes a dramatic change in the course of the bond stresses between cracks No. 1 and No. 2: the section with the zero bond stress moves nearer to crack No. 1. On the right hand side of the zero point it can be observed that due to the hysteretic behavior of the local bond-slip relationship, the change of sign of the slip results in relative small bond stresses until the relevant ribs

Fig. 2: The course of the bond stresses in the specimen 300/100T20 of Scott and Gill (1987) at different steel stress levels; top: before, bottom: after the development of the 2nd crack. (Horizontal axis: 1000 mm length with gauges, vertical axis: calculated bond stresses.)

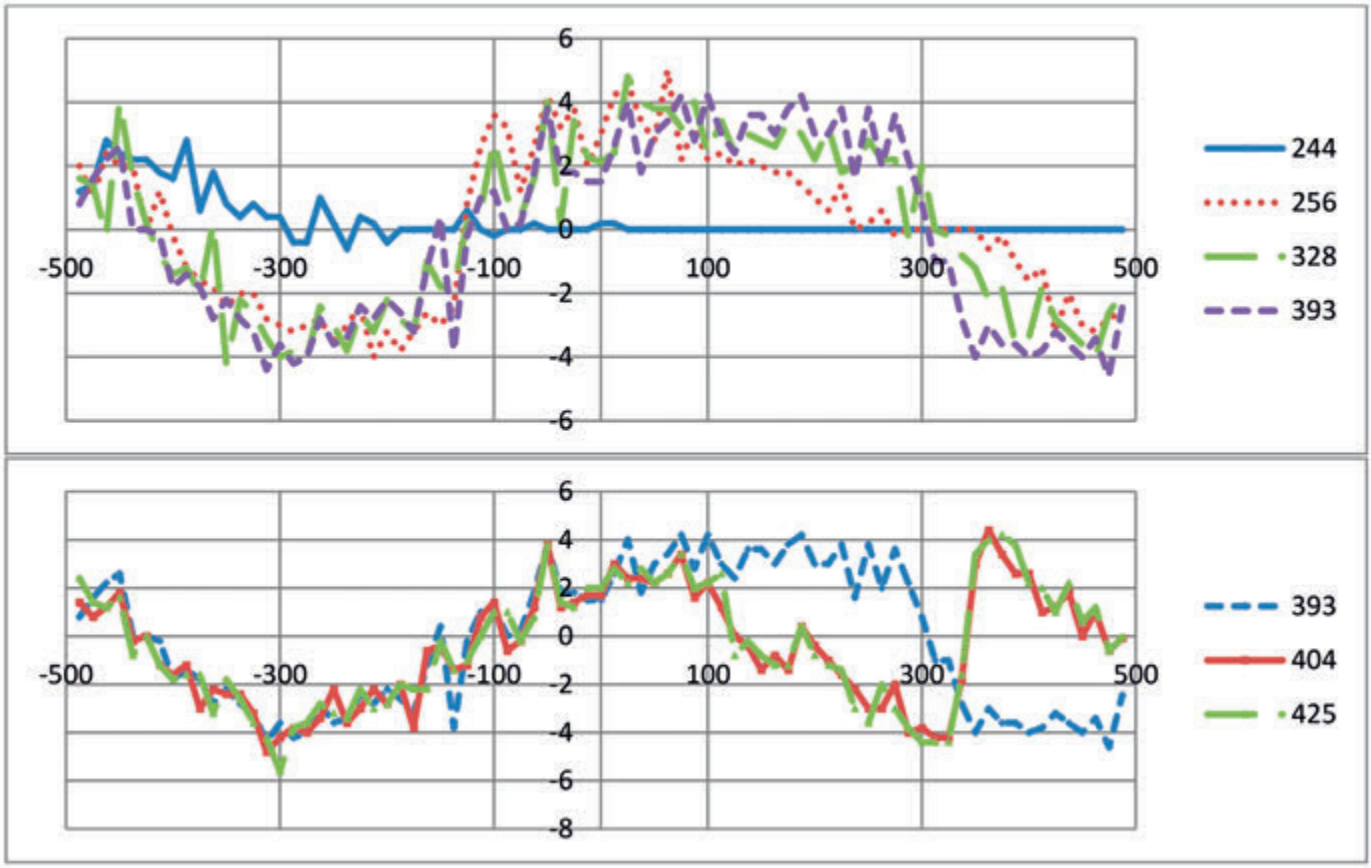

of the rebar return to their original positions and load the concrete lugs between them from the opposite direction.
- Between cracks No. 1 and No. 2 –having the distance close to the transmission length of crack No. 1- the bond stresses are of moderate magnitude hence the concrete stresses between these cracks remain small, too, therefore no further cracks can develop there.
- On both sides of crack No. 2 no development of internal Goto-cracks can be detected.

The misleading character of the databank, the accentuation of the mean values and the substitution of the slip length with the crack distance can be shown on the results of Scott and Gill, see *Table 2*:

Table 2: Comparison of crack distances and distances of points of no slip

Specimen	Crack distance, mm	Distance of points of no slip, mm
100T12	304	**322**
	393	321
	244	
Mean value	**314**	**322**
100T20	**202**	**215**
	202	215
	126	174
	162	133
		149
Mean value	**173**	**177**

Whereas the mean values of crack distance and $l_{s,max}$ are quite close together, the governing values of s_m and $l_{s,max}$ are essentially different.

3.4 BEAM TESTS OF RÜSCH AND REHM

Rüsch and Rehm (1963) tested beams with rectangular (62.5 * 30 cm²) cross section, reinforced with plain (7 pcs.) and with different deformed bars (25 pcs.). (Note: In the 1950's the optimal form of the rib pattern for deformed bars was searched for in Germany.) In 16 beams (evaluated in this paper) the reinforcements 1Ø32, 4Ø16 or 10Ø10 (each yields 804 mm² steel cross sections) were applied. The concrete compression strength (20 cm cubes) was 15 – 32 N/mm². The beams had 4 m span and two concentrated loads. Along the 200 cm long middle section with constant moment no stirrups were placed. Concrete cover was (mostly) 3 cm. The loading was increased causing 50 N/mm² stress-steps in the tensile reinforcement. The formation of cracks was observed and their width was measured in the level of reinforcement (on both sides of the cross section) and on the bottom side of the beams (mostly below the rebars in the corners). Extreme fiber strains of the concrete (near top and bottom) were measured with 20 cm or 50 cm long mechanical gauges. All results of the measurements were presented in graphs and summarized in tables. The crack widths were evaluated statistically, too, and presented also as cumulative frequency curves. Further on two more rectangular beams (120 * 45 cm²) were tested (5Ø26 and 8Ø20) with 400 cm constant moment length.

The side views of the beams with the steps of crack development and the tables lead to profound insights into the cracking per se:

- For crack width control the primary cracks are of interest.
- The mean value of crack distance and crack width are quite inert even for the most important influencing factors, like concrete class, whereas the upper fractile values reveal strong dependence.
- In many cases the max. crack width was wider than the 95% upper fractile value (which is normal). The mean value of the crack width is substantially influenced by the width of the secondary cracks which are out of interest.
- The application of more thin rebars influences very much both the crack pattern and the max. crack width.

Table 3 gives an impression about the change of the maximum crack widths while changing the diameter of the deformed (Nori) rebars. (Note: these crack widths are measured on the beam surface at the level of the rebars. The crack widths on the rebar surface are smaller.)

Table 3: Max. crack width vs. rebar diameter (in 1/100 mm)

steel stress N/mm²	reinforcement		
	1 Ø32	4 Ø16	10 Ø10
200	35	17	7
250	50	20	10
300	50	30	17
350	65	35	20
400	75	50	20

- The 1Ø32 rebar placed in the middle of the 30 cm wide cross section (certainly an unusual but quite informative pattern) hardly controls the crack widths at the corners of the cross section
- The primary cracks reveal the increase between the widths at the level of the reinforcement vs. on the bottom of the beam caused by the curvature of the beam.
- The primary cracks are perpendicular to the beam's axis and run through the tensile zone of the beam, while the secondary cracks –as they develop from Goto-cracks- are short and inclined to the relevant primary crack in their neighborhood. Note: the Goto-cracks are mostly inclined.
- The development of secondary cracks is not imperative on both sides neither of the first nor of the widest primary cracks!
- The ratio of the 90% upper fractile value to the mean crack width value changes with the loading level: at 200 N/mm² steel stress 1.56 – 2.73, at 300 N/mm² 1.38 – 2.44, i.e. it slightly decreases.
- The minimum distance of the primary cracks let estimate the upper limit value of the bond stresses (assuming uniform distribution). Values between 2 and 3 N/mm² were found.
- No strong correlation between the tensile stress at cracking of the beams and the compressive strength (cube) was found.
- Neither the value, nor the position of the maximum concrete elongation (multiplied by 20 cm gauge length) do coincide with the position and width of the widest crack, resp.

Fig. 3 shows the measured max. crack widths for the 62.5 * 30 cm² beams reinforced with different diameter and rate of reinforcements of Nori-type deformed rebars: R37 – 1Ø32, R25 – 4Ø16, R19 – 10Ø10 (all ρ=0.46), R54 – 2Ø26 (ρ=0.62), R21 -1Ø32 + 4Ø16 und R17 – 8Ø16 (ρ~0.95).
In addition to the pronounced influence of the rebar diameter

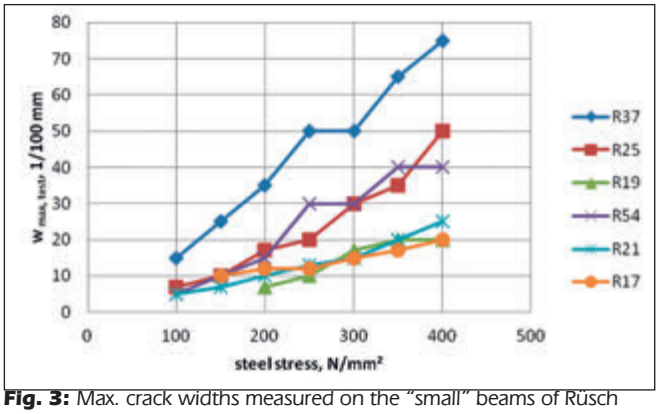

Fig. 3: Max. crack widths measured on the "small" beams of Rüsch and Rehm (1963) with different diameters and amounts of deformed bars

in case of identical rate of reinforcement, the crack width reducing effect of increasing rate of reinforcement can be realized.

A comparison of the crack patterns of the "small" (62.5 *30 cm) beams with those of the "high" beams (120 * 45 cm) reveals that

- The geometrical rate of reinforcement, μ, is a misleading characteristic: the crack patterns of beams with similar μ values but with different $b * h$ sizes are very different.
- In case of the "small" beam with 2Ø26 rebars (beam R 54, $\rho = 0.62$, clear distance between the rebars ~180 mm) no tendency of occurrence of secondary cracks can be found whereas at the "high" beam with 5Ø26 rebars in one layer (beam R 103, $\rho = 0.51$, clear distance between the rebars ~ 60 mm) a very pronounced secondary crack pattern developed. This means that the tensile stresses in the concrete due to bond strongly disperse therefore in case of big bar distances no secondary cracks can develop.
- At development of the secondary cracks the compression zone has no impact hence the tensile reinforcement with the concrete around behaves independently of the compression zone.
- As the secondary cracks originate from Goto-cracks hence their width does not result from the slips on both sides of the secondary crack but from the slips on the remote side from the relevant primary crack only. The Goto- and –as a consequence- the secondary cracks do not change the direction of the slips along the transfer length belonging to corresponding the primary crack. Accordingly the transfer lengths of this primary crack extend beyond the neighboring secondary cracks on both sides.
- The steel stress in the secondary cracks is always less than in the neighboring primary crack, nevertheless bigger than it would result from the concrete contribution along the total transmission length of the primary crack. The steel stress must balance the concrete tensile stresses which caused the secondary crack.
- After occurrence of a secondary crack its width and extension develops/increases until equilibrium is achieved.
- The distance of primary and next secondary crack is different to the transfer length one considered at development of the primary cracks as in the secondary crack the slip is not zero and the steel stress does not correspond to the concrete tensile strength.
- The Goto- and secondary cracks reduce the stiffness of the concrete around the rebar hence the concrete contribution relevant for the width of the primary crack decreases too.

4. CONCLUSIONS

Based on the re-evaluation of results of four test series from the classical literature the following conclusions can be made:

- Shortages of international code proposals for calculation of crack width are presented
- A clear distinction between primary and Goto-/secondary cracks is made.
- The design crack width belongs to a "last" primary crack with the longest transfer lengths on its both sides
- The Goto- and secondary cracks serve the compatibility between the high strains in the rebar and the very limited tensile strain of concrete around.
- The Goto- and secondary cracks "soften" the bond characteristics of the rebars.

In Part II – after a short discussion of different problem-relevant items – the well-known formula of the design value of crack width receives an advanced interpretation. All influencing factors are taken into consideration at the proper position.

5. REFERENCES

Balázs, L. Gy. et al. (2013): "Design for SLS according to *fib* Model Code 2010". *fib* Structural Concrete, 2/2013, June 2013, pp. 99-123.

Broms, B. B., Lutz, L. A. (1965): "Effects of Arrangement of Reinforcement on Crack Width and Spacing of Reinforced Concrete Members", ACI Structural Journal, Nov. 1965, No. 62-77 pp. 1395-1410. + Part II Report.

Goto, Y. (1971): "Cracks formed in concrete around deformed tension bars", ACI Journal, April 1971, pp. 244-251.

Scott, R. H., Gill, P. A. T. (1987): "Short term distributions of stand and bond stress along tension reinforcement", The Structural Engineer, 1987, 65B, No. 2, pp. 39-48.

Rüsch, H., Rehm, G. (1963): „Versuche mit Betonformstählen", Deutscher Ausschuss für Stahlbeton. Heft 140. 182 p.

EN 1992-1-1. (2003): "Eurocode 2: Design of concrete structures – Part 1-1: General rules and rules for buildings", CEN April 2003

CEB-FIP Model Code 1990 (1993), Comité Euro-International du Béton, Bulletin d'Information No. 213/214, Lausanne, May 1993

fib Model Code for Concrete Structures 2010 (2013), Ernst & Sohn, Wiley, ISBN 978-3-433-03061-5

Ferry Borges, J. (1966): "Cracking and Deformability of Reinforced Concrete Beams", IABSE Publication, Zürich, Vol. 26, pp. 75-95.

Control of Cracking of Concrete Structures (2001), ACI 224R-01, Reported by ACI Committee 224, American Concrete Institute, October 2001, 49 p.

Guide to Design Detailing to Mitigate Cracking (2013), ACI 224.4R-13, Reported by ACI Committee 224, American Concrete Institute, December 2013, 24 p.

Coleman, J. W. (2013): "Cracking… Defect or Normal? Part 1: When is cracking a construction defect?", Concrete International, Vol. 35, No. 9, Sept. 2013, pp. 35-38, "Part 2: Case law on concrete cracking", Concrete International, Vol. 35, No. 10, November 2013, pp. 29-35.

Leonhardt, F. (1987): "Cracks and Crack Control at Concrete Structures", IABSE Proceedings P-109/87, IABSE Periodica 1/1987, pp. 25-44.

Windisch, A. (1989): „Zur Berechnung von kritischen Rissbreiten in Zugstäben und Biegebalken", Werkstoff und Konstruktion II, Prof. Rehm zum 65. Geburtstag. 1989 Okt., ibidem-Verlag, Stuttgart, pp. 241-261.

NOTATIONS

$A_{c,ef}$	effective area of concrete in tension
A_c	concrete area in tension
A_s	reinforcement area
E_s	Young's Modulus of Elasticity of reinforcement
c	concrete cover, rib distance on rebar
f_{ctm}	mean value of concrete tensile strength
f_R	relative rib area
k	empirical parameter
k_1, k_2	coefficients
$l_{s,max}$	length over which slip between steel and concrete occurs
l_0	bond transfer length
s	distance of rebars
s_m, s_{rm}	mean crack distance
w_k	characteristic crack width
w_d	design crack width

α_e ratio E_s/E_c
β empirical factor to assess averaged strain within $l_{s,max}$
ε_{cm} average/mean concrete strain
ε_{cs} relevant concrete shrinkage strain
ε_{sm} average/mean steel strain
ε_s steel strain at the crack
ε_{sr} steel strain at the crack under forces causing f_{ctm}
Ø, $Ø_s$ nominal diameter of rebar
ρ A_s/A_c
ρ_r, ρ_{ef} effective reinforcement ratio ($=A_s/A_{c,ef}$)
σ_s steel stress at the crack
σ_{sr} steel stress at the crack under forces causing f_{ctm}
τ_{bk} lower fractile value of the average bond stress
τ_{bms} mean bond strength between steel and concrete

Andor Windisch PhD, Prof. h.c. retired as Technical Director of DYWIDAG-Systems International in Munich, Germany. He made his MSc and PhD at Technical University of Budapest, Hungary, where he served 18 years and is now Honorary Professor. Since 1970 he is member of different commissions of FIP, CEB and fib. He is author of more than 120 technical papers. (Dr. Andor Windisch, Schwarzhölzlstrasse 19A, D-85757 Karlsfeld, Andor.Windisch@web.de)

CREATING THE FUTURE

A-HÍD ZRt.
H-1138 BUDAPEST
KARIKÁS FRIGYES U. 20.

www.ahid.hu

A-HÍD

BUILDING BETTER CITIES

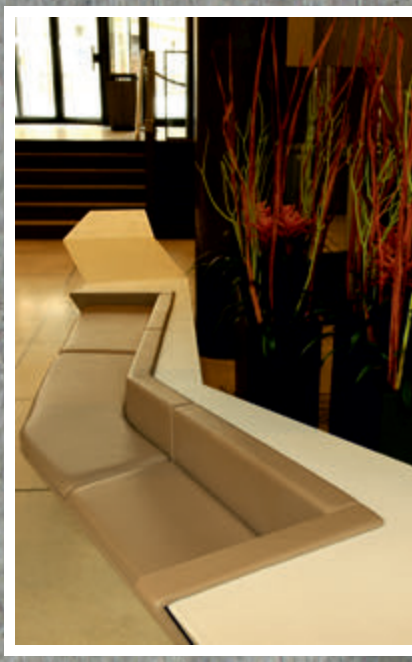

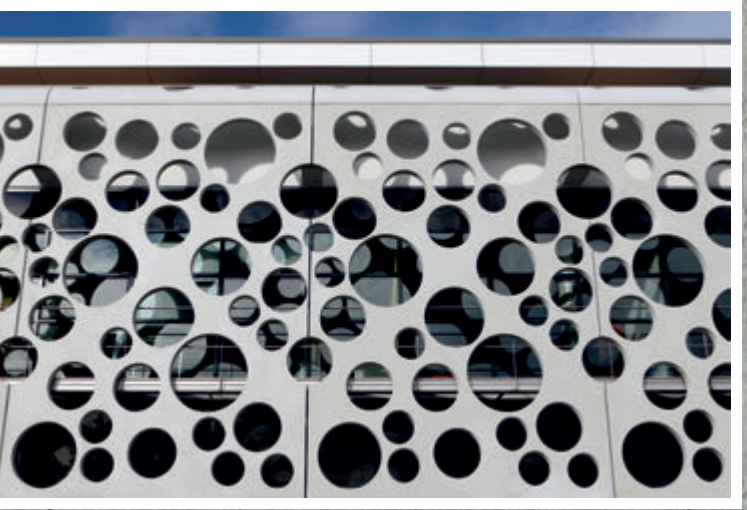

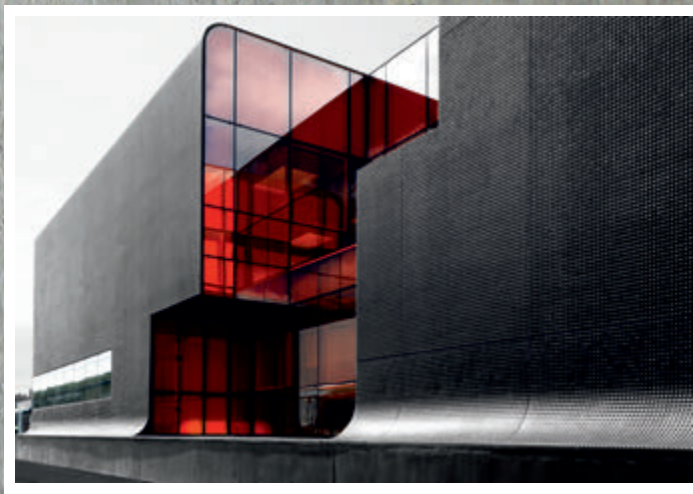

LAFARGE
Building better cities™

A member of
LafargeHolcim